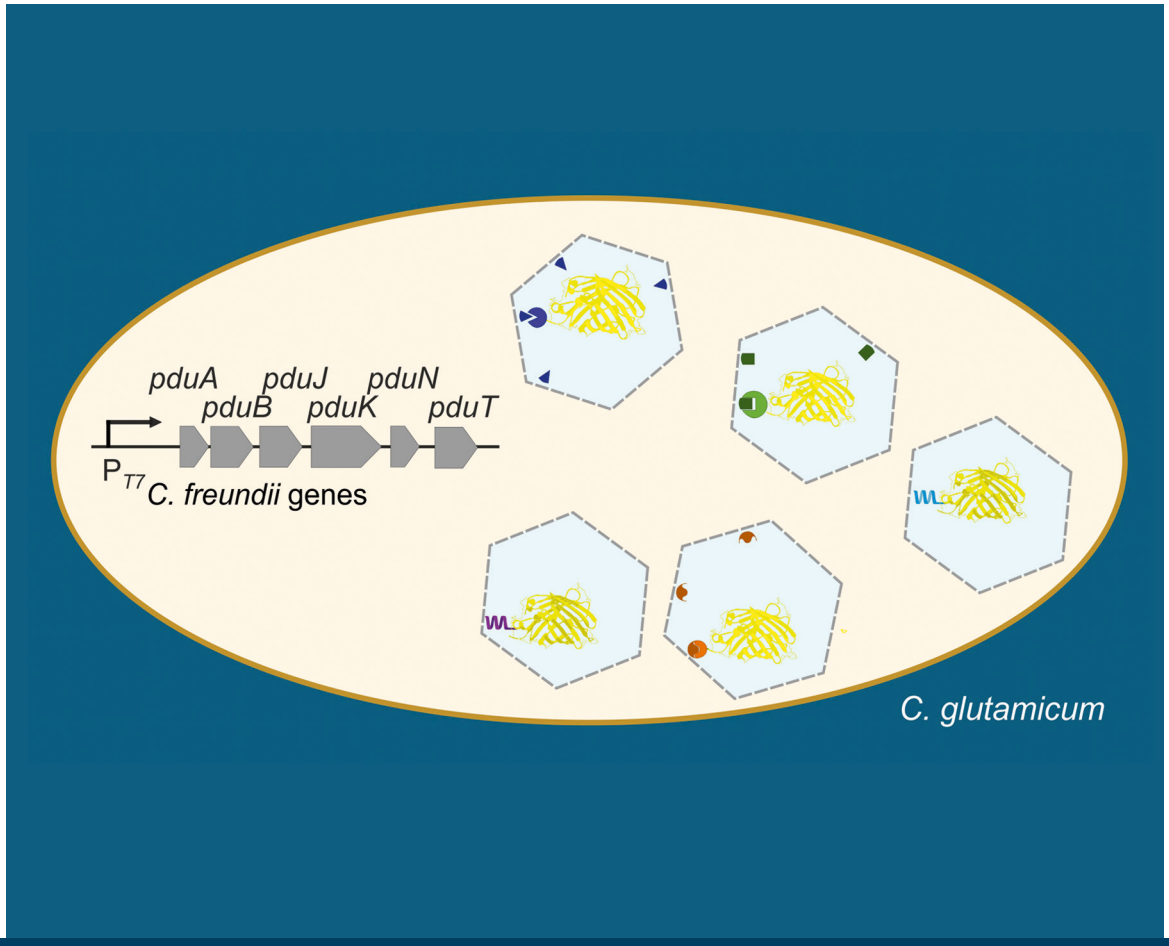

Establishment of Bacterial Microcompartments in the Industrial Production Strain *Corynebacterium glutamicum*

Isabel Huber

Schlüsseltechnologien / Key Technologies
Band / Volume 165
ISBN 978-3-95806-302-0

Mitglied der Helmholtz-Gemeinschaft

JÜLICH
Forschungszentrum

Schriften des Forschungszentrums Jülich
Reihe Schlüsseltechnologien / Key Technologies Band / Volume 165

Forschungszentrum Jülich GmbH
Institut für Bio-und Geowissenschaften
Biotechnologie (IBG-1)

Establishment of Bacterial Microcompartments in the Industrial Production Strain *Corynebacterium glutamicum*

Isabel Huber

Schriften des Forschungszentrums Jülich
Reihe Schlüsseltechnologien / Key Technologies Band / Volume 165

ISSN 1866-1807 ISBN 978-3-95806-302-0

Bibliografische Information der Deutschen Nationalbibliothek.
Die Deutsche Nationalbibliothek verzeichnet diese Publikation in der
Deutschen Nationalbibliografie; detaillierte Bibliografische Daten
sind im Internet über http://dnb.d-nb.de abrufbar.

Herausgeber und Vertrieb:	Forschungszentrum Jülich GmbH Zentralbibliothek, Verlag 52425 Jülich Tel.: +49 2461 61-5368 Fax: +49 2461 61-6103 zb-publikation@fz-juelich.de www.fz-juelich.de/zb
Umschlaggestaltung:	Grafische Medien, Forschungszentrum Jülich GmbH
Druck:	Grafische Medien, Forschungszentrum Jülich GmbH
Copyright:	Forschungszentrum Jülich 2018

Schriften des Forschungszentrums Jülich
Reihe Schlüsseltechnologien / Key Technologies, Band / Volume 165

D 61 (Diss., Düsseldorf, Univ., 2017)

ISSN 1866-1807
ISBN 978-3-95806-302-0

Vollständig frei verfügbar über das Publikationsportal des Forschungszentrums Jülich (JuSER)
unter www.fz-juelich.de/zb/openaccess.

Publications

Results described in this dissertation have been published in the following article:

Huber I., Palmer D. J., Ludwig N. K., Brown I., Warren J. M. and Frunzke J. (2017). "Construction of recombinant Pdu metabolosome shells for small molecule production in *Corynebacterium glutamicum*." ACS Synth. Biol.

Results of further projects not discussed in this thesis have been published in:

Baumgart M., **Huber I.**, Abdollahzadeh I., Gensch T. and Frunzke J. (2017). "Heterologous expression of the *Halothiobacillus neapolitanus* carboxysomal gene cluster in *Corynebacterium glutamicum*." J. Biotechnol.

Content

I List of Abbreviations

1,2-PD	1,2-propanediol	K_d	Rate constant for complex dissociation
3' UTR	3' untranslated region	LB	Lysogeny broth
a.u.	Arbitrary units	MALDI-TOF	Matrix-assisted laser desorption/ionization time of flight
Acn	Aconitase		
Adh	Alcohol dehydrogenase	MalE	Maltose binding protein
AhTet	Anhydrotetracycline	MCS	Multiple cloning site
AlcDH	Alcohol dehydrogenase	Mdh	Methanol dehydrogenases
AldDH	Aldehyde dehydrogenase	MIC	Metabolosomes with incomplete core
APase	Alkaline phosphatase	MS	Mass spectrometry
ASV	SsrA-degradation tag	N.D.	Not determined
ATCC	American type culture collection	OD_{600}	Optical density at 600 nm
BHI	Brain heart infusion	Pdc	Pyruvate decarboxylase
BHI-S	Brain Heart Infusion (+Sorbitol)	Pdu	Propanediol utilization compartment
BMC-FP	Fused/permuted BMC shell protein	PDZdom	PDZ interaction domain
BMC-H	Hexameric BMC shell protein	PDZlig	PDZ interaction ligand
BMC-P	Pentameric BMC shell protein	Phi	6-phospho-3-hexuloisomerase
BMCs	Bacterial microcompartments	P_{T7}	*T7* promoter
BMC-T	Trimeric BMC shell protein	Ptac	Phosphotransacetylase
B-PER™ II	Bacterial protein extraction reagent	P_{tac}	*Tac* promoter
Cad	Cis-aconitate decarboxylase	P_{tuf}	*Tuf* promoter
CDW	Cell dry weight	RMM	*Rhodococcus* and *Mycobacterium* microcompartment
CFP	Cyan fluorescent protein		
Cm	Chloramphenicol	RuBisCO	Ribulose 1,5-phosphate carboxylase/oxygenase
EP	Encapsulation peptide		
et al.	*et alii*	RuBP	Ribulose-1,5-bisphosphate
Etu	Ethanol utilization compartment	RuMP	Ribulose monophosphate pathway
Eut	Ethanolamine utilization compartment	SDS	Sodium dodecyl sulfate polyacrylamide
eYFP	Enhanced yellow fluorescent protein		
GBDdom	GBD interaction domain	SH3dom	SH3 interaction domain
GBDlig	GBD interaction ligand	SH3lig	SH3 interaction ligand
GFP	Green fluorescent protein	TCA	Tricarboxylic acid cycle
GRM	Glycyl-radical compartment	TEM	Transmission electron microscopy
HPLC	High performance liquid chromatography	Tet	Tetracycline
		w/v	Weight per volume
Hps	3-hexulose-6-phosphate synthase	WT	Wild type
Icd	Isocitrate dehydrogenase	Y-PER™	Dialyzable yeast protein extraction reagent
IPTG	Isopropyl-thio-β-D-galactopyranosid		
Kan	Kanamycin		

Further abbreviations not included in this section are according to international standards, as for example listed under https://www.cas.org/content/cas-standard-abbreviations.

II List of Tables

III List of Figures

Summary

Bacterial microcompartments (BMCs) have significant potential in the area of industrial biotechnology for the production of small molecules with toxic or volatile intermediates. *Corynebacterium glutamicum* is an established industrial platform organism for the production of amino acids and was made accessible for the production of diamines, dicarboxylic acids, polymers and bio-based fuels. The aim of this study was to establish BMC production in *C. glutamicum* and to provide useful tools towards a biotechnological application of BMCs as nano-bioreactors.

Within this study, optimized gene clusters for the expression of the *Citrobacter freundii* propanediol utilization compartment shell genes were constructed. Upon induction in *C. glutamicum*, transmission electron microscopy images revealed heterologous compartment production and assembly in the mid cell. Growth studies demonstrated a drastic negative impact of BMC production in *C. glutamicum* but reasonable results were obtained with the chromosomal integration of the gene cluster.

To evaluate the potential of BMCs in *C. glutamicum*, the methanol consumption and the ethanol production pathway, which both include a toxic aldehyde intermediate, and the itaconate production pathway including a transient intermediate, were used. One issue, however, was to produce the enzymes tagged with N-terminal encapsulation peptides in an active form. For the methanol consumption pathway, the enzyme Hps was inactive and also AdhB for ethanol production and MalECad for itaconate production showed reduced activities of 17% and 35% respectively. To expand the synthetic repertoire of encapsulation peptides, new strategies to target proteins of interest into the compartment lumen were investigated. Using fluorescence microscopy, it was proven that a none-native C-terminal targeting peptide from *Klebsiella pneumonia* and three synthetic scaffolding peptides are able to localize a fluorescence reporter into the compartment lumen. The establishment of the alternative the C-terminal targeting strategy now offers the opportunity to choose the optimal fusion for the particular protein of interest. This was, for example demonstrated with C-terminally targeted AdhB versions, restoring an 18% higher enzymatic activity than the N-terminally targeted AdhB version.

PduA formed bundles of filaments in *C. glutamicum* and encapsulation peptide tagged fluorescence reporters localized to those structures. This demonstrates that there is the opportunity to use the nanotube-like structures as scaffolds for directed cellular organization and pathway enhancement.

Altogether, this work provides essential fundamental groundwork on heterologous BMC or scaffold formation in *C. glutamicum* and paves the way for metabolic engineering of pathways with toxic or volatile intermediates or pathways with competing reactions.

Zusammenfassung

Bakterielle Mikrokompartimente besitzen ein großes Potential im Bereich der industriellen Biotechnologie zur Produktion von niedermolekularen Verbindungen mit giftigen oder flüchtigen Zwischenprodukten. *Corynebacterium glutamicum* ist ein industriell etablierter Plattformorganismus zur Produktion von Aminosäuren und wurde außerdem für die Produktion von Diaminen, Dicarbonsäuren, Polymeren und bio-basierten Kraftstoffen erschlossen. Das Ziel dieser Arbeit war die Etablierung der Kompartiment-Produktion in *C. glutamicum* und die Bereitstellung nützlicher Werkzeuge im Hinblick auf deren biotechnologische Anwendung als Nano-Bioreaktoren.

Während dieser Arbeit wurden optimierte Varianten eines Operons zur Expression der Hüllgene des 1,2-Propandiol nutzenden Pdu-Kompartimentes aus *Citrobacter freundii* konstruiert. Nach Induktion der Hüllgenexpression konnten Elektronenmikroskopie-Aufnahmen die heterologe Kompartiment-Assemblierung belegen. Wachstumsstudien zeigten einen drastischen Effekt der Kompartiment-Produktion in *C. glutamicum*, jedoch konnte das Wachstum durch die genomische Integration des Hüllgen-Clusters verbessert werden.

Außerdem konnte gezeigt werden, dass das Hüllprotein PduA tubuläre Strukturen in *C. glutamicum* formt und spezifische Peptidsequenzen Fluoreszenzproteine zu den Strukturen lokalisieren können. Dieses Ergebnis verdeutlicht die Möglichkeit solche Filament-Strukturen als Gerüste für eine gerichtete zelluläre Organisation von Enzymen zu nutzen und damit zur Produktivitätssteigerung von Stoffwechselwegen beizutragen.

Um das Potential der Mikrokompartimente zu beurteilen, wurden ein Methanol-Abbauweg und ein Ethanol-Produktionsweg ausgewählt, welche beide ein giftiges Aldehyd-Zwischenprodukt besitzen. Der außerdem untersuchte Itaconsäure-Produktionsweg besitzt das kurzlebige Intermediat Cis-Aconitat. Als gemeinsame Schwierigkeit stellte sich jedoch heraus, dass einige der Enzyme mit N-terminalen Lokalisations-Peptiden in ihrer Funktion eingeschränkt waren, wie etwa AdhB, ein Enzym innerhalb des Ethanol-Abbauweges und MalECad, welches für die Itaconsäure-Produktion benötigt wird. Die beiden Enzyme zeigten eine auf 17% bzw. 35% reduzierte Aktivität. Das Enzym Hps, beteiligt an der Methanol-Verwertung, war mit dem Lokalisations-Peptid inaktiv. Um das Repertoire an synthetischen Lokalisations-Peptiden zu erweitern wurden zwei alternativen Strategien zur Lokalisierung von Enzymen mittels C-terminalen Peptiden entwickelt. Dies bietet die Möglichkeit den optimalen Fusionspartner spezifisch für jedes Enzym wählen zu können. Durch die Nutzung eines C-terminalen Lokalisations-Peptids an AdhB konnte eine 18% höhere Enzymaktivität im Vergleich zur Nutzung eines N-terminalen Lokalisations-Peptids erreicht werden.

Zusammenfassend zeigt diese Arbeit, dass die heterologe Kompartiment-Produktion in *C. glutamicum* möglich ist und bietet außerdem wichtige Grundlagen für weitere Studien zur biotechnologischen Nutzung der Mikrokompartimente.

1 BACKGROUND

1.1 Bacterial microcompartments

Eukaryotic organisms have evolved a wide range of different organelles for the encapsulation of metabolic pathways like mitochondria, lysosomes, peroxisomes or chloroplasts. These organelles are able to inhabit specific functions due to their separation from cytoplasmic processes by lipid membranes. Bacteria were long thought to lack any compartmentalization of the cytosol. Even though bacterial microcompartments (BMCs) were first observed by electron microscopy almost 60 years ago (Drews and Niklowitz, 1956), increased efforts in their functional characterization were not undertaken until 20 years later (Drews and Niklowitz, 1956; Kerfeld and Erbilgin, 2015).

Genomic analyses revealed that about 20% of all sequenced bacterial species contain protein-coated microcompartments (Axen *et al.*, 2014; Kerfeld and Erbilgin, 2015). The respective genes are typically organized in large operons within the genome. Based on that and the fact that microcompartments are found within 23 different phyla, they are thought to be frequently transferred between organisms by horizontal gene transfer (Axen *et al.*, 2014).

The polyhedral shells of BMCs have a size of 90-400 nm and consist of thousands of shell proteins of different types (Figure 1). The production of BMCs allows the cell to encapsulate pathways with toxic intermediates that inhibit growth or volatile intermediates, which can diffuse through the cell membrane. BMCs can furthermore enhance ineffective reactions of enzymes with low turnover rates or suppress competing reactions by intermediate sequestration (Chen and Silver, 2012). Microcompartments fall into one of two distinct classes, carboxysomes and metabolosomes, depending on whether they encode for anabolic or catabolic processes respectively.

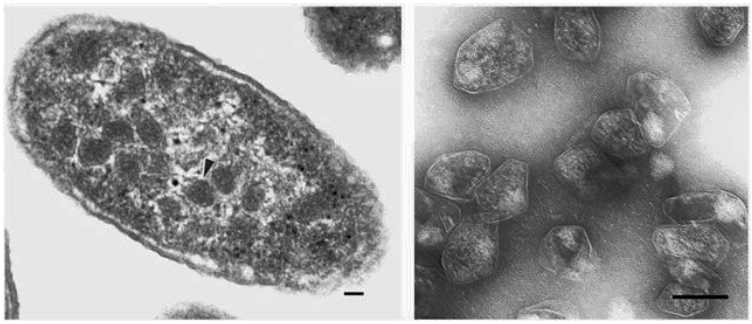

Figure 1: *Salmonella enterica* containing bacterial microcompartments and purified BMCs. Images were taken from Crowley *et al.,* 2008. Scale bar is 100 nm.

Carboxysomes are associated with the anabolic process of carbon dioxide fixation and help to generate elevated carbon dioxide levels within the BMC by enclosing carbonic anhydrase and RuBisCO, thereby enhancing carbon fixation into 3-phosphoglyceraldehyde (Kerfeld and Melnicki, 2016). Metabolosomes are associated with catabolic reactions and based on genetic evidence, it is suggested that there are at least 10 different BMC-encapsulated metabolic processes (Axen *et al.*, 2014; Kerfeld and Erbilgin, 2015).

Table 1: Diversity of bacterial microcompartments. Excerpt from a list published by Kerfeld and Erbilgin, 2015.

Name	Function	Reference
α-carboxysomes β-carboxysomes	Carbon fixation	(Rae *et al.*, 2013)
PDU	Propanediol utilization	(Kerfeld *et al.*, 2010)
EUT	Ethanolamine utilization	(Kerfeld *et al.*, 2010)
ETU	Ethanol utilization	(Heldt *et al.*, 2009)
GRM5	Fucose/rhamnose utilization (Glycyl-radical microcompartment)	(Axen *et al.*, 2014) (Petit *et al.*, 2013)
SPU	Sugar phosphate utilization	(Axen *et al.*, 2014)
RMM	Amino-2-propanol degradation (*Rhodococcus* and *Mycobacterium* microcompartment)	(Mallette and Kimber, 2017) (Axen *et al.*, 2014)

1.1.1 Catabolic processes within metabolosomes

Besides the great diversity amongst metabolosomes, there are some common enzymes present in most of the different BMC types. Genes encoding aldehyde dehydrogenases, alcohol dehydrogenases and phosphotransacetylases are the most frequent enzymes within BMC loci and represent the metabolic core for aldehyde metabolization (Figure 2A). The function of a compartment is defined by a specific aldehyde-generating enzyme, which converts the respective substrate of a BMC. These enzymes are stated as “signature enzymes” (Axen *et al.*, 2014).

The best studied metabolosomes are those associated with the catabolism of 1,2-propanediol (1,2-propanediol utilization, Pdu) from *Salmonella enterica* and *Citrobacter freundii.* The *C. freundii pdu* operon contains 21 genes, including metabolic pathway enzymes for 1,2-propanediol (1,2-PD) degradation and for the recycling of required cofactors (Figure 2C). Two additional genes upstream of the operon, which are divergently transcribed, function as regulator (*pocR*) and as transporter (*pduF*) (Havemann and Bobik, 2003). By encasing the degradation pathway of 1,2-PD, the reactive intermediate propionaldehyde is sequestered to prevent toxicity and carbon loss (Havemann *et al.*, 2002). The Pdu BMCs allow a range of bacteria to inhabit ecological niches within the intestines of eukaryotes or in soil/water, where cell wall sugars like

fructose and rhamnose are fermented to 1,2-PD under anaerobic conditions (Obradors *et al.*, 1988).

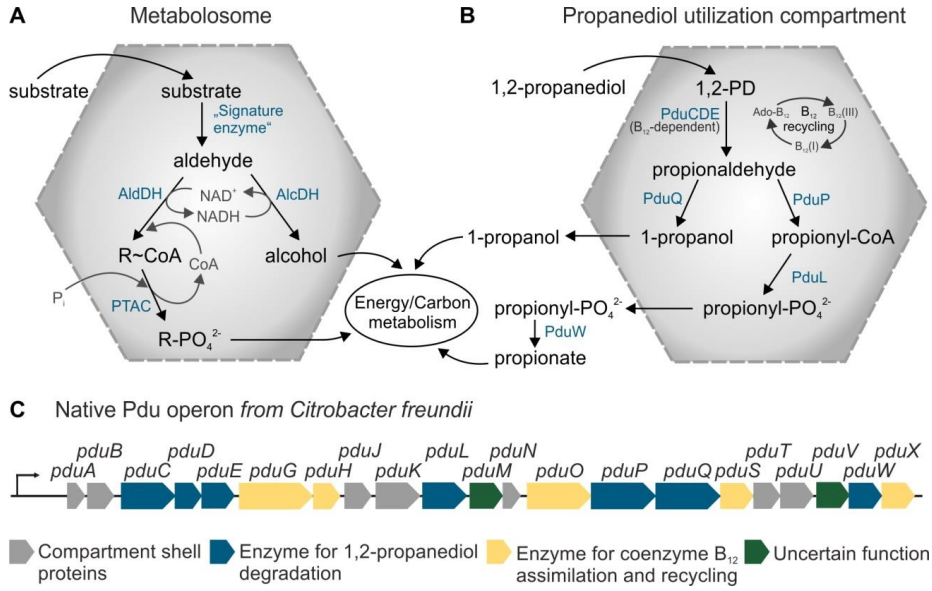

Figure 2: Schematic overview of metabolic utilization processes within BMCs. A Model of a BMC with frequent signature and core metabolic enzymes. Within the BMC, the substrate is converted to an aldehyde, which is the central intermediate. The toxic aldehyde is channeled to R-CoA or an alcohol. R-OH and R-PO_4^{2-} can feed into the central metabolism. Cofactors can be recycled internally. **B** Schematic view of a propanediol utilization compartment. By encasing the degradation pathway for 1,2-propanediol, the reactive and volatile intermediate propionaldehyde is sequestered preventing toxicity and carbon loss. **C** Genomic organization of the *Citrobacter freundii* Pdu operon. The different colors represent general gene functions as indicated. AldDH, aldehyde dehydrogenase; AlcDH, alcohol dehydrogenase; Ptac, phosphotransacetylase. The figure is adapted from Kerfeld and Erbilgin, 2015 and Chowdhury *et al.*, 2014.

Within the compartment lumen, 1,2-PD is converted to propionaldehyde by the B_{12}-dependent dioldehydratase PduCDE. In a NAD^+ and coenzyme A (CoA) dependent reaction of the aldehyde dehydrogenase PduP, propionaldehyde is converted to propionyl-CoA (Figure 2B). For the regeneration of NADH, a second reaction from propionaldehyde to 1-propanol is catalyzed by the 1-propanol dehydrogenase PduQ within the microcompartments. Propionyl-CoA can be either used in the methylcitrate pathway or is further metabolized to propionyl-phosphate *via* a phosphotransacetylase and to propionate by a reversible propionate kinase PduW. The enzyme PduCDE is coenzyme B_{12}-dependent, which can be damaged during catalysis. The reactivation of the enzyme is realized by PduS, PduP and PduGH by recycling the damaged cofactor (Cheng *et al.*, 2012).

The ethanolamine utilization (Eut) compartment is also experimentally characterized in detail. A number of bacteria are able to degrade ethanolamine and utilize it as source for

energy and carbon. Ethanolamine is formed by the degradation of phosphatidyl-ethanolamine, a major component of cell membranes in mammals. Therefore, it is not surprising that ethanolamine degrading bacteria can be frequently found within the classes of Enterobacteria (*Salmonella*, *Escherichia*, *Citrobacter*, *Enterococcus*) (Tsoy *et al.*, 2009). The mechanism of ethanolamine degradation is thereby similar to 1,2-PD degradation: a signature enzyme converts ethanolamine to acetaldehyde. Catalyzed by the core enzyme AldDH, acetyl-CoA is generated and further metabolized *via* Ptac to acetyl-PO_4^{2-} or acetate (general mechanism in Figure 2A). For the regeneration of NADH, AlcDH converts acetaldehyde to ethanol (Chowdhury *et al.*, 2014).
Less information is available for different glycyl-radical compartment (GRM) loci, whose signature enzymes are glycyl-radical enzymes. Potential functions of the different loci are mostly based on predictions by bioinformatic analyses (Axen *et al.*, 2014). However, the GRM1 locus was experimentally proven to contain an S-adenosylmethionine-dependent choline lyase producing acetaldehyde and trimethylamine (Craciun and Balskus, 2012). Also, an aldolase from the GRM5 locus is converting L-fucose and L-rhamnose to lactaldehyde (Petit *et al.*, 2013). Both characterizations fit to the model of signature enzymes producing an aldehyde, which can be further metabolized with the core enzymes (Figure 2A).

1.1.2 Microcompartment shell assembly

The shells of BMCs can self-assemble from basic building blocks to complex polyhedral organelles. These building blocks are BMC shell proteins, which all contain a characteristic BMC domain (Kerfeld *et al.*, 2005; Klein *et al.*, 2009). They are classified into three different categories on whether they form hexamers (BMC-H), pentamers (BMC-P) or trimers (BMC-T) (Figure 3A).
BMC-H proteins contain one BMC domain within their sequence and assemble into hexamers (Kerfeld *et al.*, 2005; Crowley *et al.*, 2008; Crowley *et al.*, 2010). The class of BMC-T proteins forms pseudohexameric trimers, whereby each protein contains a tandem repeat of the BMC domain. Both shell types form a central pore in the middle of the hexameric or pseudohexameric structure (Crowley *et al.*, 2010). It is suggested that BMC-H hexamers and BMC-T trimers form extended flat sheets and build the facets of assembled compartments. A conserved lysine motif (D/N-X-X-X-K) within the BMC domain was confirmed to support the interaction between adjacent hexamers (Pang *et al.*, 2014; Sinha *et al.*, 2014; Kerfeld and Erbilgin, 2015). The group of pentameric BMC-P proteins is thought to form the vertices and thereby facilitates the closure of the BMC shells (Tanaka *et al.*, 2010). This general model of shell assembly is visualized in

Figure 3A showing no symmetrical arrangement of BMC-H and BMC-T proteins at the facets.

A more detailed model for shell assembly was suggested by Lassila *et al.* based on studies on the assembly of a compartment of unknown function from *Haliangium ochraceum*. Regarding BMC-T proteins, it is proposed that the individual proteins have distinct roles, as they arrange around the vertex proteins and promote curvature of the compartment (Figure 3B) (Lassila *et al.*, 2014). Another model was offered by Malette *et al.* based on docking studies and crystal interactions of four *Rhodococcus* and *Mycobacterium* microcompartment (RMM) shell proteins from *M. smegmatis*. Additional to a BMC-H and a BMC-P shell protein, the operon contained proteins from an alternative class, determined as BMC-FP (fused, permuted or double-ringed proteins). Similar to the model from Lassila *et al.*, an inner ring around the vertex protein was proposed for one BMC-FP (Figure 3B). Additionally, the second BMC-FP protein type organized to linear strips and may line facet edges (Figure 3C). Both BMC-FPs are suggested to form face-to-face double layers, even though the function of this arrangement is unknown (Mallette and Kimber, 2017). Altogether, these models are presumptions but especially the organization of the edges is still poorly understood.

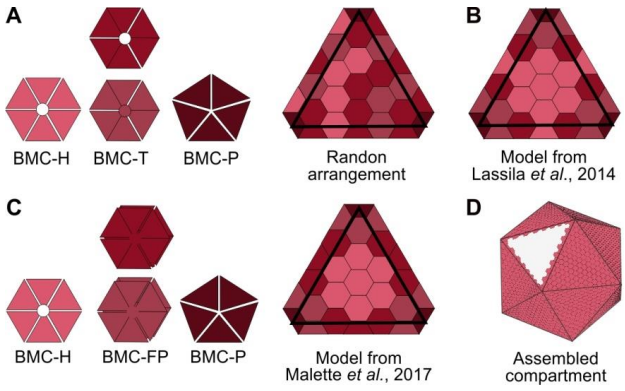

Figure 3: Compartment shell assembly. For the three types of BMC domain proteins, there are different models for their arrangement to BMC shells. BMC-P proteins form the vertices of the shells. **A** BMC-T and BMC-H proteins form the facets in random arrangements. **B** BMC-H proteins form the facets and BMC-T proteins are arranged around the vertices and promote the curvature of the BMCs. **C** Malette *et al.* provide an alternative classification of BMC domain proteins with BMC-FP proteins (fused, permuted or double ringed) present at the interfaces of the facets. **D** Polyhedral structure of a microcompartment assembled from different BMC shell proteins.

1.1.3 Protein targeting to microcompartments

For the integration of heterologous pathways into BMCs, it is of great importance to understand the mechanisms of targeting and interior organization of the incorporated enzymes. Short C- or N-terminal sequences were found to be responsible for the localization of associated pathway enzymes into the BMC lumen (Fan *et al.*, 2010). The N-terminal regions were identified by sequence alignments of PduP homologs, which were predicted to be associated with microcompartments and those which are unrelated to BMC function (Fan *et al.*, 2010). Experimental studies for PduP from *S. enterica* and *C. freundii* confirmed that the N-terminal 18 amino acids were sufficient to target the protein of interest into the compartment lumen (Fan *et al.*, 2010; Lawrence *et al.*, 2014). Using alanine scanning mutagenesis studies, the key amino acids (E7, I10 and L14) for the interaction of the N-terminal peptide from PduP with the C-terminal extension of PduA and PduJ were confirmed (Fan *et al.*, 2012).

Kinney *et al.* proposed some conserved properties for various encapsulation peptides (EPs): the size ranges from 13-22 amino acids and the peptides form an amphipathic α-helix linked to the rest of the protein by a poorly conserved linker (Kinney *et al.*, 2012). With solution structure analyses of the P18 peptide, the α-helical structure of the peptide was proven (Lawrence *et al.*, 2014). By bioinformatic analysis of over 1000 EPs from diverse BMCs, the characteristic pattern of hydrophilic and hydrophobic residues was confirmed (Aussignargues *et al.*, 2015). The general mechanism that mediates the encapsulation is also underlined by different studies showing that the interaction of shell proteins with non-native encapsulation peptides is possible. For example, some known and predicted encapsulation peptides from four different BMCs were shown to localize GFP to the *S. enterica* Pdu compartment (Choudhary *et al.*, 2012; Sargent *et al.*, 2013; Jakobson *et al.*, 2015).

Besides the targeting mechanism with EPs, additional targeting strategies are proposed as not all encapsulated enzymes contain EPs. PduQ does neither contain C- nor N-terminal extension but was demonstrated to be a luminal protein. However, PduQ was shown to bind to PduP *in vitro* and therefore may be targeted into the compartment *via* the EP of PduP as both proteins have a role in NAD^+/NADH recycling (Figure 2A and B) (Cheng *et al.*, 2012). Similarly, PduC lacks any EPs but for the packing of PduCDE, the N-terminal region of PduD was sufficient to target the whole enzyme complex into the compartment. PduE also contains a N-terminal extension but was unable to localize to BMCs when expressed alone (Fan and Bobik, 2011). These observations might be explained by the tendency of targeting peptides to interact with each other (Tobimatsu *et al.*, 2005; Lee *et al.*, 2016) and therefore the enzyme clustering might be a potential way

of recruiting enzymes without a direct interaction with the shell proteins (Aussignargues *et al.*, 2015).

1.1.4 Shell protein pores and transport mechanisms through the shells

The protein shell of a microcompartment represents the barrier between the inner lumen and the surrounding cytosolic environment. The understanding of influx and efflux mechanisms of substrates, products and cofactors through the compartment shells is highly critical for the introduction of heterologous pathways.

With crystal structures of representative hexameric BMC-H proteins, pores with a diameter of ~6 Å in the center of the hexamer have been revealed (Crowley *et al.*, 2010; Tanaka *et al.*, 2010; Yeates *et al.*, 2013). These pores are proposed to be selectively permeable to substrates and products, but inhibit the efflux of toxic or volatile intermediates. For example, the PduA pore is lined with hydrogen-bond donors and hydrogen-bond acceptors whose arrangement is suggested to facilitate the movement of the mostly polar 1,2-PD, the substrate of the Pdu pathway (Figure 2B) into the compartment but retains the less polar propionaldehyde (Crowley *et al.*, 2010). With PduA pore mutants, physiological and biochemical data confirmed the selective permeability of PduA and in particular showed that the exchange of pore-lining residues can alter substrate specificity (Chowdhury *et al.*, 2015). Similarly, mutational studies on the BMC-H protein CcmK2 from the ß-carboxysome which is closely related to PduA have been undertaken. With the exchange of critical pore residues of CcmK2 to those of the paralogs CcmK4 and CsoS1, Cai *et al.* showed that the pore of the corresponding paralog can be mimicked (Cai *et al.*, 2015).

In some cases, the typical central pore, described for BMC-H proteins is found to be blocked with a ß-barrel like in PduU. The purpose of this blockage is unknown but one hypothesis determines PduU to have other functions besides molecule transport (Crowley *et al.*, 2008). Similarly, the central pore of PduT is occupied by a Fe-S cluster and is speculated to be involved in redox-equivalent transfer for the supply electrons within the compartments or the transport of the whole Fe-S cluster into the compartment (Pang *et al.*, 2011; Bobik *et al.*, 2015).

Crystallography analysis of BMC-T proteins provided structures which are able to undergo conformational changes. The closed form of the trimeric protein revealed to have a nearly occluded small central pore and a narrow hole within each monomer, whereas the open form contains a much larger triangular central pore with a diameter of 8-11 Å (Tanaka *et al.*, 2010; Thompson *et al.*, 2015). The pores thereby provide the possibility to exchange large enzymatic cofactors like NAD^+ and CoA. It would be of

disadvantage for the compartment shells to have the large pore continuously open. Therefore it is not surprising that the pores were shown to be allosterically regulated. Ethanolamine, the substrate of the Eut compartment was demonstrated to bind the closed form of EutL and therefore ethanolamine was assumed to act as negative allosteric regulator for pore opening (Thompson *et al.*, 2015). Similarly, PduB from the *L. reuteri* Pdu and glycerol utilization compartments binds its substrate glycerol (Pang *et al.*, 2012). Controversially, Pdu and Eut compartments were shown to maintain their private cofactor pools (Cheng *et al.*, 2012; Huseby and Roth, 2013). However, whether this finding is in accordance with the pore opening theory is not completely solved.

1.2 Prospects of BMCs for metabolic engineering and pathway enhancement

1.2.1 Compartmentalization and scaffolding for synthetic biology approaches

In nature, compartmentalization for the separation of biological reactions is achieved with different strategies like membrane enclosed organelles, multi-enzyme complexes, or the previously described BMCs. Regarding synthetic biology approaches, many enzymatic pathways could benefit from compartmentalization: enzymes with low turnover rates can be provided with higher substrate concentrations; diffusion and thereby loss of volatile intermediates through the cell membrane can be limited; toxic intermediates that interfere with cytosolic processes and competing reactions are separated (Chen and Silver, 2012).

Some strategies to fulfill these requirements for the optimization of industrially relevant metabolic pathways have been successfully adapted. For example, the direct fusion of two enzymes for formaldehyde fixation (3-Hexulose-6-phosphate synthase and 6-phospho-3-hexuloisomerase) from a methylotrophic bacterium allowed a better growth and enhanced metabolization of formaldehyde in *E. coli* (Orita *et al.*, 2007).

Dueber *et al.* established synthetic protein scaffolds based on natural protein-protein interaction domains and their cognate ligands. By tagging three pathway enzymes for mevalonate production with peptide ligands specific for the interaction-domains on the scaffold, the final mevalonate yield was enhanced 77-fold (Dueber *et al.*, 2009; Liu *et al.*, 2013). Using the same polypeptide scaffold, a 5-fold increase in glucaric acid production was achieved in *E. coli* (Moon *et al.*, 2010).

Initially, these elevated product yields were explained by substrate and proximity channeling through enhanced channeling of the intermediates from one to another enzyme. In a review from Lee *et al.* this hypothesis was reformulated: It was suggested that an additional important factor for enhanced flux was the agglomeration of multiple copies of enzyme-scaffold complexes, so-called microdomains. Within these microdomains, the local concentration of intermediates is higher than outside the complex. As some enzymes of the glucaric acid and mevalonate pathway are oligomeric it is likely that multiple enzyme-scaffold complexes are able to agglomerate (Lee *et al.*, 2012).

Also, a variety of native proteinaceous encapsulation systems is present and some of those were evaluated for synthetic applications. CipA, a small 104 aa protein, forms crystalline inclusions in *Photorhabdus luminescens*. Based on the microdomain principle,

this protein was applied as scaffold to enhance violacein synthesis from L-tryptophan by tagging the five enzymes involved with the CipA peptide (Wang *et al.*, 2017).
Encapsulins are natively occurring icosahedral protein complexes with a size of up to 25 nm consisting of about 60 copies of a single protein and offer the possibility to localize proteins of interest into the structures (Sutter *et al.*, 2008; Snijder *et al.*, 2016). Other extensively studied examples of proteinaceous compartments are virus capsids. These structure were mainly characterized for the directed delivery of pharmaceuticals and vaccine development but also initial approaches for enzymatic reactions in virus capsids were made (Maity *et al.*, 2015; Giessen and Silver, 2016).

1.2.2 Synthetic BMC shell production in heterologous hosts

There are several studies on the assembly of BMC shells in the heterologous host *E. coli* by the expression of shell genes from different organisms and compartment types. The Pdu compartment from *C. freundii*, which is used throughout this work consists of seven shell proteins (BMC-H: PduA, PduJ, PduK, PduU; BMC-T: PduB, PduB', PduT; BMC-P: PduN) (Havemann and Bobik, 2003). With the production of the seven shell proteins in *E. coli*, transmission electron microscopy (TEM) images of thin sections revealed compartment-like structures with a size of ~100 nm (Parsons *et al.*, 2010). Studies on protein stoichiometry revealed that PduA, PduB, PduB' and PduJ are major components of the shells whereas the minor components PduK, PduN, PduU and PduT contribute to ~20% of the total shell protein (Havemann and Bobik, 2003; Mayer *et al.*, 2016). PduU and PduT were found to be dispensable for successful compartment formation but besides those, the deletion of other shell proteins significantly influenced compartment shape and morphology (Parsons *et al.*, 2008; Parsons *et al.*, 2010; Cheng *et al.*, 2011).
The Eut compartments from *S. enterica* consist of five different shell proteins (EutSMNLK) which self-assemble to BMCs (~100 nm) when overexpressed in *E. coli*. Furthermore, the overproduction of EutS alone was sufficient to result in shell structures (Choudhary *et al.*, 2012). A microcompartment from *H. ochraceum* encodes four shell proteins, which were placed into a synthetic operon for the production in *E. coli*. The ribosome binding sites (RBS) were designed according to known protein stoichiometries of the different BMC shell proteins. The expression of this operon led to BMC shells with a size of ~50 nm (Lassila *et al.*, 2014). Within all of these studies, the authors emphasize the utilization of the heterologous compartments for biotechnology and synthetic biology approaches.

1.2.3 Construction of an ethanol production chamber in *E. coli*

Over the last 15 years, the number of publications on functional characterization of BMCs is rapidly increasing. Nevertheless, the production of ethanol is so far the only described synthetic application of small molecule production in BMCs.

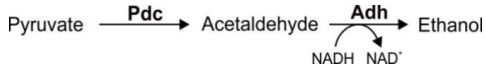

Figure 4: Reaction of pyruvate to ethanol.

The Pdu shells from *C. freundii* were successfully produced in *E. coli* by the expression of *pduABJKNUT* (*Parsons et al.,* 2010). For the purpose of ethanol production within these compartments, Pdc and Adh from *Zymomonas mobilis* were tagged with EPs for the subsequent encapsulation into the BMC shells. During the production of ethanol from pyruvate, the toxic intermediate acetaldehyde is produced by the reaction of the pyruvate decarboxylase (Pdc). The subsequent alcohol dehydrogenase (Adh) reaction catalyzes the oxidation of acetaldehyde (Figure 4) (Lawrence *et al.*, 2014).

In the absence of shell proteins, ethanol-producing strains with tagged and untagged Adh/Pdc versions yield 36-44 mM ethanol (normalized to OD_{600} = 1) with aerobic growth after 48 h in LB medium. Because of the very similar amounts of ethanol produced by all strains, it was stated that *in vivo*, no negative effect of the addition of targeting peptides to Pdc and Adh on ethanol production (without shells) was observed. In the presence of shell proteins*, E. coli D18adh/P18pdc* and *E. coli D60adh/P18pdc* reached higher ethanol titer (46 and 59 mM, respectively) than *E. coli adh/pdc* with 38 mM ethanol*.* Conclusively, the authors were able to slightly increase the ethanol production with the usage of tagged enzymes and BMC shells (Lawrence *et al.*, 2014).

1.3 The potential of *Corynebacterium glutamicum* for BMC establishment

Firmicutes, γ-Proteobacteria as well as Actinobacteria are the phyla with the highest diversity of different BMC loci found (Axen *et al.*, 2014). Actinobacteria, the phylum *C. glutamicum* belongs to, can contain *α*-carboxysomes, Pdu, Eut, Pdu/Eut fusions, GRM and MIC loci. Also, a *Rhodococcus* and *Mycobacterium* microcompartment locus was exclusively found within this phylum. The function of the RMM locus was not determined experimentally but the locus includes besides others hydrolases, a short-chain dehydrogenase and a phosphotransferase (Axen *et al.*, 2014). The short-chain dehydrogenase was previously characterized as amino-2-propanol dehydrogenase and converts amino-2-propanol to aminoacetone (Kataoka *et al.*, 2006; Urano *et al.*, 2011) which is suspected to be converted by the aminotransferase producing the toxic compound methylglyoxal (Kerfeld and Erbilgin, 2015). The structures of the shell proteins of a RMM from *M. smegmatis* were investigated by crystallography and docking studies and were described before in Section 1.1.2 (Mallette and Kimber, 2017).

No evidence for native BMC loci was found in *C. glutamicum*. To date, all studies on the establishment of engineered metabolosomes in heterologous hosts were performed in the gram-negative *E. coli*. Very recently, we published the heterologous expression of the α-carboxysomal gene cluster from *Halothiobacillus neapolitanus* in *C. glutamicum.* With the purification of microcompartment-like structures combined with a detailed microscopic analysis, the assembly of *H. neapolitanus* shells was suggested (Baumgart *et al.*, 2017).

The establishment of BMCs for synthetic applications in *C. glutamicum* could be profitable for a range of different production processes, which will be illustrated within the following sections.

1.3.1 *C. glutamicum* as industrial production strain

A sustainable bioeconomy is one of the corner stones to reach the important long-term goals for climate and resource protection, securing energy and future food supply. In the last decades, substantial progress has been made in two important key sectors towards a sustainable bioeconomy: (i) the production of a broad range of products from renewable biomasses by employing the metabolic power of microbes and (ii) the utilization of alternative carbon sources from unused industrial waste streams which do not compete with food and feed industry (Becker and Wittmann, 2015; Lee *et al.*, 2016).

On the basis of many physiological properties and a comprehensive knowledge of metabolism and regulatory networks, the gram-positive model organism *C. glutamicum* represents one of the most important biotechnological platform strains. It is used as an industrial workhorse for the large-scale production of the amino acids L-glutamate and L-lysine (about 3.1 and 2.4 million tons per year respectively) (Ajinomoto, 2016; Ajinomoto, 2017). In industrial processes, the sources for *C. glutamicum* growth and energy supply are mainly glucose (from starch), sucrose and fructose (from molasses) (Eggeling and Bott, 2005). The cultivation is based on carbon sources from renewable energy sources like sugar cane, corn or wheat. However, the production of plants as fermentation substrate competes with the demand of acreage for food production. Therefore, there is a strong interest in approaches facilitating alternative renewable carbon sources from non-competing feedstocks like lignocellulosic substrates derived from agricultural waste.
C. glutamicum already provides a broad natural substrate spectrum including sugars, organic acids (Kato *et al.*, 2010), sugar-alcohols (Laslo *et al.*, 2012) and various aromatic compounds (Shen *et al.*, 2012), which can be further expanded to the use of several additional cheap renewable carbon sources like starch (Seibold *et al.*, 2006), glycerol (Rittmann *et al.*, 2008) or lignocellulosic compounds (xylose, arabinose) (Sasaki *et al.*, 2009).
C. glutamicum has a versatile secondary metabolism which can be tailored towards the production of relevant high-value products like diamines, dicarboxylic acids, polymers and bio-based fuels by metabolic engineering (Yamamoto *et al.*, 2013; Becker and Wittmann, 2015). The large number of genetic engineering and analysis tools ('omics' technologies, high-throughput screenings) established for *C. glutamicum* strains further drives the development of new production pathways.

1.3.2 Production of the high value chemical itaconate with *C. glutamicum*

The US department of Energy published a list of 12 top-value added chemicals with a high industrial potential, which can be produced from sugars with microbial fermentation (Werpy *et al.*, 2004). Itaconic acid was placed on the list of top-value added chemicals in 2004 (Werpy *et al.*, 2004). The compound is a C5 dicarboxylic acid and has the potential to replace the petrochemically derived acrylic acid (Sauer *et al.*, 2008). The reactive compound has a broad spectrum of reactions and applications including synthetic latex, superabsorbent polymers for diapers, chelant dispersant agents, unsaturated polyester resins and detergent builders (Steiger *et al.*, 2013).
A native itaconic acid producer, *Aspergillus terreus*, is able to produce large amounts (80 g L^{-1}) from sugars. *Ustilago maydis* as natural and *Aspergillus niger* as heterologous

producer were optimized for the production of itaconic acid but the yields from *A. terreus* could not yet be exceeded (Okabe *et al.*, 2009).

The cis-aconitate decarboxylase (Cad) is the only known enzyme able to convert cis-aconitate to itaconate. In the mitochondrion of *A. terreus,* cis-aconitate is provided by the TCA cycle as an intermediate in the aconitase reaction from citrate to isocitrate. The subsequent Cad reaction is localized within the cytosol (Figure 5) (Steiger *et al.*, 2013).

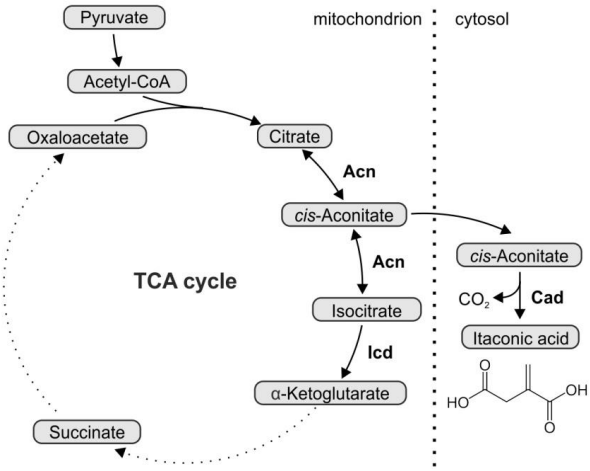

Figure 5: Itaconate production in *A. terreus*. Cis-aconitate is provided from the TCA cycle within the mitochondrion. By an unknown transport mechanism, cis-aconitate enters the cytosol and is converted to itaconic acid by the cis-aconitate decarboxylase. Acn, aconitase; Cad, cis-aconitate decarboxylase; Icd, isocitrate dehydrogenase;

The establishment of a *C. glutamicum* itaconate production strain was published before (Otten *et al.*, 2015). The *cad* gene from *A. terreus* was codon-optimized and heterologously expressed in *C. glutamicum*. Improvements in itaconate titers were achieved by the fusion of a maltose binding protein (MalE) to stabilize the protein and the application of nitrogen limited conditions. As the supply of cis-aconitate was stated to be the main bottleneck of itaconate production, the substrate availability for Cad was enhanced by lowering the isocitrate dehydrogenase (Icd) activity by modification of the Icd start codon from ATG to GTG or TTG (Otten *et al.*, 2015).

1.3.3 Methanol as alternative carbon source for *C. glutamicum*

Methanol was put into focus of scientific interest as alternative carbon source because it is a non-food raw material. Nowadays, methanol is mostly supplied from synthesis gas or directly from natural gas (Muller *et al.*, 2015) but the production from renewable

feedstocks like CO_2, biomass, municipal or industrial waste is also possible (Law *et al.*, 2013).

Methylotrophic organisms are able to utilize methanol or methane as sole carbon source for growth. In bacteria, this is achieved by the oxidation of methanol to formaldehyde by pyrroloquinoline quinone dependent or NAD^+-dependent methanol dehydrogenases (Mdh) (Arfman *et al.*, 1989; Nakagawa *et al.*, 2012). Remarkably, pathways for formaldehyde oxidation are not limited to methylotrophs but are widely distributed within bacteria. Formaldehyde is a toxic metabolite and byproduct of different reactions within the cell and within environmental processes. Therefore, mechanisms oxidizing formaldehyde to CO_2 are used as protection mechanism to reduce toxicity (Heck *et al.*, 1990). Pathways for the utilization of formaldehyde in methylotrophs are the ribulose monophosphate (RuMP) pathway, the serine cycle and the Calvin-Benson-Bassham cycle (Chistoserdova, 2011).

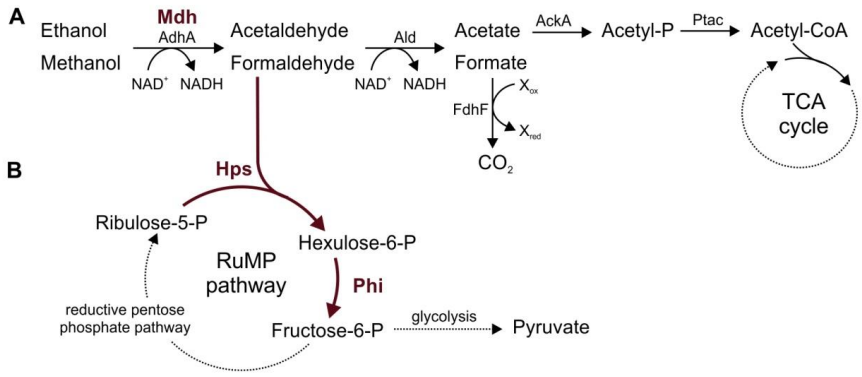

Figure 6: Native and engineered methanol catabolism pathway in *C. glutamicum.* **A** Endogenous pathway for ethanol and methanol oxidation. Both alcohols are oxidized by AdhA and Ald to acetate or formate, respectively. Acetate can feed into the TCA cycle over acetyl-P and acetyl-CoA. Formate is further oxidized to CO_2 by FdhF. **B** Engineered methanol metabolism. Heterologous enzymes (red) were introduced in *C. glutamicum* for the assimilation of formaldehyde *via* the RuMP pathway. Fructose-6-P can be used in glycolysis or the pentose phosphate pathway for regeneration of Ribulose-5-P. AldhA, alcohol dehydrogenase; Ald, acetaldehyde dehydrogenase; AckA, acetate kinase; FdhF, formate dehydrogenase; Hps, 3-hexulose-6-phosphate synthase; Mdh, methanol dehydrogenase; Phi, 6-phosphate-3-hexuloisomaerse; Ptac, phosphotransacetylase;

Even though *C. glutamicum* contains endogenous enzymes for the oxidation of methanol, it cannot be used as carbon source. The enzyme AdhA catalyzes the reaction from methanol to formaldehyde, an aldolase oxidizes formaldehyde to formate and FdhF is able to oxidize formate to CO_2 (Figure 6A) (Witthoff *et al.*, 2013).

C. glutamicum was engineered for the utilization of methanol as an auxiliary substrate (Witthoff *et al.*, 2015). The first step, the oxidation of methanol, was catalyzed by the methanol dehydrogenase (Mdh) from *Bacillus methanolicus*. For the establishment of a

functional RuMP pathway for formaldehyde assimilation, a 3-hexulose-6-phosphate synthase (Hps) and a 6-phosphate-3-hexuloisomaerse (Phi) from *Bacillus subtilis* were introduced additionally to endogenous enzymes of the central carbon metabolism of *C. glutamicum* (Figure 6B). In a defined sugar and methanol-containing medium, the cell dry weight (CDW) was increased by 18% for the *C. glutamicum* methanol consumption strains in comparison to the control strain. [^{13}C] methanol labeling experiments indicate the assimilation of carbon into biomass, but to a very low extent. 78% of the methanol was still oxidized to carbon dioxide *via* the endogenous pathway. The authors concluded that it is necessary to optimize the formaldehyde assimilation module and balance the oxidation of formaldehyde to minimize toxic formaldehyde effects for enhanced carbon assimilation (Witthoff *et al.*, 2015).

1.3.4 Ethanol production with *C. glutamicum*

Ethanol can be produced from renewable carbon sources and is primary used to replace fossil fuels for example as additive in gasoline with 10-25%. Traditionally, ethanol is produced by fermentation of the yeast *Saccharomyces cerevisiae* with glucose as substrate. Regarding sustainable resources, *S. cerevisiae* was engineered for the utilization of pentose sugars from lignocellulosic biomass (Hahn-Hagerdal *et al.*, 2007). However, this approach presents clear disadvantages with low pentose utilization rates and increased fermentation times were observed (Oreb *et al.*, 2012). Further engineering approaches also focused on *E. coli* and *C. glutamicum* (Ohta *et al.*, 1991; Inui *et al.*, 2004; Jojima *et al.*, 2015) due to their great potential to utilize alternative carbon sources (Zahoor *et al.*, 2012).

Natively, *C. glutamicum* is unable to produce ethanol, however it possess high ethanol oxidation activity when catabolizing this substrate (Figure 6). The activity of the responsible enzyme Adh is rather low, when additionally or solely glucose is present (Arndt and Eikmanns, 2007). A recombinant *C. glutamicum* strain producing Pdc and AdhB from *Z. mobilis* was genetically optimized towards ethanol production and yielded 119 g L^{-1} ethanol produced from glucose which was calculated to be 95% of the theoretical maximal yield. Ethanol production from glucose, xylose and arabinose mixed medium was determined with 83 g L^{-1} ethanol (Jojima *et al.*, 2015).

1.4 Goals and strategies of this work

The development of synthetic BMCs in the industrial platform strain *C. glutamicum* could expand the application range of *C. glutamicum*, especially for products whose synthesis involves toxic or volatile intermediates.

i. The primary aim of this dissertation is to establish the self-assembly of microcompartment shells in *C. glutamicum* by the heterologous production of BMC shell proteins. This goal represents the first approach of a transfer of metabolosomes shell genes from γ-proteobacterial origin to another phylum. The 1,2-PD utilization compartment from the Gram-negative Proteobacterium *C. freundii* is a well-studied BMC and will be used for the expression in the Gram-positive Actinobacterium *C. glutamicum*.

ii. To further direct the work towards an application of heterologously produced BMC shells, new strategies for the encapsulation of relevant pathway enzymes into compartments should be developed. The respective heterologous enzymes need to be targeted with encapsulation peptides, however, the addition of those targeting peptides often influences the enzyme activity, as it is known from literature. In order to identify the optimal tag for the particular protein of interest, it would be of great advantage to have a toolbox of different N- and C-terminal encapsulation peptides. As a proof-of-principle, the incorporation of fluorescent proteins into the BMCs with different N- and C-terminal targeting approaches is aimed.

iii. In *E. coli*, it was demonstrated that the overexpression of *pduA*, encoding a major shell protein, leads to nanotube-like structures. In this work, the aim is to establish PduA filaments in *C. glutamicum* as protein scaffolds for the localization of key metabolic pathway enzymes.

iv. To evaluate the potential of BMC shells and Pdu scaffolds in *C. glutamicum* for the production or utilization of small molecules, the strategies developed in (i), (ii) and (iii) will be applied for three metabolic pathways with significant potential: The methanol consumption and ethanol production pathway both include toxic aldehyde intermediates and could therefore profit from the implementation into the BMCs. The bottleneck of the itaconate production pathway established in *C. glutamicum* is the limited cis-aconitate availability due to alternate metabolic routes. Therefore, the performance of the two-enzyme pathway within the BMCs shall be determined.

2 MATERIAL AND METHODS

2.1 Materials, equipment and chemicals

All materials, laboratory equipment and chemicals which cannot be considered as standard technical equipment and specific chemicals are stated within the corresponding subsection of this methods part.

2.2 Media and antibiotics

The composition and preparation of required cultivation media and agar plates are given in the tables below (Table 2 and Table 3).

Table 2: Composition and preparation of different media. For agar plates, 18 g L^{-1} agar were added to the medium before autoclaving. Antibiotics were added to the final amounts as stated in Table 3.

	Component	Amount
LB medium (Sambrook and Russell, 2001)	NaCl	10 g
	Yeast extract	5 g
	Tryptone	10 g
	Add ddH_2O to 1 L and autoclave medium.	
BHI medium (Difco Laboratories, Detroit, MI, USA)	Brain Heart Infusion	37 g
	Add ddH_2O to 1 L and autoclave medium.	
BHI-S medium	Brain Heart Infusion	37 g
	Sorbitol	91 g
	Add ddH_2O to 1 L and autoclave medium.	
CGXII basis solution	$(NH_4)_2SO_4$	20 g
	Urea	5 g
	KH_2PO_4	1 g
	K_2HPO_4	1 g
	$MgSO_4$ x 7 H_2O	0.25 g
	MOPS	42 g
	Add ddH_2O to 800 mL and adjust to pH 7 with NaOH pellets, fill up to 960 mL and autoclave medium.	
Trace element solution	$FeSO_4$ x 7 H_2O	1 g
	$MnSO_4$ x H_2O	1 g
	$ZnSO_4$ x 7 H_2O	0.1 g
	$CuSO_4$	0.02 g
	$NiCl_2$ x 6 H_2O	0.002 g
	Adjust to pH 1 with conc. HCl and add ddH_2O to 100 mL. Pass solution through a sterilizing filter with 0.22 µm pore size.	
$CaCl_2$ solution	$CaCl_2$	1 g
	Add ddH_2O to 100 mL and pass solution through a sterilizing filter.	
Protocatechuic acid solution	Protocatechuic acid	0.3 g
	To dissolve add 3 mL 1 N NaOH and fill up to 10 mL with ddH_2O. Pass solution through a sterilizing filter with 0.22 µm pore size.	
50% glucose	Glucose monohydrate	55 g
	Add ddH_2O to 100 mL and autoclave.	

	Component	Amount
CGXII medium (2% glucose) (Keilhauer *et al.*, 1993)	CGXII basis solution	960 mL
	Trace element solution	1 mL
	$CaCl_2$ solution	1 mL
	Protocatechuic acid solution	1 mL
	50% glucose (w/v)	40 mL
Nitrogen-limited CGXII medium (Otten *et al.*, 2015)	Prepare as CGXII medium (2% glucose) with the following changes:	
	$(NH_4)_2SO_4$	-
	Urea	1 g

Table 3: Preparation of antibiotic stock solutions and used antibiotic concentrations.

Component	Stock solution	Final concentration	
		E. coli	*C. glutamicum*
Kanamycin	50 mg mL^{-1} in ddH_2O	50 µg mL^{-1}	25 µg mL^{-1}
Tetracycline	12.5 mg mL^{-1} in EtOH (70%)	12.5 µg mL^{-1}	5 µg mL^{-1}
Chloramphenicol	34 mg mL^{-1} in EtOH (70%)	34 µg mL^{-1}	10 µg mL^{-1}

2.3 Bacterial strains, plasmids and primers

Bacterial strains and derived mutants used in this work are listed in Table 4. All used plasmids are listed in Table 5-Table 9.

Table 4: Bacterial strains used in this work. *The *pdu* genes marked in lower case have a modified start codon.

Strain	Genotype	Reference
E. coli		
DH5α	F⁻ *endA1* Φ80d*lacZ*ΔM15 Δ(*lacZYA-argF*)U169 *recA1 relA1 hsdR17*($r_K^-m_K^+$) *deoR supE44 thi-1 gyrA96 phoA* λ^-; strain used for general cloning procedures	(Hanahan, 1983)
C. glutamicum		
MB001	Type strain ATCC13032 with deletion of prophages CGP1 (cg1507-cg1524), CGP2 (cg1746-cg1752), and CGP3 (cg1890-cg2071)	(Baumgart *et al.*, 2013)
MB001(DE3)	MB001 derivative with chromosomally encoded T7 gene *1* (cg1122-P_{lacI}-*lacI* P_{lacUV5} –*lacZ*α-T7 gene *1*-cg1121)	(Kortmann *et al.*, 2015)
MB001(DE3)::*icd*(A1T)	MB001(DE3) derivative with exchange of the start codon ATG to TTG in the *icd* gene (cg0766)	This work
MB001(DE3)::*icd*(A1G)	MB001(DE3) derivative with exchange of the start codon ATG to GTG in the *icd* gene (cg0766)	This work
MB001(DE3)::*D18$_{ATG}$acn*	MB001(DE3) derivative with D18 targeting peptide tagged of *acn* gene (Cg1737)	This work
MB001(DE3)::*D18$_{GTG}$acn*	MB001(DE3) derivative with D18 targeting peptide tagged of *acn* gene (Cg1737)	This work
MB001(DE3)::*icd*(A1G):: P_{T7}*pduA*	MB001(DE3)::*icd*(A1G) derivative with *pduA* from *C. freundii* under control of P_{T7} in the CGP1 region	This work
MB001(DE3)::*icd*(A1G):: P_{T7}*pduABJknt**	MB001(DE3)::*icd*(A1G) derivative with *pduABJknt* from *C. freundii* under control of P_{T7} in the CGP1 region	This work
MB001(DE3):: P_{T7}*pduABJKNUT*	MB001(DE3) derivative with *pduABJKNUT* from *C. freundii* under control of P_{T7} in the CGP1 region	This work
MB001(DE3):: P_{T7}*pduA*	MB001(DE3) derivative with *pduA* from *C. freundii* under control of P_{T7} in the CGP1 region	This work
MB001(DE3):: P_{T7}*pduABJknt**	MB001(DE3) derivative with *pduABJknt* from *C. freundii* under control of P_{T7} in the CGP1 region	This work

Table 5: Summary of empty plasmids used in this work.

Plasmid	Relevant characteristics	Reference
pAN6	Kan^R; *C. glutamicum*/*E. coli* shuttle plasmid for regulated gene expression using P_{tac} (P_{tac} *lacI*^{q} pBL1 *ori*V_{Cg} pUC18 *ori*V_{Ec})	(Frunzke *et al.*, 2008)
pEC-P_{tetR}	Cm^R; *C. glutamicum*/*E. coli* shuttle plasmid for regulated gene expression using P_{tetR}(pGA1 *ori*V_{Cg}, *ori*V_{Ec})	This work
pEC-XC99E	Cm^R; *C. glutamicum*/*E. coli* shuttle plasmid for regulated gene expression using P_{trc}(P_{trc} *lacI*^{q} pGA1 *ori*V_{Cg}, *ori*V_{Ec})	(Kirchner and Tauch, 2003)
pEKEx2	Kan^R; *C. glutamicum*/*E. coli* shuttle vector for regulated gene expression using P_{tac} (P_{tac} *lacI*^{q} pBL1 *ori*V_{Cg} pUC18 *ori*V_{Ec})	(Eikmanns *et al.*, 1991)
pMKEx1	Kan^R; *E. coli*/*C. glutamicum* shuttle vector based on pJC1 for expression of target genes under control of the T7 promoter (P*lacI*, *lacI*, PT7, *lacO1*, N-term. Strep-tagII, MCS, C-term. His-tag, pHM1519 *oriCg*; pACYC177 *oriEc*)	(Kortmann *et al.*, 2015)

Plasmid	Relevant characteristics	Reference
pVWEx2	Tet^R; *C. glutamicum*/ *E. coli* shuttle vector for regulated gene expression; (Ptac, *lacIQ*, pCG1 *oriVC.g.*, pUC18 *oriV E.c.*)	(Peters-Wendisch *et al.*, 2001)

Table 6: Plasmids for the production of Pdu compartment proteins from *C. freundii*. * The *pdu* genes marked in lower case have a modified start codon.

Plasmid	Relevant characteristics	Reference
pET3a_*pduABJKNUT*	Amp^R; overexpression vector with T7 promoter for expression of seven shell genes	(Parsons *et al.*, 2010)
pET14b-pdu65	Amp^R; cloning vector containing *pduA, pduB, pduC, pduD, pduE, pduG, pduH, pduJ, pduK, pduL, pduM, pduN, pduO, pduP, pduQ, pduS, pduT, pduX*	(Parsons *et al.*, 2008)
pAN6_*pduA-X*	Kan^R; P_{tac}; overexpression vector for production of all pdu genes (as present on pET14b-pdu65)	This work
pMKEx1_*pduABJKNUT*	Kan^R; P_{T7}; overexpression vector for production of all pdu shell genes	This work
pMKEx1_ *mcherryPduABJKNUT*	Kan^R; P_{T7}; overexpression vector for production of mCherryPduABJKNUT	This work
pMKEx1_*pduA*	Kan^R; P_{T7}; overexpression vector for production of PduA	This work
pMKEx1_*mcherrypduA*	Kan^R; P_{T7}; overexpression vector for production of mCherryPduA	This work
pMKEx1_ $pduABJKNTU_{native}$	Kan^R; P_{T7}; overexpression vector for expression of the native PduABJKNTU operon	This work
pMKEx1_*pduABJKN*	Kan^R; P_{T7}; overexpression vector for production of PduABJKN	This work
pMKEx1_*pduABJKNU*	Kan^R; P_{T7}; overexpression vector for production of PduABJKNU	This work
pMKEx1_*pduABJkN**	Kan^R; P_{T7}; overexpression vector for production of PduABJkN	This work
pMKEx1_*pduABJkNu**	Kan^R; P_{T7}; overexpression vector for production of PduABJkNu	This work
pMKEx1_*pduABJkNut**	Kan^R; P_{T7}; overexpression vector for production of PduABJkNut	This work
pMKEx1_*pduABJkn**	Kan^R; P_{T7}; overexpression vector for production of PduABJkn	This work
pMKEx1_*pduABJknt**	Kan^R; P_{T7}; overexpression vector for production of PduABJknt	This work
pMKEx1_*pduABJkNt**	Kan^R; P_{T7}; overexpression vector for production of PduABJkNt	This work
pMKEx1_*pduABJkn**	Kan^R; P_{T7}; overexpression vector for production of PduABJkn	This work
pMKEx1_*pduJ*	Kan^R; P_{T7}; overexpression vector for production of PduJ	This work
pMKEx1_*pduABJK*	Kan^R; P_{T7}; overexpression vector for production of PduABJK	This work
pMKEx1_*pduABJKn**	Kan^R; P_{T7}; overexpression vector for production of PduABJKn	This work
pMKEx1_*pduBJKN*	Kan^R; P_{T7}; overexpression vector for production of PduBJKN	This work
pMKEx1_*pduABJKnut**	Kan^R; P_{T7}; overexpression vector for production of pduABJKnut	This work
pMKEx1_*pduABJKnt**	Kan^R; P_{T7}; overexpression vector for production of PduABJKnt	This work

Plasmid	Relevant characteristics	Reference
pMKEx1_*pduA*$_{PDZlig}$	Kan^R; P_{T7}; overexpression vector for production of PduA C-terminally tagged with PDZligand (GGCGTGAAGGAATCCCTGGTG); Linker: GGATCTGGTTCCGGCTCCGGTTCCGGC [$(GS)_4G$]	This work
pMKEx1_*pduA*$_{SH3lig}$	Kan^R; P_{T7}; overexpression vector for production of PduA C-terminally tagged withSH3ligand (CCACCACCAGCACTGCCACCAAAGCGCCGCCGC); Linker: [$(GS)_4G$]	This work
pMKEx1_*pduA*$_{GBDlig}$	Kan^R; P_{T7}; overexpression vector for production of PduA C-terminally tagged with GBDligand (Sequence S1); Linker: [$(GS)_4G$]	This work
pMKEx1_*pduA*$_{PDZlig}$*BJknt**	Kan^R; P_{T7}; overexpression vector for production of PduABJknt with PduA C-terminally tagged with PDZligand	This work
pMKEx1_*pduA*$_{SH3lig}$*BJknt**	Kan^R; P_{T7}; overexpression vector for production of pduABJknt with PduA C-terminally tagged with SH3ligand	This work
pMKEx1_*pduA*$_{GBDlig}$*BJknt**	Kan^R; P_{T7}; overexpression vector for production of PduABJknt with PduA C-terminally tagged with GBDligand	This work

Table 7: Plasmids for genomic integrations in *C. glutamicum*.

Plasmid	Relevant characteristics	Reference
pK19*mobSacB*	Kan^R; vector for allelic exchange in *C. glutamicum* (oriT oriV_{Ec} *sacB lacZ*α)	*(Schäfer et al., 1994)*
pK19_*D18*$_{GTG}$*acn*	Kan^R; pK19*mobSacB* derivative for allelic exchange of the start codon ATG to GTG of acn gene (Cg1737) and targeting with D18 peptide	This work
pK19_*D18*$_{ATG}$*acn*	Kan^R; pK19*mobSacB* derivative for allelic exchange of the start codon GTG to GTG of acn gene (Cg1737) and targeting with D18 peptide	This work
pK19_*icd*(A1G)	Kan^R; pK19*mobSacB* derivative for allelic exchange of the start codon ATG to GTG in the *icd* gene (cg0766)	(Otten *et al.*, 2015)
pK19_*icd*(A1T)	Kan^R; pK19*mobSacB* derivative for allelic exchange of the start codon ATG to TTG in the *icd* gene (cg0766)	(Otten *et al.*, 2015)
pK19_CGP1int_P_{T7}*eyfp*	Kan^R; pK19*mobSacB* derivative for allelic integration of *eyfp* under control of P_{T7} into CGP1 region	Meike Baumgart
pK19_P_{T7}*pduABJKNUT*	Kan^R; Derivative of pK19-CGP1int_P_{T7}-*eYFP*, *eYFP* was exchanged with *pduABJKNUT*	This work
pK19_P_{T7}*mcherryPduABJKNUT*	Kan^R; Derivative of pK19-CGP1int_P_{T7}-*eYFP*, *eYFP* was exchanged with mcherry*pduABJKNUT*	This work
pK19_P_{T7}*pduA*	Kan^R; Derivative of pK19-CGP1int_P_{T7}-*eYFP*, *eYFP* was exchanged with *pduA*	This work

Table 8: Plasmids based on pEC-P_{tetR} used in this work.

Plasmid	Relevant characteristics	Reference
pEC-XC99E	Cm^R; *C. glutamicum*/*E. coli* shuttle plasmid for regulated gene expression using P_{trc} (P_{trc} *lacI*^{q} pGA1 *ori*V_{Cg}, *ori*V_{Ec})	(Kirchner and Tauch, 2003)

pEC-P_{tetR}	Cm^R; *C. glutamicum*/*E. coli* shuttle plasmid for regulated gene expression using P_{tetR} (pGA1 $oriV_{Cg}$, $oriV_{Ec}$), based on pEC-XC99E	This work
pEC_*eyfp*	Cm^R; derivative of pEC-P_{TetR}; regulated expression of *eyfp*	This work
pEC_*P18eyfp*	Cm^R; derivative of pEC_$P_{tetR;}$ regulated expression of *eyfp* tagged with P18 targeting peptide (ATGAACACTTCAGAACTTGAAACCCTTATTCG TAACATTTTGAGTGAGCAACTT); Linker: AGATCT [BglII]	This work
pEC_*P18eyfp*$_{ASV}$	Cm^R; derivative of pEC_P_{tetR}; regulated expression of *eyfp* tagged with P18 targeting peptide and ASV degradation peptide, linker: [BglII]; ASV tag (GCAGCAGAAAAGAGCCAACGTGATTACGCTGCATCAGTT)	This work
pEC_*P18eyfp*$_{AAV}$	Cm^R; P_{tetR}; regulated expression of *eyfp* tagged with P18 targeting peptide and aav degradation peptide; linker: [BglII]; AAV tag (GCAGCAGAAAAGAGCCAACGTGATTACGCAGCAGCTGTT	This work
pEC_*D18eyfp*	Cm^R; derivative of pEC_P_{tetR}; regulated expression of *eyfp* tagged with D18 targeting peptide (ATGGAAATCAATGAAAAGCTGCTGCGCCAGATTATTGAAGACG TACTGTCTGAA); linker: [BglII]	This work
pEC_*D18eyfp*$_{ASV}$	Cm^R; P_{tetR}; regulated expression of *eyfp* tagged with D18 targeting peptide and ASV degradation peptide; Linker: [BglII]	This work
pEC_*D18eyfp*$_{AAV}$	Cm^R; P_{tetR}; regulated expression of *eyfp* tagged with D18 targeting peptide and AAV degradation peptide; linker: [BglII];	This work
pEC_*D18eyfp-P18cfp*	Cm^R; P_{tetR}; regulated expression of *eyfp* tagged with D18 targeting peptide and *cfp* tagged with P18 targeting peptide; Linker: AGATCT [BglII]	This work
pEC_*eyfp-PDZ*$_{dom}$	Cm^R; P_{tetR}; regulated expression of *eyfp* tagged with C-terminal *PDZdomain* (Sequence S1); Linker: GGATCTGGTTCCGGCTCCGGTTCCGGC [$(GS)_4G$]	This work
pEC_*eyfp-SH3*$_{dom}$	Cm^R; P_{tetR}; regulated expression of *eyfp* tagged with C-terminal *SH3domain* (Appendix Sequence S1); Linker: [$(GS)_4G$]	This work
pEC_*eyfp-GBD*$_{dom}$	Cm^R; P_{tetR}; regulated expression of *eyfp* tagged with C-terminal *GBDdomain* (Appendix Sequence S1); Linker: [$(GS)_4G$]	This work
pEC_*eYFP-C17*$_{K.p}$	Cm^R; P_{tetR}; regulated expression of *eyfp* tagged with C-terminal targeting peptide from *K. pneumonia* (AACGAACAGAACGTGGA ACGCGTGATCCGCCAGGTGCTGGAACGCCTGGCAAAG) Linker: GGCGGTGGCTCCGGCGGCGGTTCCGGCGGT [$(GGGS)_2GG$]	This work
pEC_*eyfp-C17*$_{P.m}$	Cm^R; P_{tetR}; regulated expression of *eyfp* tagged with C-terminal targeting peptide from *P. mirabilis;* Linker: [$(GGGS)_2GG$]; C18 peptide (ACCGAAGAAAACGTGGAACGCATCATCAAGGAAGTGCTGGGC CGCCTGGGCAAG)	This work
pEC_*eyfp-P18*	Cm^R; P_{tetR}; regulated expression of *eyfp* C-terminally tagged with P18 targeting peptide; Linker: [$(GGGS)_2GG$]	This work

Table 9: Plasmids encoding enzymes for the production of different compounds.

Plasmid	Relevant characteristics	Reference
pVWEx2_*Bm(mdh)*	Tet^R; P_{tuf}; expression of methanol dehydrogenase (*mdh*) from *Bacillus methanolicus*	This work
pVWEx2_*Bm(D18mdh*)	Tet^R; P_{tuf}; expression of *mdh* with D18 targeting peptide; Linker: AGATCT [BglII]	This work

Plasmid	Relevant characteristics	Reference
pVWEx2_*Bm(D18mdh _act)*	Tet^R; P_{tuf}; expression of *mdh* with D18 targeting peptide; Linker: [BglII] and Mdh activator protein (Act) from *B. methanolicus*	This work
pVWEx2_*Bm(mdh_act)*	Tet^R; P_{tuf}; expression of *mdh* with D18 targeting peptide; Linker: [BglII] and Mdh activator protein (Act)	(Witthoff *et al.*, 2015)
pEKEx2_*Bs(hps_phi)*	Tet^R; P_{tuf}; pEKEx2 derivative for constitutive expression of 3-hexulose-6-phosphate synthase (Hps) and 6-phosphate-3-hexuloisomerase (Phi) from *B. subtilis*	(Witthoff *et al.*, 2015)
pEKEx2_*Bs*(*D18hps_P18phi*)	Tet^R; P_{tuf}; expression of *hps* with D18 targeting peptide and *phi* with P18 targeting peptide	This work
pEKEx2_*Bs*(*D18hps_phi*)	Tet^R; P_{tuf}; pEKEx2 derivative for expression of *hps* with D18 targeting peptide; Linker: [BglII] and *phi*	This work
pEKEx2_*Bs*(*D18-GS-hps_phi*)	Tet^R; P_{tuf}; pEKEx2 derivative for expression of *hps* with D18 targeting peptide; Linker: GGCTCC [GS] and *phi*	This work
pEKEx2_*Bs*(*D18-GGSG-hps_phi*)	Tet^R; P_{tuf}; pEKEx2 derivative for expression of *hps* with D18 targeting peptide; Linker: GGCGGTTCCGGC [GGSG] and *phi*	This work
pEKEx2_*Bs*(*D18-10aa-hps_phi*)	Tet^R; P_{tuf}; pEKEx2 derivative for expression of *hps* with D18 targeting peptide; Linker: AGGGCTCTGGATCGACATCAGGCTCCGGT [10 aa] and *phi*	This work
pEKEx2-P_{tac}*malEcad*	Kan^R; P_{tac}; pEKEx2 derivative for inducible expression of codon-optimized *cad* from *A. terreus* in fusion with maltose binding protein MalE from *E. coli*	(Otten *et al.*, 2015)
pEKEx2-P_{tac}*P18malEcad*	Kan^R; $P_{tac;}$ expression of codon-optimized *malEcad* fused to N-terminal P18 targeting peptide; Linker: GGCTCC [GS]	This work
pEKEx2-P_{tac}*acn*	Kan^R; P_{tac}; pEKEx2 derivative for inducible expression of aconitase (*acn,* cg1737)	This work
pEKEx2-P_{tac}*D18acn*	Kan^R; P_{tac}; inducible expression of *acn* with N-terminal D18 targeting peptide; Linker: GGCGGTTCCGGC [GGSG]	This work
pVWEx2_*malEcad*	Tet^R; P_{tuf}; pVWEx2 derivative for constitutive expression of codon-optimized *malEcad*	This work
pVWEx2_*P18malEcad*	Tet^R; P_{tuf}; constitutive expression of codon-optimized *P18malEcad,* Linker: [GS]	This work
pVWEx2_*acn_malEcad*	Tet^R; P_{tuf}; constitutive expression of *malEcad* and *acn*	This work
pVWEx2_*D18acn_P18malEcad*	Tet^R; P_{tuf}; constitutive expression of *P18malEcad,* Linker: [GS] and *D18acn,* Linker: [GGSG]	This work
pVWEx2_*adhB*	Tet^R; $P_{tuf;}$ pVWEx2 derivative for constitutive expression of *adhB* (GenBank: AFN57379.1) from *Z. mobilis*	This work
pVWEx2_*D18-GSGS-adhB*	Tet^R; $P_{tuf;}$ *D18adhB* expression; Linker: GGTTCTGGCTCC [GSGS]	This work
pVWEx2_*D18-10aa-adhB*	Tet^R; $P_{tuf;}$ *D18adhB* expression; Linker: AGGGCTCTGGATCGACATCAGGCTCCGGT [10 aa]	This work
pVWEx2_*D60-adhB*	Tet^R; $P_{tuf;}$ *D60adhB* expression; No linker	This work
pVWEx2_*adhB-*GBD_{dom}	Tet^R; $P_{tuf;}$ *adhB-*GBD_{dom} expression; Linker: GGATCTGGTTCCGGCTCCGGTTCCGGC $[(GS)_4G]$	This work
pVWEx2_*adhB-*$SH3_{dom}$	Tet^R; $P_{tuf;}$ *adhB-*$SH3_{dom}$ expression; Linker: $[(GS)_4G]$	This work
pVWEx2_*adhB-*PDZ_{dom}	Tet^R; $P_{tuf;}$ *adhB-*PDZ_{dom} expression; Linker: $[(GS)_4G]$	This work
pVWEx2-*adhB_pdc*	Tet^R; $P_{tuf;}$ *adhB* and *pdc* expression	This work
pVWEx2_*D18-GSGS-*	Tet^R; $P_{tuf;}$ *D18adhB* and *P18pdc* expression; Linker	This work

Plasmid	Relevant characteristics	Reference
adhB_P18pdc	between *D18* and *adhB*: [GSGS]; Linker between *P18* and *pdc*: [NdeI]	
pVWEx2_*D18-10aa-adhB_P18pdc*	Tet^R; P_{tuf}; *D18adhB* and *P18pdc* expression; Linker between *D18* and *adhB*: [10aa]; Linker between *P18* and *pdc*: [NdeI]	This work

2.4 DNA techniques

The plasmids and strains specified in the Tables 4-9 were created applying the methods introduced in the following sections. The detailed Gibson Assembly or cloning procedure of each plasmid can be found in the Appendix Section 6.1.

2.4.1 Isolation of plasmid DNA

The isolation of plasmids from *E. coli* was carried out by alkaline lysis (Birnboim and Doly, 1979) with subsequent clean-up steps and concentration of the plasmid trough a silica matrix. For this purpose, the GeneJet Plasmid Miniprep Kit (Thermo Fisher Scientific, Waltham, USA) was used. For generation of cell material, a single colony was picked and grown overnight in 6 mL LB medium (37 °C, 300 rpm) with appropriate antibiotic and the culture was treated afterwards following manufacturer's protocols. The success of the plasmid isolation was determined by measuring the DNA concentration and a diagnostic digest of the plasmid followed by agarose gel electrophoresis.

2.4.2 DNA concentration measurement

The concentration of nucleic acids in samples was determined photometrically with a NanoDrop™ spectrophotometer (Thermo Fisher Scientific, Waltham, USA) at a wavelength of λ = 260 nm with 1.5 µL of nucleic acid solution per sample. The DNA concentration was calculated automatically by the NanoDrop® ND-1000 software.

2.4.3 Agarose gel electrophoresis

Mini-Sub® cell GT and wide Mini-Sub® cell GT DNA electrophoresis systems (Bio-Rad Laboratories, Hercules, USA) were used with agarose gels containing 1-2% agarose (w/v) in TA buffer (Table 10). The samples were mixed with 6x DNA Gel loading dye (Thermo Fisher Scientific, Waltham, USA) and up to 30 µL of the mixture were loaded into one gel compartment depending on the intended purpose. One of the pockets was filled with GeneRuler™ 1 kb DNA Ladder (Thermo Fisher Scientific). A voltage of 100 V was applied for 35 min for the electrophoretic separation of the DNA fragments. The gel was stained for 10 min in ethidium bromide solution. For visualization of the DNA bands, the gel was illuminated with UV-light using the BioDoc Analyzer (Biometra, Göttingen, Germany) and digitalized with a CCD camera.

Table 10: Composition and preparation of TA buffer.

	Component	Amount
50x TA buffer	Tris	242 g
	Glacial acetic acid	57.1 mL
	Add ddH_2O to a volume of 1 L.	
TA buffer	Use 20 mL 50x TA buffer and add 980 mL ddH_2O.	

2.4.4 Polymerase chain reaction

For amplification of DNA fragments for Gibson Assembly or to gain DNA fragments with the required restriction enzyme target sites, Q5® High-Fidelity 2X Master Mix (New England Biolabs, Frankfurt, Germany) was used. The confirmation of positive clones was performed with DreamTaq Green PCR Master Mix (2X) (Thermo Fisher Scientific, Waltham, USA). Both master mixes were used according to manufacturer's instructions and with appropriate primers. After the PCR reaction, the success of the amplification was confirmed by agarose gel electrophoresis. Successfully amplified DNA fragments for sequencing, cloning or Gibson Assembly were extracted applying the NucleoSpin Gel and PCR Clean-up (Macherey-Nagel, Düren, Germany) following manufacturer's instructions and stored at -20 ˚C until use.

2.4.5 Restriction enzyme digests

Depending on purpose, different protocols and volumes for enzyme digest reactions were used (Table 11). Digested plasmids as well as PCR products were purified with agarose gel extraction and the NucleoSpin Gel and PCR Clean-up Kit (Macherey-Nagel, Düren, Germany) following manufacturer's instructions.

Table 11: Different compositions of DNA digest reactions.

	Diagnostic digest	Plasmid cloning digest	Digest of PCR products
10x FastDigest buffer	1 µL	4 µL	2 µL
Fast digest enzyme 1	0.5 µL	2 µL	1 µL
Fast digest enzyme 2	0.5 µL	2 µL	1 µL
Plasmid	2 µL	2-4 ng	~ 100 µg
	Total volume: 10 µL Incubation for 20 min	Total volume: 40 µL Incubation for 1 h	Total volume: 20 µL Incubation for 1 h

2.4.6 Cloning of plasmid vectors

For traditional cloning approaches, a suitable plasmid backbone was digested and purified as stated in Section 2.4.5. The inserts for ligations into the plasmid backbone were either amplified by PCR with appropriate restriction site containing overhangs

or extracted from agarose gels after digestion out of existing plasmids (Section 2.4.3 and Section 2.4.5). To reduce recircularization of digested plasmid backbones, the 5'-termini were dephosphorylated with the shrimp alkaline phosphatase for 45 min at 37 °C (2 µL 10x APase buffer, 1 µl APase, 17 µL digested plasmid backbone). 50 ng plasmid backbone and insert (3x higher molarity than plasmid backbone) were ligated afterwards at 22 °C for 30 min using rapid ligase according to manufacturer's protocol (New England Biolabs, Frankfurt, Germany). Approximately 2.5 µL of the ligation mixture was used for the transformation in *E. coli* DH5α cells (Section 2.5.2).

2.4.7 Gibson Assembly

The Gibson Assembly was performed as described previously (Gibson *et al.*, 2009). The primers were designed with 15-20 base pair overlaps to the intended joining regions. To generate the sequences with the complementary overlaps, PCR using the Q5® High-Fidelity 2X Master Mix (New England Biolabs, Frankfurt, Germany) was conducted and DNA fragments were purified with NucleoSpin Gel and PCR Clean-up Kit (Macherey-Nagel, Düren, Germany) following manufacturer's instructions.

Table 12: Reaction mix composition of Gibson Assembly master mix. NEB, New England Biolabs;

	Components	Volume/amount
Assembly mixture	5x isothermal reaction buffer	320 µL
	10 U mL^{-1} T5 exonuclease (NEB)	0.64 µL
	2 U mL^{-1} Phusion HF DNA polymerase (NEB)	20 µL
	40 U mL^{-1} *Taq* DNA ligase (NEB)	160 µL
	Add ddH_2O to a volume of 1.2 mL and aliquot the solution to 15 µL. Store the mixture at -20 °C.	
5x isothermal reaction buffer	1 M Tris-HCl (pH 7.5)	3 mL
	2 M $MgCl_2$	150 µL
	100 mM dGTP	60 µL
	100 mM dATP	60 µL
	100 mM dTTP	60 µL
	100 mM dCTP	60 µL
	1 M DTT	300 µL
	PEG-8000	1.5 g
	100 mM NAD	300 µL
	Add precooled ddH_2O to a volume of 6 mL and store the aliquots at -20 °C.	

15 µL Gibson Assembly mixture (Table 12) and 5 µL of purified DNA fragments (50 ng of each fragment) were incubated at 50 °C for 60 min. Afterwards, 5 µL of the mixture were transformed into *E. coli* DH5α competent cells (Section 2.5.2) followed by plating on LB selection plates.

2.4.8 Control of correct plasmid assembly

Positive clones from the transformation of ligation reactions or Gibson Assembly were verified through Colony PCR. Positive clones were cultivated and the plasmids were isolated. As an additional control, restriction enzyme digests with the isolated plasmids were performed and plasmids with the correct digestion pattern were sent for sequencing.

2.4.9 Sequencing

Sequencing was performed at Eurofins MWG Operon (Ebersfeld, Germany) using premixed samples. Samples were prepared according to company guidelines with 15 µL plasmid template (~50 ng μL^{-1}) or 15 µL PCR product (10-30 ng μL^{-1}) and 2 µL primers (10 µM).

2.5 Bacterial strains and growth conditions

2.5.1 Generation of *E. coli* calcium chloride competent cells

The protocol for the generation of calcium chloride competent cells was performed after the protocol published from Hanahan (Hanahan, 1983).

2.5.2 Transformation of calcium chloride competent *E. coli* DH5α cells

The transformation of competent cells was performed using the protocol "NEB 10-beta Competent *E. coli* (High Efficiency) (C3019I)" (New England Biolabs, Frankfurt, Germany). Therefore, 4 ng plasmid, 2 µL ligation reaction or 5 µL Gibson Assembly were added to 50 µL calcium chloride competent *E. coli* cells before transformation. After the heat shock, 900 µL SOC medium (Table 3.20) were added and the cells were incubated at 37 ˚C for one hour. If the cells were transformed with Gibson Assembly or ligation reaction, they were centrifuged for 2 min at 1,000 *g* and the supernatant was decanted. The remaining medium was used to solubilize the pellet and the cells were plated on LB agar plates with antibiotics. For transformation of plasmids, 50 µL cells were plated.

Table 13: Composition and preparation of SOC medium.

	Component	Volume/amount
SOC basis solution	Tryptone	20 g
	Yeast extract	5 g
	NaCl	0.5 g
	KCl	0.19 g
	Add ddH_2O to a volume of 1 L, set pH to 7 with NaOH and autoclave.	
SOC medium	SOC basis solution	100 mL
	50% glucose (w/v) (sterile)	0.72 mL
	1 M $MgCl_2$ (sterile)	1 mL

2.5.3 Glycerin cultures for maintenance of *E. coli* transformants

For long term storage of assembled plasmids, 400 µL of a transformant over night *E. coli* culture were mixed with 600 µL of 50% glycerol (w/v) in 2 mL tubes with screw plastic vials. Immediately after mixing, vials were snap frozen in liquid nitrogen and stored at -80 °C.

2.5.4 Generation of *C. glutamicum* competent cells

To generate *C. glutamicum* competent cells, an adapted protocol was used (van der Rest *et al.*, 1999). All steps were carried out ensuring sterile conditions. A *C. glutamicum*

strain was streaked out on a BHI media plate with appropriate antibiotics and incubated overnight at 30 °C. One single colony was used to inoculate 4 mL BHI-S and cultivated for 16 h at 170 rpm and 30 °C in a rotary shaker. 50 mL BHI-S were inoculated with 1 mL pre-culture in a 500 mL Erlenmeyer flask. Cultivation was performed at 30 °C and 120 rpm until an OD_{600} of 0.6. After the addition of 15 µL ampicillin (5 mg mL^{-1} stock) and 2 mL isoniazid (0.1 g mL^{-1} stock, pass through sterilizing filter), cultivation was continued for 1 h. Cells were harvested by centrifugation at 4000 rpm for 7 min at 4 °C and taken up in 30 mL EPB1 buffer. After two washing steps with 30 mL EBP1 buffer, the cells were taken up in 750 µL EPB2 buffer and aliquots of 100 µL were prepared in precooled 1.5 ml Eppendorf tubes. The aliquots were frozen in liquid nitrogen and stored at -80 °C.

Table 14: Buffers for the preparation of competent *C. glutamicum* cells.

	Component	Volume/amount
EPB1 buffer	HEPES (0.5 M)	20 ml
	Glycerin (87%)	28.74 ml
	Addition ddH_2O up to 500 ml and autoclave.	
EPB2 buffer	HEPES (0.5 M)	2 mL
	Glycerin (87%)	34.48 mL
	Addition of ddH_2O up to 200 ml and autoclave.	
HEPES 0.5 M (pH 7.2)	HEPES	5.96 g
	Adjust pH with NaOH and add to 50 ml with ddH_2O.	

2.5.5 Transformation of *C. glutamicum via* electroporation

The transformation of *C. glutamicum* was done exactly as described previously (Eggeling and Bott, 2005). For the transformation of single plasmids, 500 ng of plasmid DNA were added. For the cotransformation of two plasmids at the same time, up to 1 µg of each plasmid were used, not exceeding a total volume of 10 µL. For transformation of two plasmids or pK19*mobsacB* derivatives, the BHI-S culture was centrifuged for 5 min at 4000 rpm and all cells were plated on appropriate BHI-S selection agar. For single plasmid transformations, 100 µL of cell suspension were plated.

2.5.6 Glycerin cultures for long term storage of *C. glutamicum* strains

For long term storage of *C. glutamicum* chromosomal mutants, wild types and plasmid-containing strains, 400 µL of a *C. glutamicum* over night culture were mixed with 600 µL of 50% glycerol (w/v) in 2 mL screw plastic vials. Immediately after mixing, vials were snap frozen in liquid nitrogen and stored at -80 °C.

2.5.7 Construction of chromosomal integrations and exchanges

Integrations into the *C. glutamicum* genome were performed with pK19*mobsacB* integration plasmids, which contained 500 bps of the integration sites flanking the sequences of interest. The plasmids used in this work are listed in Table 7. After transformation of the plasmids, the protocol was performed as previously described (Niebisch and Bott, 2001). To test the success of the two homologous recombinations, kanamycin sensitive and sucrose-resistant clones were tested with Colony PCR on and sequencing of the region of interest. Strains containing the wanted modification were stored as glycerin cultures.

2.5.8 Preculture handling for C. *glutamicum*

Single colonies of *C. glutamicum* strains, either obtained through previous transformation or streaked out the day before from glycerin culture, were used to inoculate 4-5 mL liquid BHI with appropriate antibiotics. The cultures were cultivated at 30 °C and 170 rpm for about 8 h using a rotary shaker. Depending on purpose, up to 20 mL of CGXII supplemented with 2% (w/v) glucose medium were inoculated with BHI preculture to an OD_{600} of 1 and further cultivated until used for inoculation of a main culture.

2.5.9 Cultivation for ethanol production

The preculture handling was performed as described before. The main culture, 50 mL CGXII supplemented with 4% (w/v) glucose and 50 µM IPTG, was inoculated to an OD_{600} of 1 and cultivated in a 100 mL conical shaking flask at 30 °C and 130 rpm. After 24 h, 30 h, 48 h and 60 h, 1 mL culture samples were taken and HPLC analysis was performed to determine ethanol concentration as described in Section 2.6.6.

2.5.10 Cultivation in a microbioreactor system (BioLector)

For high throughput growth experiments, microscale cultivations were performed in 48 parallel cultivations in 48-well Flowerplates™ incubated in a BioLector® (Microbioreactor for high-throughput fermentations, m2p-labs GmbH, Baesweiler, Germany). Precultures were prepared as stated in Section 2.5.8 in biological triplicates. The cultivation volume of the CGXII preculture was 4 mL. After a washing step with CGXII basis solution, the OD_{600} of the cultures was determined and 1 mL of fresh medium was inoculated to an OD_{600} of 1. 750 µL of each sample were transferred to the 48 well plate, which was sealed with a gas permeable membrane to minimize evaporation. If not stated otherwise, following cultivation conditions were set: orbital shaker with a shaking diameter of 3 mm

and a shaking frequency of 1200 rpm, 30 °C, a relative humidity of 80%, and measurement of the backscatter signal with a gain of 5, 10 and 20 every 15 min.
To determine the growth rates, first, the values were baseline-corrected by the average of the backscatter values 2-4. Then, the values were transformed to logarithmic scale. The growth rate was calculated by determining the linear regression within the exponential phase (values for at least 4 h).

2.6 Protein biochemical methods

2.6.1 Cell lysis methods

Glass-bead homogenization

The cells lysis of *C. glutamicum* cells for subsequent enzymatic assays with culture lysate was performed with a Precellys® 24 homogenizer (Bertin instruments, Montigny-le-Bretonneux, France). Up to 25 mL cultures were solubilized in 1 mL appropriate buffer and transferred in 2 mL screw cap tubes containing 250 mg glass beads with a diameter of 0.1 mm. The cell lysis was done by 3x 20 sec intervals at 6000 rpm in the Precellys® 24 homogenizer with 2 min cooling on ice in between. The crude extract was obtained by separating cell debris with two centrifugation steps at 12,000 *g* for 15 min at 4 °C.

Cell lysis with French Press

For compartment purification approaches, *C. glutamicum* cells were lysed using the HTU DIGI-F-Press (Model F-013G, G. Heinemann Ultraschall- und Labortechnik, Schwäbisch Gmünd, Germany). Cell pellets were solubilized in respective buffer solution containing cOmplete™, Mini, EDTA-free Protease Inhibitor Cocktail tablets (Roche Diagnostics, Mannheim, Germany). The cells were disrupted by 5-6 passages through the French pressure cell with a lysis pressure of 15,000 psi. In between the lysis steps, cells were cooled on ice.

Cell lysis with ultrasonic cell homogenizer

Sonication was performed either following a French Pressure treatment or without former cell lysis steps. In rosette cooling cells, the cells were disrupted by sonication (Intensity: 8, duty cycle: 50%, 1 min disruption and 30 sec cooling intervals) with a Branson Sonifier 250 (G. Heinemann Ultraschall- und Labortechnik, Schwäbisch Gmünd, Germany).

2.6.2 Enzymatic assays

Enzyme assays for the methanol degradation pathway enzymes

Strains were cultivated in 50 ml CGXII defined medium with 1% glucose and 120 mM methanol at 30 °C and 120 rpm in shake flasks and harvested at OD_{600} = 5 or after 12 h of cultivation (4,500 *g*, 15 min, 4 °C). Cells were washed with 100 mM glycine-KOH buffer (pH 9.4) for the methanol dehydrogenase assay and 50 mM potassium phosphate buffer (pH 7.6) containing 1 mM DTT and 3 mM $MgCl_2$ for the coupled Hps-Phi assay and solubilized in 350 µl and 500 µl buffer respectively. The cells were mechanically

lysed as described in Section 2.6.1 with glass beads. Both assays were carried out in an a volume of 200 µL at 30 °C within an Infinite® 200 PRO microplate reader (Tecan Group AG, Männedorf, Switzerland).

Table 15: Methanol dehydrogenase (Mdh) assay mixture.

	Component	Volume	Final concentration
Mdh assay mixture	1 M glycine-KOH buffer (pH 9.4)	20 µL	100 mM
	50 mM $MgSO_4$	20 µL	5 mM
	10 mM DTT	20 µL	1 mM
	10 mM NAD^+	20 µL	1 mM
	ddH_2O	80 µL	-
	cell extract (different dilutions)	40 µL	-
	5 M methanol	20 µL	500 mM

The methanol dehydrogenase activity was measured *via* the reduction of NAD^+ to NADH at a wavelength of 340 nm and was performed as described before (Hektor *et al.*, 2002; Witthoff *et al.*, 2015). The reaction was initiated with the addition of methanol with the injection system to a final concentration of 500 mM into the premixed assay mixture (Table 15). The increase of absorbance with the production of NADH was followed for 15 min. One unit (U) of Mdh activity was defined as the reduction of 1 µmol NAD^+ to NADH per minute. Specific activity refers to the activity per mg protein in the crude extract. Protein amount in the extracts were quantified with the Pierce™ BCA Protein Assay Kit (Thermo Fisher Scientific, Waltham, USA) and BSA as protein standard.

The coupled Hps and Phi activity was measured *via* the reduction of $NADP^+$ to NADPH (Figure 7) as described before (Arfman *et al.*, 1990; Witthoff *et al.*, 2015). The reaction mixture (Table 16) was equilibrated for 5 min at 30 °C and the reaction was initiated with the addition of formaldehyde to a final concentration of 5 mM with the injection system of the microplate reader. 1 U of coupled Hps/Phi activity was defined as the reduction of 1 µmol $NADP^+$ to NADPH per minute.

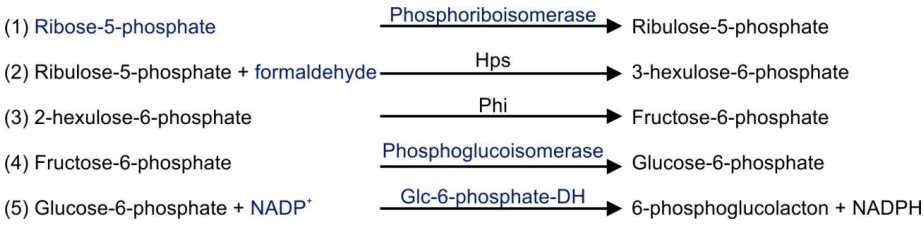

Figure 7: Assay for coupled measurement of *in vitro* enzyme activities of Hps and Phi. The absorbance at 340 nm was measured after the addition of $NADP^+$ for determination of NADPH production. The reagents marked in blue were added to the assay mixture. Figure and assay were adapted from Sabrina Witthoff (Witthoff *et al.*, 2015).

Specific activity refers to the activity per mg protein in the crude extract. The protein amounts in the extracts were quantified with the Pierce™ BCA Protein Assay Kit (Thermo Fisher Scientific, Waltham, USA) and BSA as protein standard.

Table 16: Coupled Hps/Phi activity assay mixture. The enzymes for the reaction were applied as followed: Phosphoglucoisomerase (PGI) from yeast (Roche Diagnostics Deutschland GmbH, Mannheim, Germany); Glc-6-phosphate (G6PDH) from yeast (grade II, Roche Diagnostics Deutschland GmbH, Mannheim, Germany); Phosphoriboisomerase (PRI) from spinach (Type I, partially purified powder, Sigma-Aldrich, St. Louis, MO, USA); PP buffer, potassium phosphate buffer;

	Component	Volume	Final concentration
Coupled Hps-Phi activity assay mixture	Cell extract (different dilutions)	40 µL	-
	500 mM potassium phosphate buffer, pH 7.6	14 µL	50 mM
	50 mM $MgCl_2$	20 µL	5 mM
	50 mM ribose-5-phosphate in 50 mM PP buffer	20 µL	5 mM
	25 mM $NADP^+$ in 50 mM PP buffer	20 µL	2.5 mM
	PGI from yeast	Dependent on charge	5 U
	G6PDH from yeast		5 U
	PRI from spinach in 50 mM PP buffer		5 U
	50 mM formaldehyde (37%)	20 µL	5 mM
	Add ddH_2O to a final volume of 2 mL.		

Measurement of aconitase activity

The aconitase activity assays were performed as described before (Baumgart and Bott, 2011). Precultivation of *C. glutamicum* cells was done as described in Section 2.5.8. Main cultivations were inoculated to an OD_{600} of 1 in 50 mL CGXII medium supplemented with 2% glucose. For plasmid-based aconitase production, the overexpression was initiated with the induction of the P_{tac} promoter with 500 µM IPTG. At OD_{600} = 5, cells were harvested and washed with PBS buffer. The pellet from 25 mL cell culture was solubilized in 1 ml 100 mM Tris-HCl, pH 8.0 containing cOmplete™, Mini, EDTA-free Protease Inhibitor Cocktail (Roche Diagnostics, Mannheim, Germany). Cells were disrupted with glass beads (Section 2.6.1) and the cell lysate was immediately used for enzymatic assays, since aconitase is oxygen sensitive. The specific aconitase activity in crude cell extracts was determined with isocitrate as substrate. The assay mixture is given in Table 17. The reaction was performed in 1 mL reactions in UV Suprasil® quartz absorption cuvettes with a spectral range of 200-2,500 nm (Hellma, Müllheim, Germany) and the absorbance was measured at 240 nm. 1 U is defined as the formation of 1 µmol cis-aconitate within 1 min. Specific activity refers to the activity per mg protein in the crude extract. Protein amounts in the extracts were quantified with the Pierce™ BCA Protein Assay Kit (Thermo Fisher Scientific, Waltham, USA) and BSA as protein standard.

Table 17: Aconitase assay mixture. Cell extract, buffer and ddH_2O were premixed within the reaction cuvettes. The reaction was started with the addition of 100 µL isocitrate.

	Component	Volume	Final concentration
Aconitase assay mixture	Cell extract (undiluted)	10 µL	-
	1 M Tris-HCl (pH 8.0)	100 µL	100 mM
	200 mM isocitrate	100 µL	20 mM
	ddH_2O	790 µL	-

Cis-aconitate decarboxylase activity

The enzymatic activity of cis-aconitate decarboxylase (Cad) was measured as described before (Bentley and Thiessen, 1957; Otten *et al.*, 2015). Cells were harvested after 24 h of cultivation and can be frozen with liquid nitrogen and stored at -20 °C until use. Cells from 25 mL cultivation were solubilized in 1 mL of 200 mM sodium phosphate buffer (pH 6.5) containing cOmplete™, Mini, EDTA-free Protease Inhibitor Cocktail (Roche Diagnostics, Mannheim, Germany) and lysed with glass beads (Section 2.6.1). The protein concentration was measured with BCA assay. 800 µL of 30 °C prewarmed buffer with 100 µL undiluted cell extract and the reaction was started with 100 µL cis-aconitate. After 10 min incubation at 30 °C, the reaction was stopped with 50 µL 25% HCl. The reaction mixtures were centrifuged 2x 15 min at 12,000 *g* and the final supernatant was used to measure the concentration of the produced itaconate *via* HPLC analysis (Section 2.6.5). One unit corresponds to the activity converting 1 µmol cis-aconitate to itaconate within 1 min. Specific activity refers to the activity per mg protein in the crude extract. Protein amount in the extracts were quantified with the Pierce™ BCA Protein Assay Kit (Thermo Fisher Scientific, Waltham, USA) and BSA as protein standard.

Table 18: Cad assay mixture. Buffer and cell extract were premixed in Eppendorf tubes and the reaction was started with the addition of 100 µL cis-aconitate.

	Component	Volume	Final concentration
Cis-aconitate decarboxylase assay mixture	250 mM sodium phosphate buffer (pH 6.5)	800 µL	200 mM
	Cell extract (different dilutions)	100 µL	-
	80 mM cis-aconitate	100 µL	8 mM

Alcohol dehydrogenase activity assay

For AdhB assays, cells of a 20 mL main culture (OD_{600} of 5) were harvested and snap-frozen in liquid nitrogen until use. Subsequently, the cells were resuspended in 500 µL and lysed using the bead mill homogenizer Precellys® 24 (Peqlab, Bonn, Germany) at 6,000 rpm three times for 20 sec and cooled on ice in between. Cell lysate was collected by transferring the supernatant to new Eppendorf tubes after centrifugation at 16,000 rpm for 30 min at 4 °C. The assay was based on previous work (Kinoshita *et al.*, 1985), but was performed in 96-well microplate format and measured with the Infinite PRO 200 microplate reader (Tecan, Männedorf, Switzerland). 20 µL of 1:20 diluted cell-free extract

were mixed with 160 µL assay buffer (50 mM Tris-HCl, pH 8.5, 10 mM NAD^+) and added to the plate. The reader was pre-heated to 30 °C and the reaction was started with the addition of 20 µL 4% (v/v) ethanol solution in 50 mM Tris-HCl, pH 8.5 *via* the injector system. The absorption at 340 nm was measured directly after the addition of the substrate in 40 sec intervals for 10 min. One unit of specific activity was defined as conversion of 1 µmol NAD^+ per minute. Specific activity refers to the activity in the crude cell extract per mg protein. Protein amounts in the extracts were quantified with the Pierce™ BCA Protein Assay Kit (Thermo Fisher Scientific, Waltham, USA) and BSA as protein standard.

Table 19: AdhB assay mixture. The reaction was started with the addition of 20 µL 4% ethanol.

	Component	Volume	Final concentration
AdhB assay mixture	50 mM Tris-HCl, pH 8.5	140 µL	50 mM
	100 mM NAD^+ in 50 mM Tris-HCl, pH 8.5	20 µL	10 mM
	Cell extract (1:20 dilution)	20 µL	-
	4% (v/v) ethanol in 50 mM Tris-HCl, pH 8.5	20 µL	0.4%

2.6.3 Compartment purification

Sucrose gradient purification

For compartment purification from *C. glutamicum* MB001(DE3) *pduABJKNUT*, 250 mL CGXII medium supplemented with 2% glucose and 50 µM IPTG were inoculated with precultures to an OD_{600} of 0.5 and cultivated for 16 h at 20 °C. Afterwards, the cells were harvested and washed once with TEMP buffer. The pellet was suspended in 50 mL TEMP buffer (50 mM Tris-HCl, 1 mM EDTA, 0.6 mM sucrose and 0.2% 1,2-propanediol) containing 2 mg mL^{-1} lysozyme. Subsequently, the cells were centrifuged at 5000 *g* for 10 min and the pellet was suspended in 30 mL TEMP supplemented with 5 mM $CaCl_2$ and 50 µg mL^{-1} DNAseI. The cell lysis was achieved by passing them three times through a French Press (Section 2.6.1). The cell debris was separated from the supernatant by two centrifugation steps at 11,000 *g* for 15 min at 4 °C. The supernatant was collected and centrifuged for 90 min at 48,000 *g*. The pellet was subsequently suspend in 2 mL TEMP and clarified for 2 min at 11,000 *g*. The final supernatant was layered on top of a 10-50% sucrose gradient and centrifuged for 16 h at 25,000 rpm in a SW-28.1 rotor. The different protein fractions were separated using self-made gels with an 18% separation gel and a 6% stacking gel.

Dialysis purification approach

A second purification approach was performed with *C. glutamicum* MB001(DE3) *mcherrypduABJKNUT*. The main culture was performed as described for the previous

paragraph. The pellet was suspended in 30 mL YPER™ Plus and the cell suspension was passed five times through a French Press (Section 2.6.1). The cell debris was separated from the supernatant by a centrifugation step at 11,000 *g* for 30 min at 4 °C. The supernatant was collected and centrifuged for 30 min at 20,000 *g*. Afterwards, the pellet was suspended in 3 mL YPER™ Plus centrifuged at 12.000 *g*. The resulting red layer on top of the pellet was suspended in TEMP buffer. The suspension was loaded into a 3 mL 3 kDa Slide-A-Lyzer™ Dialysis Cassette (Thermo Fischer Scientific, Waltham, USA) and dialyzed over night according to manufacturer's protocol. The final supernatant was concentrated in an Amicon® Ultra-4 Centrifugal Filter Units (30 kDa, Merck Millipore, Darmstadt, Germany). The concentrated supernatant was separated using a 4-20% Mini-PROTEAN® TGX™ Precast Protein Gels (Bio-Rad, Hercules, USA).

YPER™ Plus purification

For compartment purification from *C. glutamicum* MB001(DE3) *pduABJknt*, 200 mL CGXII medium supplemented with 2% glucose and 50 µM IPTG were inoculated with precultures to an OD_{600} of 0.5 and cultivated for 16 h at 25 °C. Before cell lysis, the cells were harvested and washed with lysozyme buffer (50 mM Tris-HCl, pH 8, 5 mM EDTA, 0.6 M sucrose, 0.2% 1,2-propanediol, w/o lysozyme). The cell pellet was resuspended in 100 mL lysozyme buffer (containing 2 mg ml^{-1} lysozyme) and incubated for 1 h at room temperature. Afterwards, the cells were washed with lysozyme buffer and re-suspended in 50 mL Y-PER™ Plus Dialyzable Yeast Protein Extraction Reagent (Thermo Fischer Scientific, Waltham, USA) supplemented with EDTA-free Protease Inhibitor Cocktail tablets (Roche Diagnostics, Mannheim, Germany) and Benzonase® nuclease and incubated at room temperature for 1 h. The cell suspension was sonicated for 10 min with 1 min sonication (Amplitude: 80%; Output: 8; Branson Sonifier 250 G; Heinemann Ultraschall- und Labortechnik, Schwäbisch Gmünd, Germany) and 1 min cooling intervals. Cell debris and intact cells were separated from cell lysate by centrifugation at 4,000 *g* for 15 min at 4 °C. Starting from the cell lysate, a previously published protocol was followed (Lawrence *et al.*, 2014). In contrast to the original protocol, the NaCl concentration was raised to 160 mM NaCl (instead of 80 mM) to precipitate the compartment shells. The different protein fractions were separated using 4-20% Mini-PROTEAN® TGX™ Precast Protein Gels (Bio-Rad, Hercules, USA).

2.6.4 SDS polyacrylamide gel electrophoresis (SDS-PAGE)

For separation and detection of proteins, discontinuous SDS-PAGE (Sodium dodecyl sulfate polyacrylamide gel electrophoresis) was used. If determined, the protein concentration was measured with the Pierce™ BCA Protein Assay Kit (Thermo Fisher

Scientific, Waltham, USA) and BSA as protein standard. Each protein sample was mixed with 6x SDS sample buffer (Table 20), incubated at 95 °C for 5 min, thoroughly mixed afterwards and stored on ice until use.

Table 20: Preparation of 6x SDS sample buffer.

	Component	Final concentration
6x SDS sample buffer	Tris-HCl (pH 6.8)	375 mM
	SDS, solid	6%
	Glycerol	48% (v/v)
	DTT	9%
	bromophenol blue	0.03%

Protein separation was conducted in vertical gels with a thickness of 0.75 mm using self-made gels with different percentages (Table 21) or 4-20% Mini-PROTEAN® TGX™ Precast Protein Gels (Bio-Rad, Hercules, USA).

Table 21: Components of separation and stacking gels for SDS-PAGE.

Components	Separation gel			Stacking gel	
	12%	15%	18%	6%	8%
ddH_2O	3.35 mL	2.35 mL	1.35 mL	2.7 mL	2.36 mL
0.5 M Tris, pH 6.8	-	-	-	1.25 mL	1.25 mL
1.5 M Tris, pH 8.8	2.5 mL	2.5	2.5 mL	-	-
Acrylamide/Bisacrylamide	4 mL	5 mL	6 mL	1 mL	1.33 mL
10% SDS	100 µL	100 µL	100 µL	50 µL	50 µL
10% APS	65 µL	65 µL	65 µL	30 µL	30 µL
TEMED	12.5 µL	12.5 µL	12.5 µL	6.5 µL	6.5 µL

The Mini-PROTEAN Tetra Cell System (Bio-Rad, Hercules, USA) was used with 1x SDS running buffer (Table 22). For the determination of protein sizes, 5 µL Precision Plus Protein™ Dual Color Standard (Bio-Rad, Hercules, USA) or Spectra™ Multicolor Low Range Protein Ladder (Thermo Fisher Scientific, Waltham, USA) were also applied in one lane. The electrophoresis was carried out at 100 V for 15 min until samples lined up at the separation gel. Then, electrophoresis was run for further ~60 min at 150 V. After gel electrophoresis, the gel was rinsed with water for 15 min and stained with Rapid Stain™ (G-Biosciences, St. Louis, USA) for 1 h. To remove excess stain, the gels were rinsed with dH_2O. Pictures of each gel were taken for documentation with a standard office scanner.

Table 22: Composition and preparation of 10x SDS running buffer.

	Components	Amount	Final concentration
10x SDS running buffer	Tris	60.4 g	250 mM
	Glycine	288.4 g	1.92 M
	SDS	20 g	1% (w/v)
	Add ddH_2O to a final volume of 2 L. Test pH with indicator strips (pH 8.4–8.9), but do not adjust pH.		
1x SDS running buffer	Mix 100 mL of 10x SDS running solution with 900 mL ddH_2O.		

2.6.5 HPLC analysis of itaconate production

For the quantitative analysis of itaconic acid in culture supernatants and Cad assay samples was performed by HPLC analysis in an 1100 series HPLC value system (Agilent Technologies, Santa Clara, USA). The cell suspensions were clarified by 2x 15 min centrifugation at 16,000 *g*. Depending on growth phase of the cultures, the final supernatants were diluted 1:3 as high glucose concentrations in the sample should be avoided. Each sample was run for 38 min with a constant flow of 0.4 mL min^{-1} in 0.1 M H_2SO_4 running buffer at 40 °C over an Organic-Acid Resin column (300 x 8 mm; Column-No: 1711-13; CS-Chromatographie-Service GmbH, Langerwehe, Germany). Eluted organic acids were detected with an Agilent 1100 diode array detector at a wavelength of 215 nm at a retention times of ~24.5 min. Itaconate was quantified by measuring the area (mAU*s) under the chromatographic peak by integration using the Agilent Chem Station software. With an external standard a calibration curve with known itaconate concentrations (linear measurement range from 0.01 mM to 1.75 mM) was calculated (Figure 8).

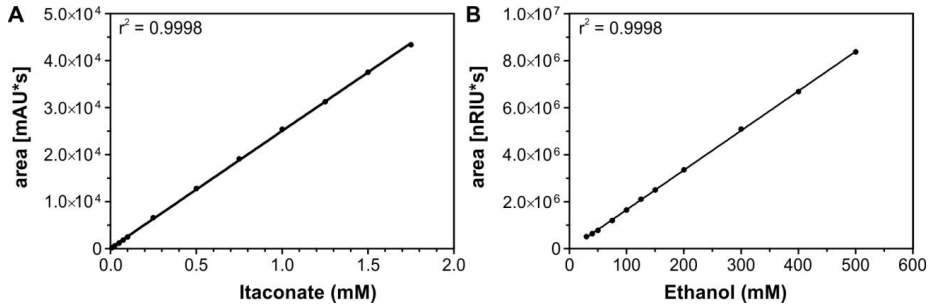

Figure 8: Itaconate and ethanol standard curves for quantitative concentration measurements. A Itaconate concentration of 0,01 mM, 0.025 mM, 0.05 mM, 0.075 mM, 0.1 mM, 0.25 mM, 0. 5 mM 0.75 mM, 1 mM, 1.25 mM, 1.5 mM and 1.75 mM were measured and lie within the linear measuring range. **B** For ethanol determination, concentrations of 30 mM, 40 mM, 50 mM, 75 mM, 100 mM, 125 mM, 150 mM, 200 mM, 300 mM, 400 mM and 500 mM were used to determine a standard curve.

2.6.6 HPLC analysis of ethanol production

The quantification of ethanol content in culture supernatant of ethanol production strains was performed *via* HPLC analysis. After 24, 30, 48 and 60 h of cultivation, 500 µL supernatant were taken from the cultures and cells were removed with two centrifugation steps at 16,000 *g* for 15 min at 4 °C. The undiluted culture supernatants were applied into the HPLC vials. Ethanol standards with known concentrations (30-500 mM) were prepared in ddH_2O and were used as references for a standard a calibration curve (Figure 8).

The HPLC run was performed as described in Section 2.6.5 but with an elongated run time of 45 min. Ethanol was detected with the refractive index detector (RID) signal after ~39.5 min. The quantification of ethanol was performed by calculating the area (nRIU*s) under the chromatographic peak by integration using the Agilent Chem Station software.

2.6.7 Fluorescence microscopy

Main cultures for fluorescence microscopy analyses were cultivated in 20 mL CGXII supplemented with 2% (w/v) glucose inoculated with a CGXII preculture (Section 2.5.8) to a starting OD_{600} of 1 in baffled shake flasks at 30 °C for 2 h. The production of shell and fluorescence proteins was induced with different amounts of IPTG to induce BMC shell production and 50 ng ml^{-1} anhydrotetracycline to induce fluorescence reporter production.

To reduce the movement of the cells for microscopy, agar pads with 1% (w/v) agarose were prepared between two microscopy slides. 3 µL of a sample were placed on the agar pad and a cover slip was immediately placed above. The fluorescence microscopy has been performed with the AxioImager M2 microscope with AxioCam MRm using a Plan-Apochromat 100x, 1.40 Oil phase contrast oil-immersion objective (Carl Zeiss MicroImaging GmbH, Göttingen, Germany). The optimal exposure time for the different fluorescence images was determined with the automatic measurement option of the AxioVision Rel. 4.8 software (Carl Zeiss MicroImaging GmbH), which was also used for analyzing the images.

2.6.8 Transmission electron microscopy

The main cultures, CGXII supplemented with 2% (w/v) glucose, were inoculated to an OD_{600} of 1 and cultivated for 2 h at 30 °C. Compartment gene induction was triggered by the addition of 50 µM IPTG to the culture and the cells were cultivated for further 4 h. Bacteria were embedded, sectioned and stained as described previously (Parsons *et al.*, 2010; Lawrence *et al.*, 2014) with the addition that vacuum steps were applied during the

glutaraldehyde, osmium tetroxide and 100% resin steps. During these steps the pellets were resuspended in the appropriate solution and placed in a vacuum desiccator. A vacuum was applied for 1 min and released to aid infiltration of the solutions into the cells. This process was repeated twice before incubations in the aforementioned solutions and was carried out according to the protocol. Images were obtained using a JEOL-1230 transmission electron microscope equipped with a Gatan multiscan digital camera operated at an accelerating voltage of 80 kV.

3 RESULTS

3.1 Assembly of 1,2-PD utilization metabolosome shells

3.1.1 *C. freundii pdu* operon design for expression in *C. glutamicum*

The aim of this study was the establishment of synthetic Pdu BMCs in the biotechnological platform organism *C. glutamicum*. In a first experiment, the *pdu* operon from *C. freundii* was introduced into *C. glutamicum* to test its transferability to a Gram-positive organism. For this purpose, three basic designs were tested: First, the native 21 gene operon (*pduA-X* (Parsons *et al.*, 2008); Figure 9A) was cloned into the pAN6 vector under control of the inducible P_{tac} promoter. Second, the empty shell operon *pduABJKNUT* illustrated in Figure 9B (Parsons *et al.*, 2010) was cloned under control of an IPTG inducible P_{T7} promoter in the pMKEx1 vector. The synthetic operon contains 40 bp upstream regions including a ribosome binding site in front of *pduAB*, p*duJ*, *pduK*, *pduN*, *pduU* and *pduT* (Parsons *et al.*, 2010). This operon version was additionally designed with a fusion of *mcherry* to the N-terminus of *pduA*. As a third variant, the synthetic operon was placed under control of the native 3' untranslated regions (3'UTR) of the shell genes (*pduABJKNTU*$_{native}$) (Figure 9C). All operon versions were tested on their ability to form BMCs in *C. glutamicum*.

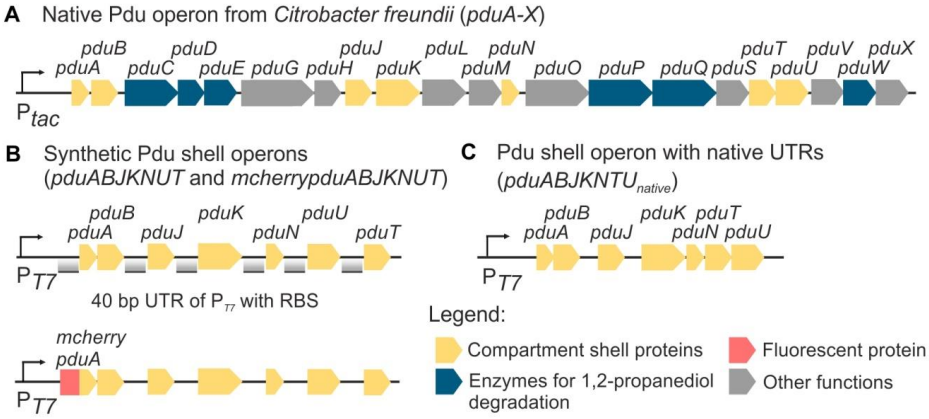

Figure 9: Propanediol utilization operon design. **A** The whole *pdu* operon (*pduA-X*) consists of 21 genes, encoding for shell proteins (yellow), enzymes for 1,2-PD degradation (blue) and proteins with other functions (grey). The seven shell proteins should self-assemble to hexameric compartment structures without cargo proteins (**B** (*mcherry*)*pduABJKNUT* and **C** *pduABJKNTU*$_{native}$). The whole operon and the different *pdu* shell operon versions were tested on their performance on BMC assembly in *C. glutamicum*.

3.1.2 Tracking compartment assembly by fluorescence reporter systems

As outlined in the introduction, proteins of interest can be targeted into the BMC lumen by fusing them to the first 18 amino acids of PduP and PduD (further named P18 and

D18, respectively) (Fan *et al.*, 2010; Fan *et al.*, 2012; Lawrence *et al.*, 2014; Lee *et al.*, 2016). Therefore, a toolbox of different eYFP reporter plasmids was created as described in the following (Figure 10). The plasmid pEC-XC99E (Kirchner and Tauch, 2003) was modified by the addition of an anhydrotetracycline inducible P_{tetR} promoter and an adapted multiple cloning site (MCS) (Figure 10A). The resulting plasmid pEC-P_{tetR} was used as backbone for all further modifications. The D18 and P18 targeting peptide sequences as well as *eyfp* are interchangeable with other genes of interest by usage of the respective enzyme digest sites (Figure 10B). The *eyfp* version $eyfp_{ASV}$ contained the SsrA-degradation tag *C. g.* AAEKSQRDYAASV (*C. g.* ASV (Hentschel *et al.*, 2013)) fused to the C-terminus of *eyfp*. Within the cytoplasm, ASV-tagged proteins are susceptible for tail-specific proteases (Herman *et al.*, 1998), whereas encapsulated proteins are protected from degradation.

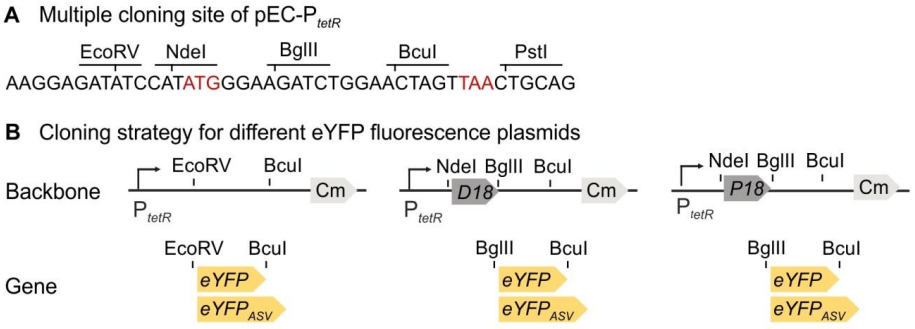

Figure 10: pEC-P_{tetR} based plasmid construction. A MCS sequence of pEC-P_{tetR} with unique enzyme digest sites. **B** Schematic overview of *eyfp* expression vectors. The fluorescence reporter *eyfp* was fused N-terminally to either no, the D18, or the P18 signal sequence and C-terminally to the SsrA peptide sequence *C. g.* ASV or no targeting signal.

For a first visualization of the structures resulting from the expression of the before mentioned pdu operons (Figure 9) in *C. glutamicum* MB001(DE3), *P18eyfp* was coexpressed in the respective strains (Figure 11). For the native 21 gene operon *pduA-X*, filamentous structures as well as adjacent round structures were formed. As a control, no interaction was observed when untagged eYFP was coproduced with PduA-X. Hence, the eYFP signal was evenly distributed within the cytosol. Consistently, the coproduction of shell proteins with their native upstream regions ($PduABJKNTU_{native}$) and P18eYFP resulted in the formation of similar structures as observed for PduA-X. These findings, however, suggest some kind of assembly problems of the Pdu proteins within the cell rather than the functional assembly of BMCs. Previous studies have also reported the formation of aberrant structures including laminar structures with the overexpression or deletion of single or multiple shell proteins (Parsons *et al.*, 2010; Pang *et al.*, 2014). In *E. coli pduA-X*, all shell proteins (PduA,-B,-B',-J,-K,-U,-T), apart from

PduN, were shown to have a negative influence on compartment assembly when overexpressed (Parsons *et al.*, 2008). Based on these observations, it can be assumed that imbalances in protein complex stoichiometry hindered the correct assembly of Pdu BMCs when expressed from the native operon. The expression of the synthetic shell operons *pduABJKNUT* and *mcherrypduABJKNUT* revealed distinct foci within the cytosol, which could be linked to the formation of BMC structures. For MB001(DE3) *mcherrypduABJKNUT P18eyfp*, both fluorescence proteins colocalized within the cells. This demonstrated that P18eYFP and the shell protein PduA are present at the same location suggesting the recruitment of P18eYFP to compartment shell proteins.

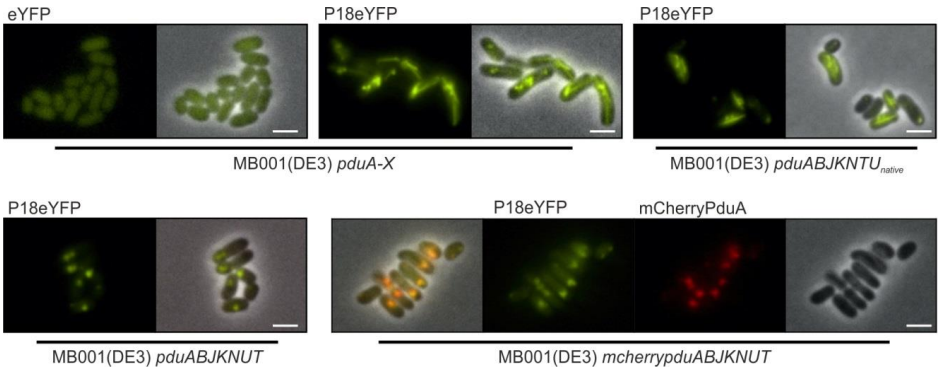

Figure 11: Coexpression of *P18eyfp* with different *pdu* operons in *C. glutamicum* MB001(DE3). The protein production was induced after 2 h of cultivation in CGXII + 2% (w/v) glucose with 50 µM IPTG and 50 ng mL^{-1} anhydrotetracycline. The strains were cultivated for 4 h after induction. The production of (mCherry)PduABJKNUT led to distinct eYFP localizations within the cells, the production of PduA-X and PduABJKNTU$_{native}$ showed filamentous as well as adjacent round structures. *pduA-X*: native 21 gene operon; *pduABJKNUT*: synthetic operon contains 40 bp upstream regions including a RBS in front of *pduAB*, *pduJ*, *pduK*, *pduN*, *pduU* and *pduT*; *mcherrypduABJKNUT*: *pduABJKNUT* with *mcherry* fused to *pduA*; *pduABJKNTU$_{native}$*: synthetic shell operon with native 3'UTR of the shell genes; Scale bar is 2 µm.

3.1.3 Analysis of a *C. glutamicum* (mCherry)PduABJKNUT production strains

The fluorescence signals observed for MB001(DE3) *pduABJKNUT* and MB001(DE3) *mcherrypduABJKNUT* showed promising localization patterns (Figure 11) and were further investigated. With the objective to determine an optimal cultivation strategy that achieves maximum compartment yields, different cultivation conditions were examined. First, the formation of the compartments over the course of time was investigated. In MB001(DE3) *pduABJKNUT P18eyfp* and MB001(DE3) *mcherrypduABJKNUT,* Pdu production was induced with a medium concentration of 50 µM IPTG and strains were further cultivated at 30 °C. After 2 h, distinct localizations of fluorescence signal were present for both strains (Figure 12A). With longer cultivation

time, the fluorescence signals accumulated (4 h and 6 h) and were visible almost throughout the whole cytosol after 24 h.

Since the fluorescence signals were already very distinct after 4 h of cultivation, this time point was chosen to evaluate the effect of different IPTG inducer concentrations (20 µM, 50 µM, 100 µM and 500 µM IPTG) on *mcherrypduABJKNUT* expression (Figure 12B). Cultivated with 20 µM IPTG, most cells showed one distinct localization signal within the cytosol. With higher IPTG concentrations the mCherry fluorescence signal became more indistinguishable and started to aggregate or accumulate within the cytosol similar to what was observed for cultivations with 50 µM IPTG after 6 h and 24 h. The cultivation temperature (20 °C, 25 °C, 30 °C or 37 °C) had a similar effect on mCherry distribution as different IPTG concentrations at 30 °C after 4 h of cultivation (Figure 12C).

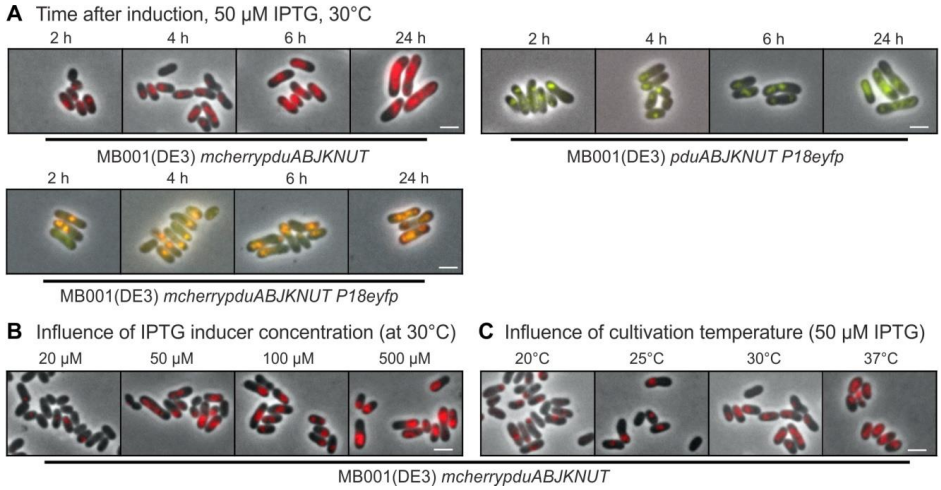

Figure 12: Influence of temperature and IPTG concentration on Pdu shell production in *C. glutamicum* MB001(DE3). MB001(DE3) *mcherrypduABJKNUT* and MB001(DE3) *pduABJKNUT P18eyfp* were cultivated in CGXII supplemented with 2% (w/v) glucose at different temperatures and IPTG concentrations. The BMC formation was examined under the microscope after different time points. 2 h after cultivation, Pdu production resulted in fluorescent foci but even with lower cultivation temperature and decreased IPTG concentration, an aggregation of fluorescence signal occurred afterwards. Scale bar is 2 µm.

It can be concluded that the distinct localizations were observable already after 2 h of induction with low IPTG concentration or with low cultivation temperature. With higher inducer concentrations, higher temperatures and longer cultivation time the fluorescent structures remain localized but accumulate to large aggregates within the whole cytosol. Further examinations of MB001(DE3) *pduABJKNUT* and MB001(DE3) *mcherrypduABJKNUT* were performed by transmission electron microscopy after 4 h of cultivation with 50 µM IPTG. The analysis revealed the presence of large and unstructured aggregates with no defined borders (Figure 13). These aggregates were

exclusive to MB001(DE3) *pduABJKNUT* and MB001(DE3) *mcherrypduABJKNUT*. No aggregated were found in the MB001(DE3) parental, suggesting they had formed from aggregated shell proteins.

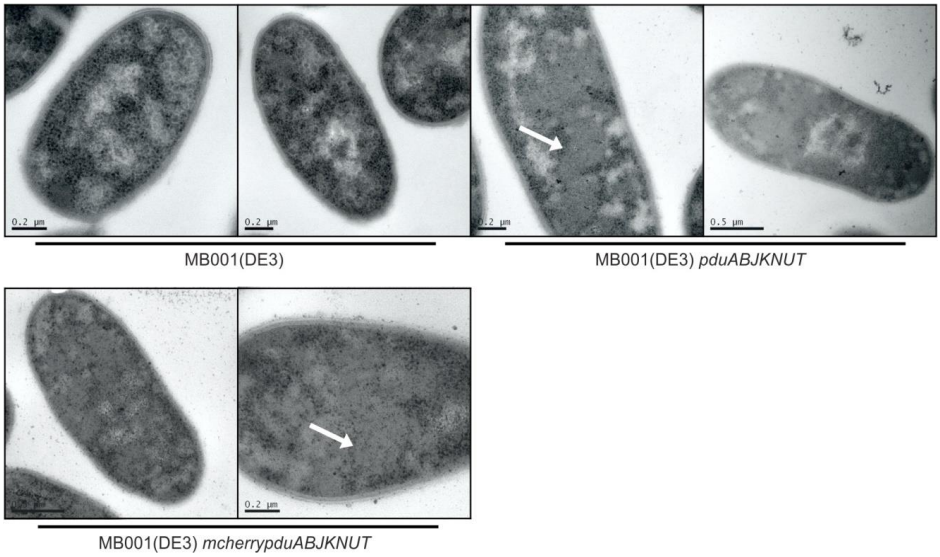

Figure 13: Transmission electron microscopy analysis of BMC production strains *C. glutamicum* MB001(DE3) *(mcherry)pduABJKNUT* and MB001(DE3) WT. For the thin sections, MB001(DE3) *pduABJKNUT* and *mcherrypduABJKNUT* were grown in CGXII supplemented with 2% glucose for 4 h after induction of Pdu production with 50 µM IPTG. The production of PduABJKNUT and mCherryPduABJKNUT led to large accumulations of proteins without detached structures (exemplary regions are marked with a white arrow), concluding that BMCs were not successfully formed.

3.1.4 Importance of protein stoichiometry on compartment assembly

To prevent the production of aggregates and misshaped BMC protein assemblies, attempts to optimize protein stoichiometry to facilitate proper assembly in *C. glutamicum* were undertaken. Based on the analysis of the molar ratios of the Pdu shell proteins purified from *S. enterica* from Havemann *et al*., the shell proteins were classified into three groups: High abundancy (PduA,B,B',J; ~16-28 % each), low abundancy (PduK,U,T; ~3 % each) and minor abundancy (PduN, not detectable) (Havemann and Bobik, 2003). The adaptation of protein stoichiometry was achieved by modification of start codons of single or combinations of shell proteins from ATG (100%) to GTG (~40% (Otten *et al.*, 2015) for *pduK*, *pduU* and *pduT* or TTG (~1%) (Otten *et al.*, 2015) for *pduN*. This was combined with the deletion of *pduU* and/or *pduT*. Hereafter, small letters within the operon notation represents the modification of the start codon to GTG or TTG. Twelve operon versions based on *pduABJKNUT* were designed and are presented in Figure 14.

A first screening of the different operons was performed by coexpression of the *pdu* operons and *P18eyfp*$_{ASV}$ in *C. glutamicum* MB001(DE3). Interestingly, the different Pdu production strains caused very divergent fluorescence patterns with the coproduction of the protease susceptible P18eYFP$_{ASV}$ (Figure 14).

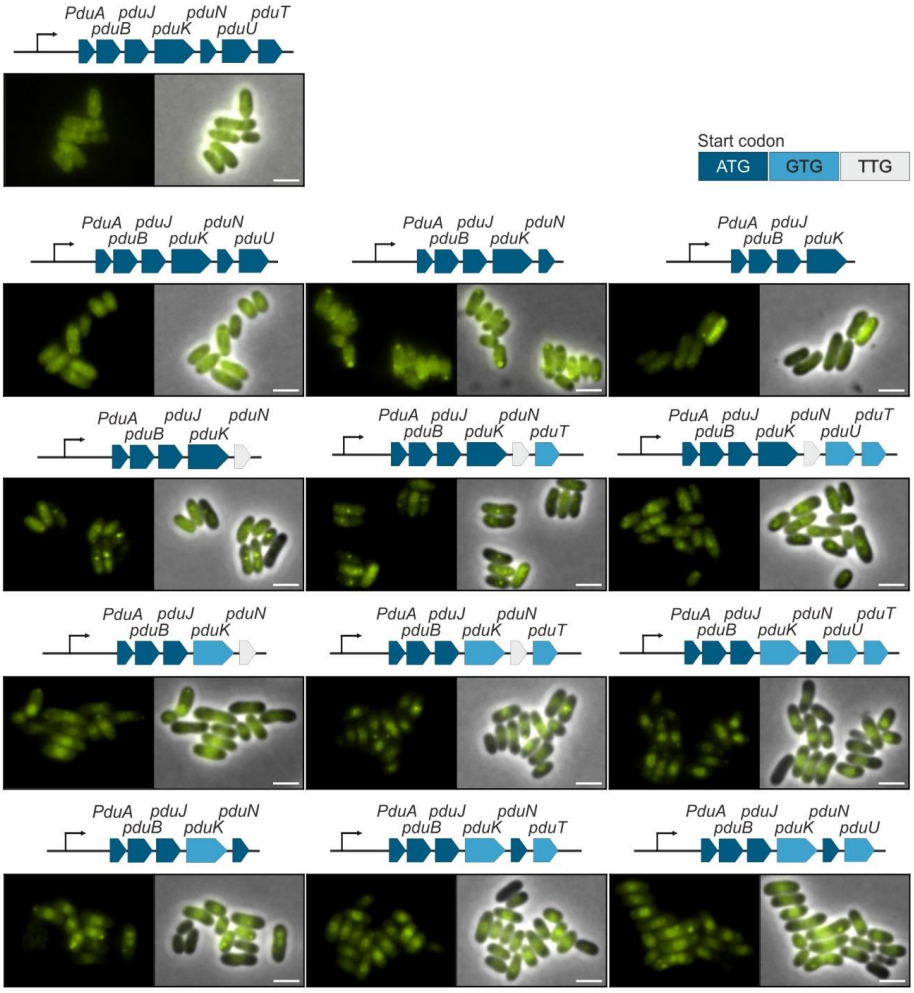

Figure 14: Effect of changes in protein stoichiometry on Pdu shell formation in *C. glutamicum* MB001(DE3). The operon expression was induced with 50 µM IPTG, strains were further cultivated at 30 °C and fluorescence microscopy images were taken 4 h after induction of BMC and P18eYFP$_{ASV}$ production. The analysis revealed diverse fluorescence phenotypes depending on the different operons. Scale bar is 2 µm.

PduA,-B,-J,-K and PduN were published as minimal requirement for heterologous shell formation in *E. coli* (Parsons *et al.*, 2010). In this work, the absence of PduU and PduT in the operons *pduABJKNU* and *pduABJKN* led to a phenotype similar to *pduABJKNUT*, which was disconfirmed to produce BMCs, upon expression in MB001(DE3) with a

fluorescence signal rather distributed within the cytosol and few weak distinct localizations. For MB001(DE3) *pduABJKn* and MB001(DE3) *pduABJKnt*, the shell production led to a single distinct focus and some weak localizations as described for the abovementioned operons. The most significant difference was found with the downregulation of $PduK_{ATG}$ to $PduK_{GTG}$. For example in MB001(DE3) *pduABJkn* and MB001(DE3) *pduABJknt* distinct fluorescence patterns in the mid part of the cell with some delineated contours occurred. The influence of PduU, PduT and PduN could not be determined with fluorescence microscopy, because the direct comparison of relevant strains did not reveal visible differences. For example, comparing MB001(DE3) *pduABJkN* with MB001(DE3) *pduABJkNt* or MB001(DE3) *pduABJkNt* with MB001(DE3) *pduABJkNut*, the same fluorescence phenotypes were displayed.

To further evaluate differences indistinguishable by fluorescence microscopy, eight representative Pdu production strains were further investigated by transmission electron microscopy and results are given in Figure 15. Comparing the thin section of MB001(DE3) *pduABJKNUT* (Figure 15A), *pduABJKnut* (Figure 15C), and *pduABJKnt* (Figure 15D), the introduced changes resulted in no obvious effect and cells were observed to contain aggregated proteins rather than BMC-like structures.

In all strains containing plasmid where PduK was downregulated, the shape of the structures was positively influenced and compartment-like structures with defined borders could be observed within the cells (Figure 15E-J). In contrast, the modulation of PduN abundancy resulted in no visible effect. This becomes obvious when comparing the thin sections of the strains MB001(DE3) *pduABJkn* (Figure 15I) with MB001(DE3) *pduABJkN* (Figure 15J) as well as MB001(DE3) *pduABJknt* (Figure 15G) with MB001(DE3) *pduABJkNt* (Figure 15H).

Therefore, the influence of *pduU* on compartment assembly was analyzed by comparing the strains expressing *pduABJkNu* (Figure 15F), *pduABJkN* (Figure 15J), *pduABJkNut* (Figure 15E) and *pduABJkNt* (Figure 15H). Analysis of the thin sections revealed no obvious differences correlated with the production or absence of PduU. In contrast, thin sections revealed that strains including *pduT* within the operon have more distinct borders defining the individual compartments (compare *pduABJkNut* (Figure 15E) with *pduABJkNu* (Figure 15F); *pduABJknt* (Figure 15G) with *PduABJkn* (Figure 15I); *pduABJkNt* (Figure 15H) with *pduABJkN* (Figure 15J)). Interestingly, the two strains lacking PduU and PduT contained BMC-like structures in 26% and 29% of the cells respectively, whereby in MB001(DE3) *pduABJknt*, MB001(DE3) *pduABJkNt* and MB001(DE3) *pduABJkNut,* the number of cells containing visible BMC-like structures was higher with 46%, 38%, and 53%, respectively (Table S8).

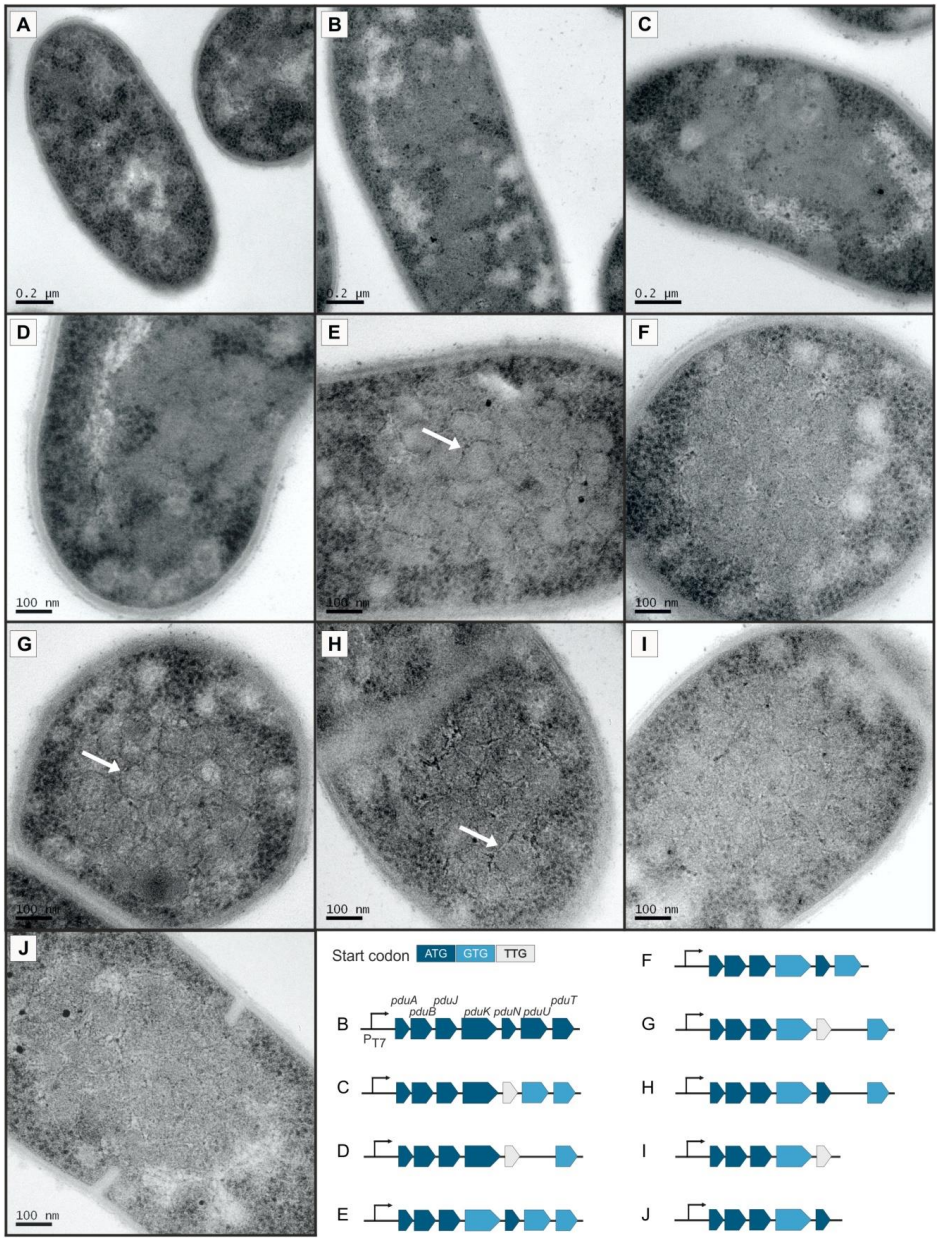

Figure 15: Transmission electron microscopy analysis of *C. glutamicum* MB001(DE3) WT (A) and different *C. glutamicum* MB001(DE3) Pdu production strains (B-J). The cells were grown in CGXII 2% glucose for 4 h after induction of Pdu production with 50 µM IPTG. Downregulation of different genes are indicated by lower cases. White arrows point to exemplary defined BMC-like structures. **A** MB001(DE3) WT; **B** MB001(DE3) *pduABJKNUT*; **C** MB001(DE3) *pduABJKnut;* **D** MB001(DE3) *pduABJKnt*; **E** MB001(DE3) *pduABJkNut*; **F** MB001(DE3) *pduABJkNu*; **G** MB001(DE3) *pduABJknt*; **H** MB001(DE3) *pduABJkNt*; **I** MB001(DE3) *pduABJkn*; **J** MB001(DE3) *pduABJkN*; More images can be found in Figure 13 and in the Appendix in Figure S1.

In the MB001(DE3) initial strain, 4% of the total analyzed cells showed unknown structures accounted as 'BMC-like' (Figure 16). Nevertheless, the occurrence within Pdu production strains is much higher, and hence, these structures described before were thought to be specific for BMC-producing strains.

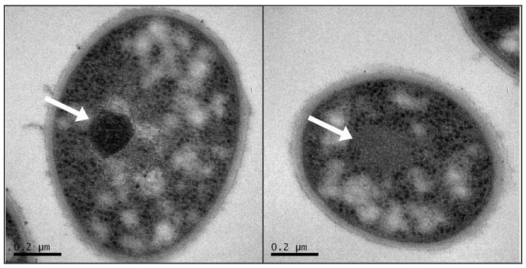

Figure 16: Transmission electron microscopy of *C. glutamicum* MB001(DE3). Arrow in the left image marks volutin granule (Pallerla *et al.*, 2005) and arrow within the right image an unknown artefact.

Based on the obtained data, it was considered that the structures observed in ~50% of the cells from MB001(DE3) *pduABJkNut* and MB001(DE3) *pduABJknt* represent arrangements of compartment-like structures with delimiting boundaries (Figure 15E and G and Table S8), whereby some structures produced within the respective strains seemed to be poorly formed, not fully closed and ranged widely in size. Although the produced BMCs are arranged together in the mid part of the cells rather than being distributed across the cytoplasm, which is similar to the clustering of heterologously produced BMCs in *E. coli* (Parsons *et al.*, 2010; Lawrence *et al.*, 2014; Lee *et al.*, 2016). Furthermore, the TEM image analysis (Figure 15) showed that the appearance of distinct foci in the fluorescence microscopy experiments (Figure 14) did not necessarily hint to BMC formation. Hence, the strains showing larger fluorescent clusters in the mid of cells successfully produced BMC-like structures.

3.1.5 Growth of plasmid-based BMC production strains

With the goal to establish BMCs as a profitable technology, it is important to evaluate the influence of compartment production on growth of *C. glutamicum*. The growth was analyzed using a microbioreactor system (BioLector®). The production of Pdu shell proteins (50 µM IPTG) was found to dramatically influence the growth in the respective *C. glutamicum* strains (Figure 17A and Table S6).

It has to be mentioned, that the IPTG induction of the empty vector control MB001(DE3) pMKEx1 already had an negative effect on the growth rate with a drop from 0.491 ± 0.004 h^{-1} to 0.354 ± 0.009 h^{-1} but reaching the same final backscatter as the uninduced control. Unfortunately, it cannot be differentiated if the growth effects observed for Pdu

production strains after addition of 50 µM IPTG are additional effects of pMKEx1 impairment and Pdu production or the exclusive influence of Pdu production (Appendix 6.2 for more information).

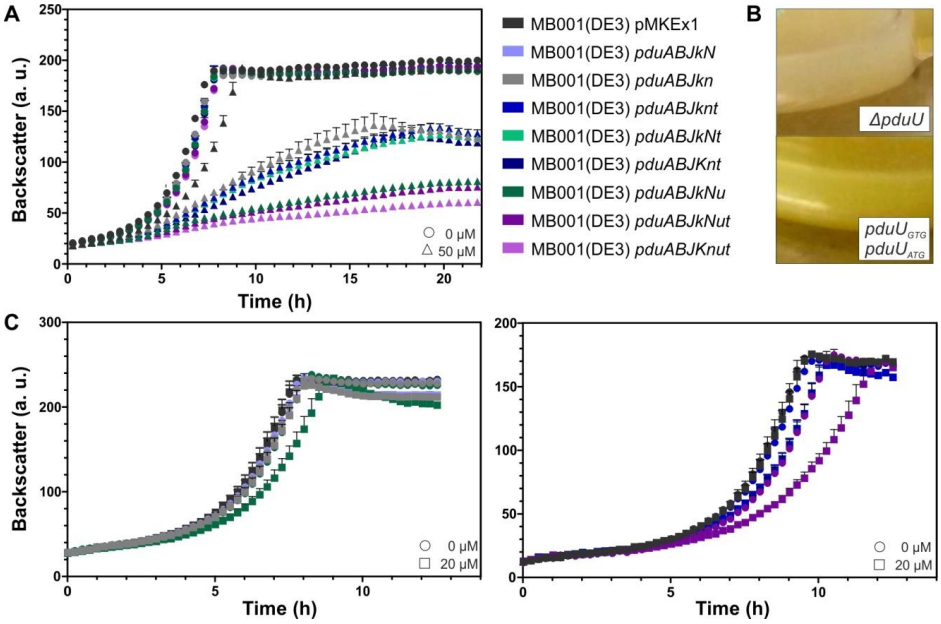

Figure 17: Growth of different Pdu production strains. Cultures were grown in CGXII + 2% (w/v) glucose and induction of operon expression was performed with **A** 0 µM and 50 µM IPTG and additionally with **C** 0 and 20 µM IPTG for Pdu production strains, which were confirmed to build BMC-like structures; Circles: 0 µM IPTG; Squares: 20 µM IPTG; Triangles: 50 µM IPTG; **B** Cultures containing *pduU* have a strong yellow phenotype of the cells.

Nevertheless, growth analyses showed that the production of PduU had the most dramatic influence on growth as MB001(DE3) *pduABJkNu*, MB001(DE3) *pduABJkNut* and MB001(DE3) *pduABJKnut* reached the lowest final backscatter signals and had comparably low growth rates. Interestingly, the cells of all strains containing *pduU* showed a yellow phenotype as shown in Figure 17B, even when the heterologous genes were uninduced. MB001(DE3) *pduABJkn* and *MB001(DE3) pduABJknt* performed best with growth rates of 0.319 ± 0.003 h^{-1} and 0.318 ± 0.005 h^{-1}.

Because a reduced growth is not ideal for a BMC production strain, strains which were confirmed by electron microscopy analyses to build BMC-like structures were additionally cultivated in CGXII + 2% (w/v) glucose with a reduced amount of 20 µM IPTG within the BioLector® microbioreactor device (Figure 17C). With 20 µM IPTG, the control strain MB001(DE3) pMKEx1 did not show impaired growth (Figure 17C) and therefore, growth declines of Pdu production strains can be assigned to Pdu production.

With the reduction of operon induction, the growth decline was minimized for MB001(DE3) *pduABJkn*, MB001(DE3) *pduABJkN* and MB001(DE3) *pduABJknt*. A slight reduction in growth was observed for MB001(DE3) *pduABJkNu* and a stronger growth decline for *pduABJkNut* but all strains reached the same final backscatter.

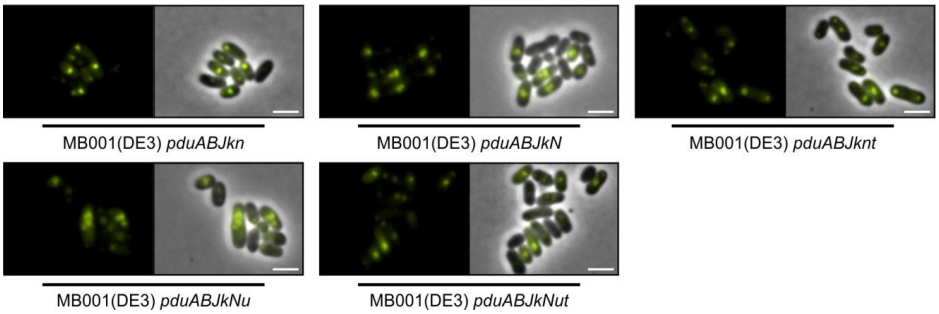

Figure 18: Coexpression of *P18eyfp* with different *pdu* operons in *C. glutamicum* MB001(DE3). The Pdu production strains were cultivated in CGXII + 2% (w/v) glucose induced with 20 µM IPTG for 4.5 h. Fluorescent foci were observed for within cells of all Pdu production strains. Scale bar is 2 µm.

Pdu production was followed by additional coproduction of P18eYFP and subsequent fluorescence microscopy analyses. Figure 18 shows the formation of distinct fluorescence signals after supply of a lowered IPTG concentration of 20 µM IPTG. It could be speculated that the induction was sufficient for BMC formation, but further transmission electron microscopy analyses are necessary for confirmation of these assumptions.

3.1.6 Chromosomal integration of the *pduABJknt* shell operon

In order to generate a more stable expression system, the optimized *pdu* shell operon *pduABJknt* was integrated under control of the P_{T7} promoter into an intergenic region on the chromosome of *C. glutamicum* MB001(DE3) between the genes cg1121 and cg1122. The growth performance of the resulting strain was tested with different IPTG inducer concentrations and compared to the MB001(DE3) WT (Figure 19A). For the control strain MB001(DE3), the growth rates were determined with 0.548 ± 0.008 h^{-1} in the absence of IPTG and 0.540 ± 0.003 h^{-1} in the presence of 150 µM IPTG.

With increasing IPTG levels, a moderate influence on the growth rate of MB001(DE3)::P_{T7}*pduABJknt* was observed (0.558 ± 0.011 h^{-1} without IPTG induction, 0.522 ± 0.005 h^{-1} with 20 µM IPTG, 0.452 ± 0.009 h^{-1} with 50 µM IPTG and 0.428 ± 0.009 h^{-1} with 150 µM IPTG). The compartment production was investigated by fluorescence microscopy after induction of the *pdu* operon with 50 µM IPTG and the coproduction of different eYFP versions (Figure 19A). In the control strain MB001(DE3)

pduABJknt eyfp, eYFP fluorescence was evenly distributed throughout the cytosol. It was possible to confirm that P18eYFP and D18eYFP both localized to foci within the cells when coproduced with PduABJknt (Figure 19A). Additionally, a SsrA-degradation tag variant AAEKSQRDYAASV (ASV) (Hentschel *et al.*, 2013) was fused to the C-terminus of D18eYFP and P18eYFP resulting in D18eYFP$_{ASV}$ and P18eYFP$_{ASV}$. By addition of this tag, the proteins are susceptible to tail-specific proteases in the cytoplasm (Herman *et al.*, 1998), whilst the encapsulation protected them from degradation. With the production of shell proteins and D18eYFP$_{ASV}$, eYFP was protected from degradation within the compartments and a fluorescence signal was detected. Similar results were obtained with the maximal expression (250 µM IPTG) of the operon (Figure 19A).

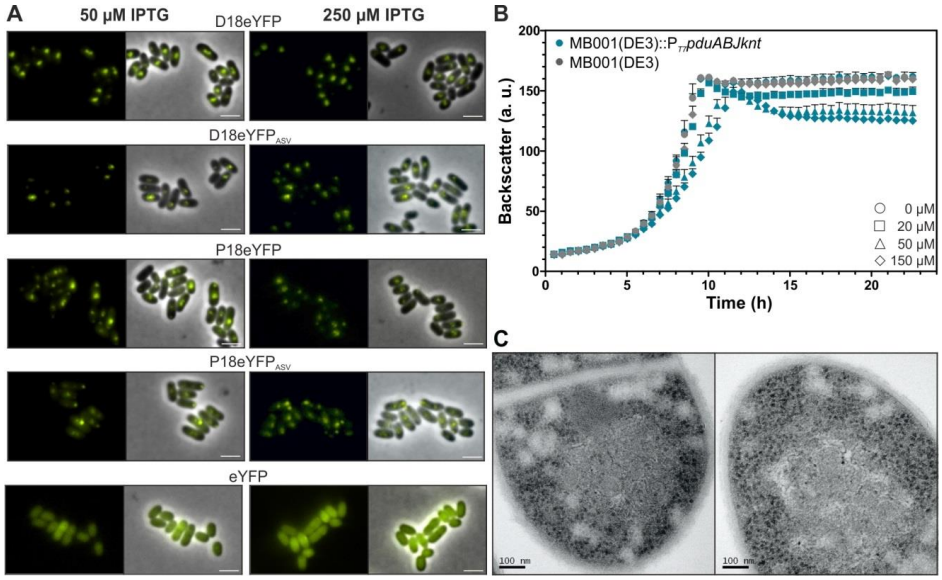

Figure 19: Characterization of BMC production strain *C. glutamicum* MB001(DE3)::P$_{T7}$*pduABJknt*. A Fluorescence microscopy analyses showed the distribution of D18eYFP/P18eYFP variants with coproduction of PduABJknt (50 µM and 250 µM IPTG). Scale bar is 2 µm. ASV: SsrA-degradation tag variant AAEKSQRDYAASV; **B** Growth of MB001(DE3) (grey) and MB001(DE3)::P$_{T7}$*pduABJknt* (blue) induced with 0, 20, 50 or 150 µM IPTG. The optimized *pdu* gene cluster was chromosomally integrated into the intergenic region between cg1121 and cg1122. **C** TEM images of MB001(DE3)::P$_{T7}$*pduABJknt* cells grown in CGXII 2% glucose with 50 µM IPTG for 4 h after induction of Pdu production showed BMC-like structures within the cytoplasm.

For transmission electron microscopy studies, MB001(DE3)::P$_{T7}$*pduABJknt* was cultivated for 4 h after induction with 50 µM IPTG. BMC-like structures were observed (Figure 19C) in 19% of the cells examined. However, the boundaries of the BMC-like structures were not as distinct as seen for the plasmid-based BMC production strain MB001(DE3) *pduABJknt* (Figure 15G). Apparently, the correct adaption of expression

strength also has an impact on compartment formation, as the induction with 50 µM IPTG in MB001(DE3)::P_{T7}*pduABJknt* may not be sufficient to induce compartment formation in a great proportion of cells as it was seen for the plasmid-based expression strains.

3.1.7 Approaches for BMC purification from *C. glutamicum*

A broad range of purification protocols is available for the purification of BMCs (Lassila, 2015). For an optimal purification, different parameters have to be considered such as cultivation conditions (cultivation temperature, expression strength, cultivation time) as well as the method of cell lysis and choice of purification protocol.

In the beginning of this work, all purification approaches were conducted with the strains MB001(DE3) *pduABJKNUT* and MB001(DE3) *mCherrypduABJKNUT*. Within the scope of this study, both strains were shown to be unable to form BMC structures under the tested condition. Nevertheless, some major issues should be mentioned for prospective optimization approaches.

i. Purification approaches including a sucrose gradient, and also YPER™ Plus based purifications, led to the copurification of ribosomal proteins, which made it difficult to discriminate between Pdu shell proteins and ribosomal proteins. A typical result is shown in Figure 20A. Different possibilities to circumvent ribosome copurification will be addressed in the discussion (chapter 4.1.3).
ii. MB001(DE3) *mCherryPduABJKNUT* was chosen to follow purification steps by visual examination and *via* fluorescence microscopy. However, tracking of the mCherry signal during purification was hindered by the strong yellow phenotype of strains producing PduU (Figure 20B). This could be avoided by the usage of production strains lacking *pduU*.
iii. The fluorescence microscopy analysis of different fractions and purification approaches of MB001(DE3) *mCherrypduABJKNUT* revealed insolubility and aggregation of fluorescence reporter proteins to cell debris, which hinted to issues in either compartment production or compartment purification (Figure 20C). However, it was possible to solubilize parts of those aggregates by dialysis which then could be purified with relatively high purity, even though the structures were most like not correctly assembled BMCs. By MADLI-TOF MS analysis, the production of five from seven shell proteins could be confirmed (Figure 20D).
iv. Fractions of a PduABJKNUT purification approach were analyzed *via* TEM and revealed the presence of structures with clear angles and boundaries (Figure 20D). However, this result highlights the challenges in differentiation between BMCs and

lipid structures by TEM. The observed structures arose most likely due to a high lipid content of the samples occurring from treatment with detergents (YPER™ Plus).

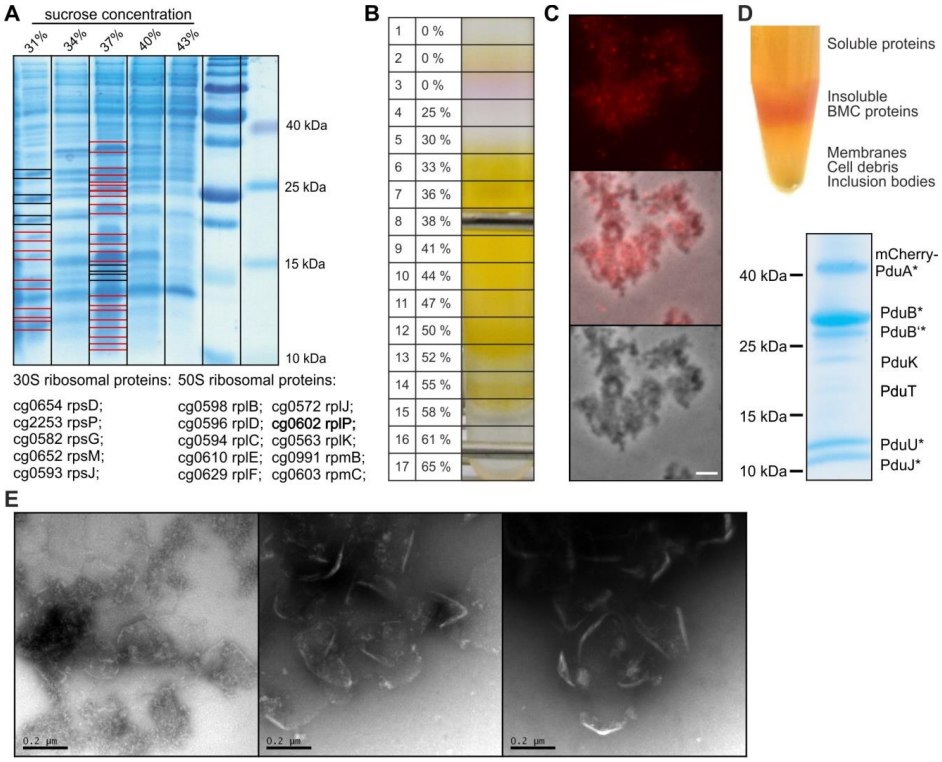

Figure 20: Approaches for (mCherry)PduABJKNUT purification. A Exemplary sucrose gradient during compartment purification (Sucrose gradient purification method in Section 2.6.3). Bands marked with a square were analyzed *via* MALDI-TOF-MS and red squares present the identification of ribosomal proteins. **B** Exemplary sucrose gradient within a 15 mL centrifuge tube. Within the middle of the gradient, the yellow color overlaid possible mCherry signal which can be seen in soluble Fraction 3. **C** Distinct mCherry foci localized to cell debris. Scale bar is 2 µm. **D** Eppendorf tube containing cell lysate within YPER™ Plus, centrifuged for 10 min at 11.000 *g*. Insoluble BMC fraction was found on top of cell debris. The purification of this fraction revealed relatively pure Pdu shell proteins, even though BMCs were most likely not properly formed (Dialysis purification method in Section 2.6.3). Proteins marked with an asterisk were identified by MALDI-TOF-MS. **E** TEM analysis of different PduABJKNUT purification fractions from YPER™ Plus purification (YPER™ Plus purification method in Section 2.6.3) showed structures, which could be considered as BMC-like structures, but are most probably artefacts.

After the production of BMC-like structures was confirmed for MB001(DE3) *pduABJkNut* and MB001(DE3) *pduABJknt* as reported in Section 3.1.4, further purification approaches were performed based on a previously published protocol (Lawrence *et al.*, 2014). After lysozyme digest, mechanical disruption methods with either sonication or French Press treatment were applied to lyse the cells. In Figure 21, an exemplary BMC purification with cell disruption by 10 min of sonication is shown. The fractions P1, S2 and FS should contain BMCs, however, not obvious enrichment of BMC proteins was

observed. The obtained protein yield in the final supernatant (FS) was very low, but three of six compartment shell proteins were detected by MALDI-TOF-MS. Overall, the purification did not significantly contribute to the verification of assembled compartment structures as the purified compartment fraction was not further analyzed by transmission electron microscopy. A similar purification approach using French Press treatment instead of sonication also did not result in concentration of compartment proteins (data not shown). It is assumed that purification approaches were hampered by the thick *C. glutamicum* cell wall which demands long and intense sonication for efficient cell breakup.

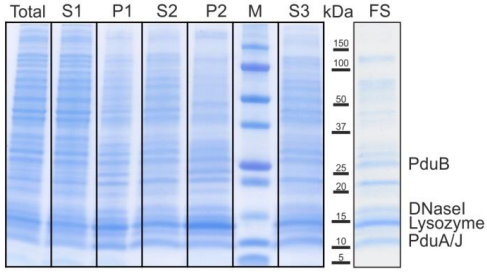

Figure 21: PduABJknt purification approach. (Total) Cell lysate of *C. glutamicum* MB001(DE3) *pduABJknt* in YPER™ Plus after centrifugation at 4000 *g*. (S1) Supernatant and (P1) BMC-containing pellet fraction after centrifugation at 11,000 *g* in YPER™ Plus. (S2) and (P2) from subsequent centrifugation at 11,000 *g* in 20 mM Tris-HCl, 20 mM NaCl; Supernatant should contain BMCs; After addition of 160 mM NaCl, BMCs should pellet into (P3) which was solubilized clarified with centrifugation step at 11,000 *g* and revealed (FS). The whole purification is described in Material and Methods Section 2.6.3 (YPER™ Plus purification).

3.1.8 Comparison of disruption methods for *C. glutamicum*

C. glutamicum showed a high tolerance to chemical and biochemical disruption methods like lytic enzymes as well as detergent-based lysis methods such as the commercially available Y-PER Yeast Protein Extraction Reagent and B-PER Bacterial Protein Extraction Reagents (data no shown). Commonly, mechanical disruption methods such as sonication, glass-bead homogenization and French Press treatment are used but these are intrusive methods to lyse *C. glutamicum*. Pdu BMCs are huge multiprotein complexes with a size of 100-200 nm in diameter and with harsh mechanical lysis methods, these structures are more likely to be damaged during cell disruption. With view on efficient compartment shell release more gentle methods of cell disruption would be preferable.

To reduce the mechanical forces applied on *C. glutamicum* to two mutant strains, *C. glutamicum* ATCC13032 Δ*ipsA* and *C. glutamicum* ATCC13032::P_{cg2732}*lcpA*, were tested as potential candidates for improved cell lysis. Both strains showed a significantly

reduced cell wall stability when lacking myoinositol or gluconate (Baumgart *et al.*, 2013; Baumgart *et al.*, 2016), These strains and *C. glutamicum* MB001(DE3) were precultivated in BHI complex medium. After washing and subsequent transfer of the cells into CGXII supplemented with 2% glucose, cells were cultivated for 16 h. The depletion of myoinositol caused an elongated phenotype of *C. glutamicum* ATCC13032 Δ*ipsA* and the absence of gluconate led to swollen *C. glutamicum* ATCC13032::P_{cg2732}*lcpA* cells as presented in Figure 22D. The cultures were harvested and used for lysis *via* lysozyme treatment, sonication and French Press treatment. The mutant strains and the control strain MB001(DE3) were treated with 4 mg mL^{-1} lysozyme for 6 h (Figure 22A).

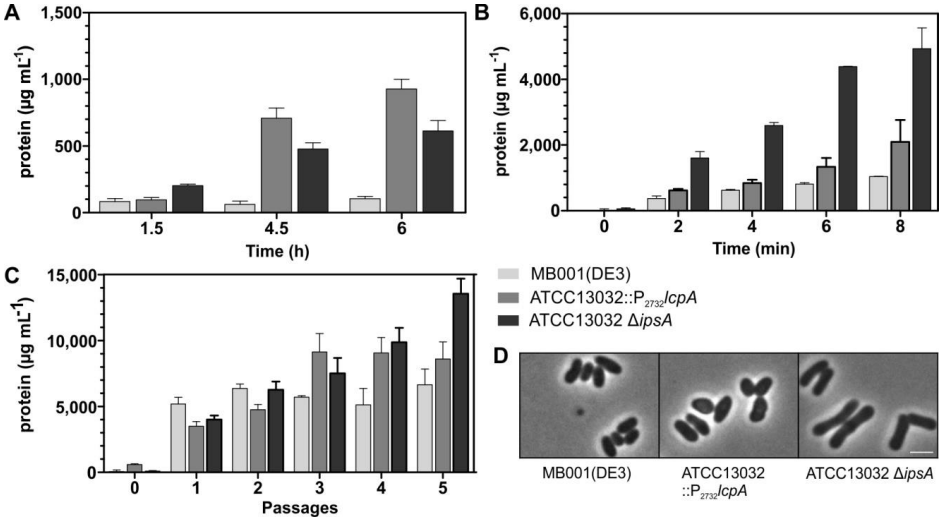

Figure 22: Treatment of cells suspensions with different lysis methods. A The protein concentrations were determined after incubation with 4 mg mL^{-1} lysozyme. **B** Ultrasonic cell homogenization was applied for 8 min (50% amplitude, 1 min intervals with 30 sec cooling, Branson Sonifier 250). **C** Cells were passed 5x through a French Press with a pressure of 20,000 psi. All protein concentrations were determined in technical triplicates. **D** Microscopy images of strains after 16 h of cultivation before cell lysis. Scale bar is 2 µm.

After 1.5 h incubation, the protein concentration in cell supernatant was measured and a slight effect was visible for both mutant strains with 1.2 and 2.4 times higher protein concentrations. After 4.5 h incubation, the protein release was significantly increased for ATCC13032 Δ*ipsA* and ATCC13032::P_{cg2732}*lcpA*. For sonication, 5 mL cell suspension in TEMP buffer was treated at an amplitude of 50% in 1 min intervals with 30 sec cooling in a Branson Sonifier 250. Protein concentration in the lysate supernatant was determined every 2 min (Figure 22B). After 2 min sonication, ATCC13032 Δ*ipsA* showed a higher sensitivity to sonication treatment than ATCC13032::P_{cg2732}*lcpA* and MB001(DE3). After 8 min, the amount of protein in the cell lysate supernatant of ATCC 13032::P_{cg2732}*lcpA* with 2,000 µg mL^{-1} protein and of ATCC13032 Δ*ipsA* with 4,931 µg mL^{-1} protein was

significantly higher than for the control strain MB001(DE3) with a concentration of 1,036 µg mL^{-1} protein. During French Press treatment, the cells were disrupted by passing them through a tiny hole with a pressure of 20,000 psi. ATCC13032 Δ*ipsA* was more susceptible to the treatment than the other two strains with a protein concentration of 13 µg mL^{-1} after 5 passages.

Summarizing, ATCC13032 Δ*ipsA* was significantly more sensitive to lysozyme incubation, sonication and French Press treatment than MB001(DE3) and might be an alternative strain for BMC production and subsequent BMC purification approaches.

3.2 Targeting of proteins of interest into BMCs

3.2.1 C-terminal targeting to BMCs with native and non-native encapsulation peptides

For the integration of heterologous pathways into BMCs, it would be of great advantage to choose between N- and C-terminal tag versions in order to identify the optimal tag for the particular protein of interest. From literature, it is known that the addition of targeting peptides often influences enzymatic activity (Lee *et al.*, 2016), which was also observed in this work (described in Sections 3.4.1-3.4.3).

Native targeting peptides have been described as amphipathic α-helices at the N- or C-terminus of enzymes. The proposed common mechanism is the interaction of the peptides with C-terminal α-helices of certain shell proteins or the epitopes of hexamer-hexamer interfaces (Kinney *et al.*, 2012; Aussignargues *et al.*, 2015). Therefore, it was investigated if the interaction of the P18 peptide with the shell proteins is still possible when it is moved to the C-terminus of the fluorescent protein. Additionally, two putative encapsulation peptides, natively present at the C-terminus of the aldehyde dehydrogenases (AdhDH) from compartments of unknown function from *Klebsiella pneumonia* ($C17_{K.p.}$) and *Proteus mirabilis* ($C17_{P.m.}$) (Aussignargues *et al.*, 2015), were tested. The composition of hydrophilic and aliphatic amino acids is very similar between the selected encapsulation peptides from AdhDH and the P18/D18 peptides (Table 23).

Table 23: Amino acid composition of different C- and N-terminal targeting peptides. The percentage of single or groups of amino acids is given. Adapted from Aussignargues *et al.*, 2015.

	Aliphatic I,L,V	Aromatic F,W,Y	Hydrophylic K,R,D,E,Q,N	Tiny G,A,S	H	C	M,T	P
AldhDH_C17, *Klebsiella pneumoniae*								
NEQNVERVIRQVLERLA	35.3%	0.0%	58.8%	5.9%	0.0%	0.0%	0.0%	0.0%
AldhDH_C17, *Proteus mirabilis*								
TEENVERIIKEVLGRLG	35.3%	0.0%	47.1%	11.8%	0.0%	0.0%	5.9%	0.0%
PduD(2-18), *Citrobacter freundii*								
NEKLLRQIIEDVLSEMQ	35.3%	0.0%	52.9%	5.9%	0.0%	0.0%	5.9%	0.0%
PduP(2-18), *Citrobacter freundii*								
NTSELETLIRNILSEQL	35.3 %	0.0 %	41.1 %	11.8%	0.0%	0.0%	11.8%	0.0%

According to fluorescence microscopy evaluation, the localization of eYFP to the compartments with the C-terminal P18 and $C17_{K.p.}$ peptides was observed, whereby the localization was more distinct for eYFP-P18 (Figure 23). With the C-terminal AdhDH sequence from *P. mirabilis*, localization of eYFP to the compartments could not be

observed. With this fluorescence microscopy studies, it cannot be stated to which extend eYFP-P18 and eYFP-C17$_{K.p.}$ are incorporated in comparison to P18eYFP.
Concluding, these data suggest that the P18 peptide may be used as N- or C-terminal fusion for the targeting of cargo protein into the PduABJknt lumen. Additionally, the C17$_{K.p.}$ peptide, which was not experimentally examined before, appeared to be sufficient to target eYFP to the compartment-like structures.

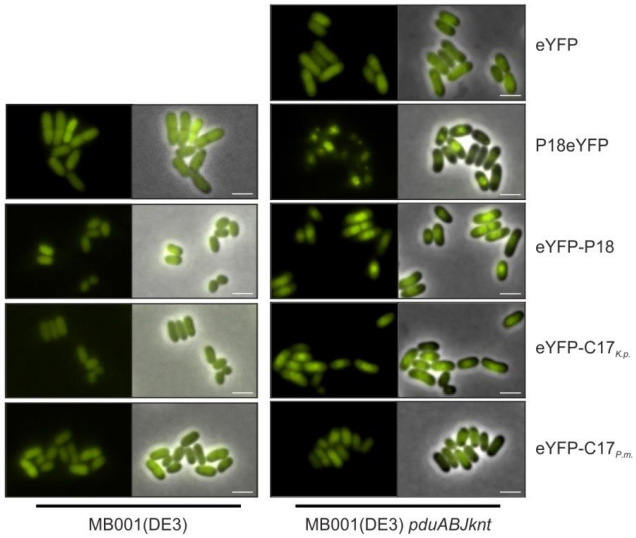

Figure 23: C-terminal targeting of eYFP to PduABJknt production strains. The fluorescence reporter eYFP was used to determine the localization of eYFP fused with different C- and N-terminal targeting peptides during coproduction of PduABJknt (50 µM IPTG) in *C. glutamicum* MB001(DE3). P18eYFP, eYFP-P18 and eYFP-C17$_{K.p.}$ showed clear localization in the mid part of the cell where the structures were proven to be located by TEM (Figure 15G).

3.2.2 Implementation of protein scaffolds for BMC targeting

Non-catalytic synthetic scaffolding proteins can provide engineered interactions between proteins. For example, combinations of interaction ligands and domains (namely PDZ, GBD and SH3 interaction partners) were utilized to target pathway enzymes to synthetic protein scaffolds (Dueber *et al.*, 2009). To enlarge the toolbox for synthetic BMC targeting peptides, the suitability of these scaffolds to C-terminally target a fluorescence reporter (tagged with the interaction domain) into the bacterial microcompartment lumen *via* PduA (tagged with the cognate interaction peptide ligand) was tested. For this purpose, the operon *pduABJknt* was adapted as follows: one of the three ligands (PDZ, GBD, and SH3) was C-terminally fused to *pduA* and an additional ribosome binding site was inserted between *pduA* and *pduB*, because the two genes overlap in the original operon structure.

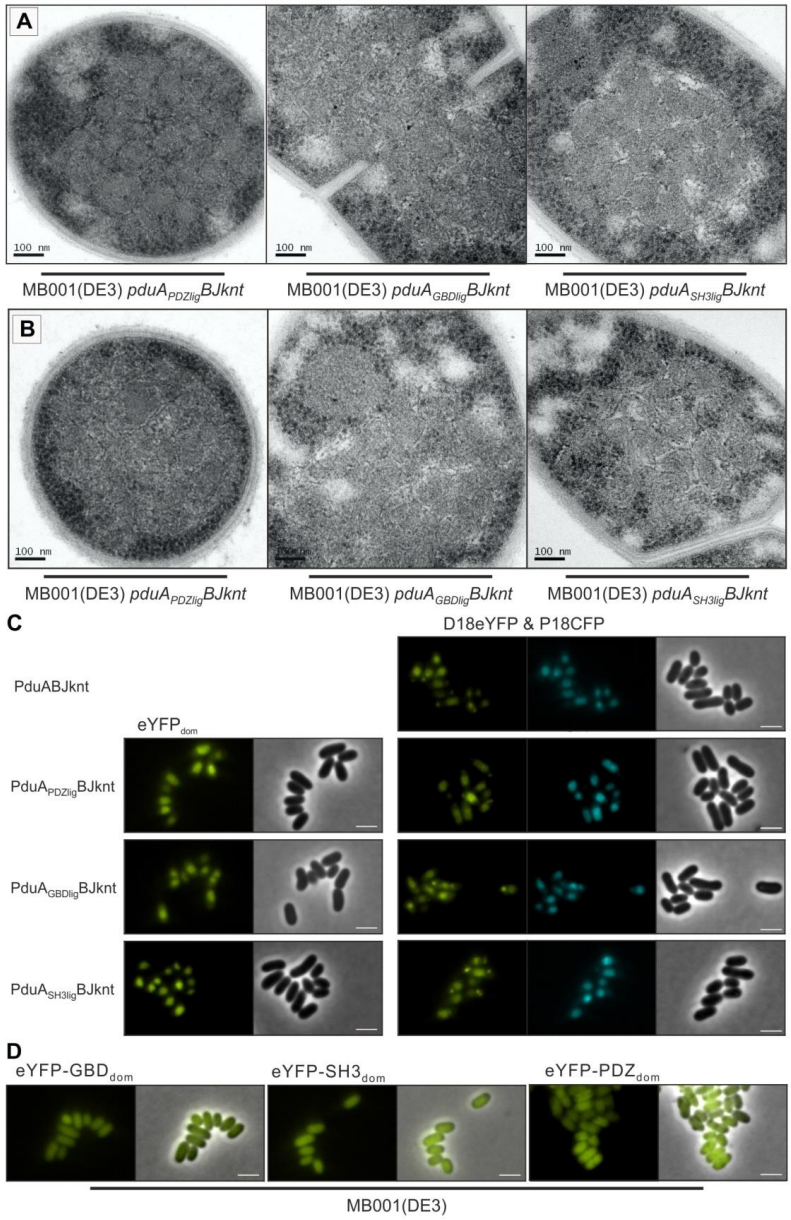

Figure 24: Production of PduA$_{lig}$BJknt BMCs and establishment of C-terminal targeting strategies. Thin sections of MB001(DE3) *pduA$_{PDZlig}$BJknt* MB001(DE3) *pduA$_{GBDlig}$BJknt* and MB001(DE3) *pduA$_{SH3lig}$BJknt* reveal **A** BMC-like structures and **B** incompletely formed BMCs within the cytosol 4 h after induction of protein production with 50 µM IPTG. **C** Localization of C- and N-terminally targeted fluorescence reporter (D18eYFP, P18CFP, eYFP$_{dom}$) to the cognate PduA$_{lig}$BJknt BMCs. The fluorescence pattern of eYFP$_{dom}$ was similar to those observed for the control MB001(DE3) *pduABJknt D18eyfp-P18cfp*. **D** Within the control strains MB001(DE3) *eyfp-GBD$_{dom}$*, MB001(DE3) *eyfp-SH3$_{dom}$* and MB001(DE3) *eyfp-PDZ$_{dom}$*, eYFP was equally distributed within the cytosol. Scale bar is 2 µm.

To verify that the ligand addition to one of the shell proteins does not interfere with the compartment assembly, TEM analysis was performed with MB001(DE3) *pduA*$_{PDZlig}$*BJknt*, MB001(DE3) *pduA*$_{GBDlig}$*BJknt* and MB001(DE3) *pduA*$_{SH3lig}$*BJknt* (Figure 24A/B).

The images provide evidence that the strains are able to form compartment-like structures with the additional ligands fused to PduA and were of similar shape as those produced in MB001(DE3) *pduABJknt*. Depending on the nature of the ligand at the C-terminus of PduA, BMC-like structures can be observed within 58% (PDZ_{lig}), 34% (GBD_{lig}) and 23% ($SH3_{lig}$) of the cells suggesting a measurable effect of the addition of synthetic scaffolds. However, it has to be noted that also misshaped structures and protein aggregates appeared in a considerable fraction of cells of all imaged samples (Figure 24B).

To test for intracellular colocalization, plasmids for the production of the BMC shell operons were cotransformed with plasmids encoding the cognate eYFP-PDZ_{dom}, eYFP-GBD_{dom} and eYFP-$SH3_{dom}$ interaction partners. For all three strains, the respective $eYFP_{dom}$ signal localized within the mid part of the cells suggesting that they had been entrapped within the compartments (Figure 24C). As control, *D18eyfp* and *P18cfp* were cotransformed with each *pduA*$_{lig}$*BJknt* version into MB001(DE3) and upon BMC and eYFP production, D18eYFP and P18CFP were able to localize to the compartments showing fluorescence patterns similar to those of $eYFP_{dom}$.

It appears that the addition of the C-terminal ligand does not interfere with interactions of PduA during BMC assembly or the functionality of native D18 or P18 peptides. Thus, in principle, both the C- and N-terminal versions can be combined to target different proteins into the lumen of $PduA_{PDZ}$BJknt, as this strain showed the highest number of cells with BMCs.

3.2.3 Activity of ethanol production enzymes enhanced by C-terminal targeting

As proof-of-principle, alcohol dehydrogenase (AdhB) tagged with one of the three synthetic C-terminal interaction domains SH3, GBD and PDZ and enzymatic activities should be determined. The constitutive P_{tuf} promoter was used for the production of the enzymes in MB001(DE3). The untagged AdhB version had an activity of 0.376 ± 0.045 U mg^{-1} cell extract (Figure 25). All C-terminal tagged AdhB versions (AdhB-GBD_{dom}, AdhB-PDZ_{dom}, AdhB-$SH3_{dom}$) had a similarly reduced activity with 0.119 ± 0.014 U mg^{-1}, 0.127 ± 0.016 U mg^{-1} and 0.133 ± 0.030 U mg^{-1} cell extract and were twice as high as the best D18-AdhB version with 0.067 ± 0.005 U mg^{-1} cell extract.

In comparison to the untagged AdhB version, the $AdhB_{dom}$ versions maintained 30% of their activity. With that, the C-terminal targeting of AdhB was proven to enhance enzyme

activity in comparison to the N-terminally tagged versions and provides a novel alternative for enzyme targeting into BMCs.

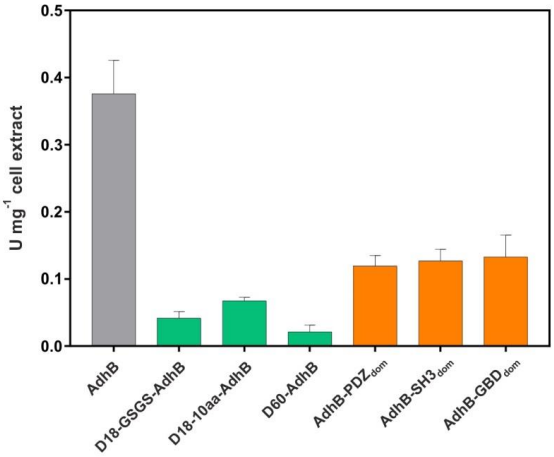

Figure 25: Activity measurements of AdhB versions in crude cell extracts of respective *C. glutamicum* MB001(DE3) production strains. The highest AdhB activity was observed for the untagged *adhB* variant (grey). For the C-terminally tagged *adhB* versions (orange) higher activities were determined than for N-terminally tagged *adhB* versions (green). One unit of specific activity was defined as conversion of 1 µmol NAD^+ per minute.

It could be inferred that the enhancement of activity with C-terminal targeting can be transferred to other metabolic enzymes of interest. It seems plausible to assume that the opportunity to choose between N- and C-terminal targeting peptides for each enzyme individually will increase the chances for the successful establishment of a respective pathway (see also Section 4.2 for further discussion).

3.3 Targeting proteins of interest onto Pdu-based scaffolds

3.3.1 PduA and PduJ form filaments in *C. glutamicum*

In several studies, it was demonstrated in different studies that the overexpression of *pduA* from *C. freundii*, encoding a major shell protein, leads to the formation of nanotube-like structures within the cytosol of *E. coli* cells (Parsons *et al.*, 2010; Pang *et al.*, 2014). Besides the potential of PduABJknt or PduABJkNut for the establishment of synthetic nanobioreactors, the usage of PduA filaments as protein scaffolds for the localization of key metabolic pathway enzymes was considered for *C. glutamicum.* Targeting of specific proteins of interest to PduA scaffolds may enhance metabolic pathway flux by substrate channeling and microdomain organization (James and Viola, 2002; Orita *et al.*, 2007; Chen and Silver, 2012; Lee *et al.*, 2012).

In this study, PduA was overproduced in *C. glutamicum* MB001(DE3) *pduA* by the addition of 50 µM IPTG to the cultivation medium. After 4 hours, TEM analysis of thin sections revealed that PduA did form large bundles of regular filaments within the cell with a diameter of ~17-20 nm for single filaments (Figure 26A). Since PduJ shares 80% sequence similarity to PduA, it was further investigated whether PduJ is also able to form similar filaments in *C. glutamicum*. TEM analysis of PduJ samples showed the regular and linear filamentous structures (20 ± 5 nm) as well as large linear structures which rolled up consisting of single filaments with a diameter of 4 ± 1.3 nm (Figure 26B). The finding that PduJ does not only to form filaments, but also angular structures, is consistent with the common opinion that PduJ is present at the edges to join the facets of the compartments allowing a proper closure of the compartment (Cheng *et al.*, 2011).

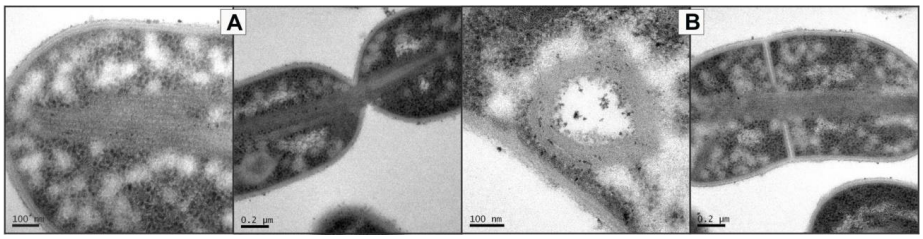

Figure 26: PduA and PduJ form filaments in *C. glutamicum*. A Upon induction with 50 µM IPTG, MB001(DE3) *pduA* produced large bundles of regular filaments. **B** PduJ formed linear filaments or rolled up filamentous structures.

3.3.2 N-terminal targeting peptides recruit eYFP to PduA scaffolds

In the two proteins PduA and PduJ, a C-terminal amphipathic motif is present which is thought to interact with the P18 and D18 peptide (Fan *et al.*, 2012). To investigate the

interaction of the two targeting peptides P18 and D18 with the PduA and PduJ structures in *C. glutamicum*, the genes were coexpressed with either *P18eyfp* or *D18eyfp*. Fluorescence microscopy analysis of the resulting strains revealed the successful recruitment of the reporter proteins D18eYFP and P18eYFP to PduA tubes (Figure 27A). With the production of P18eYFP$_{ASV}$ and PduA, no filaments were visible, suggesting the susceptibility of P18eYFP$_{ASV}$ to proteases. Furthermore, the MB001(DE3) *mcherrypduA* strain was investigated for the ability of PduA to produce filaments with the N-terminal addition of mCherry. It would be of advantage to have the opportunity to directly tag a fluorescence reporter to a BMC shell protein. However, mCherryPduA was unable to form filamentous structures and mCherry and eYFP signals in the respective strains were distributed within the whole cytosol (Figure 27B).

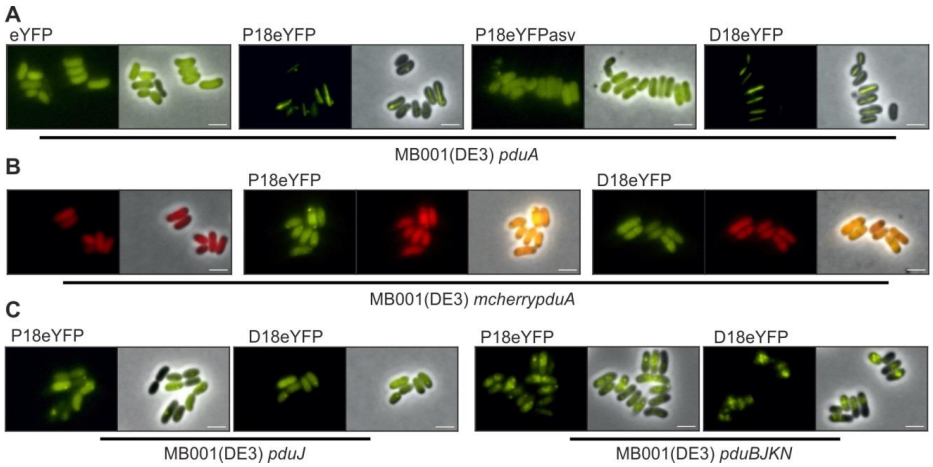

Figure 27: Characterization of P18 and D18 interaction with PduA and PduJ. A PduA and **B** mCherryPduA were coproduced with different eYFP fluorescence reporters in *C. glutamicum* MB001(DE3) and fluorescence microscopy analysis revealed colocalization of PduA with P18eYFP and D18eYFP. **C** No direct interaction of P18 and D18 peptides with PduJ filaments were observable, but interactions with one or more proteins encoded in the *pduBJKN* operon are indicated by the distinct localizations. Scale bar is 2 µm.

The fact that PduJ is able to form filaments was proven by TEM. However, no localization of eYFP to PduJ filaments was achieved with the D18/P18 peptides. By fluorescence microscopy, it cannot be concluded whether PduJ is targeted by the encapsulation peptides P18 or D18. Anyhow, a strain containing the operon *pduBJKN*, which was not intended to form compartments, was used to study further interaction partners of P18 and D18. The production of P18eYFP and D18eYFP with PduBJKN revealed distinct loci within the cells providing evidence that at least one of the shell proteins, besides PduA, is able to bind the targeting peptides (Figure 27C).

Based on these data and with regard to an application of the shell proteins as scaffolds, PduA seems to be the most promising candidate. To have a stable PduA production

strain, the *pduA* gene was genomically integrated into the same genomic locus as described before for *pduABJknt*. Growth studies revealed a more significant influence of the PduA production on cellular growth than the production of PduABJknt (comparing Figure 19B and Figure 28A). It is likely to assume that the filamentous structures have a stronger impact on the growth than the BMC structures, since the filaments may interfere strongly with cell division machinery as shown by TEM images (Figure 26A). Using plasmid-expressed D18eYFP and P18eYFP, the assembly of PduA filaments in MB001(DE3)::P_{T7}*pduA* was confirmed by fluorescence microscopy (Figure 28B).

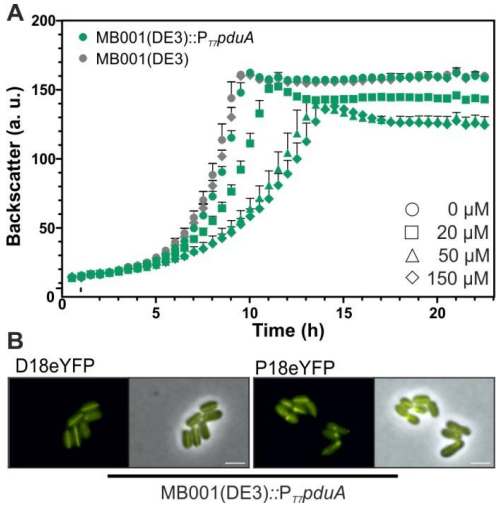

Figure 28: Growth and fluorescence microscopy analysis of *C. glutamicum* MB001(DE3)::P_{T7}*pduA* strains. A The growth performance was determined by cultivation experiments in standard CGXII medium supplemented with 2% (w/v) glucose using the BioLector® device and different IPTG inducer concentrations (0, 20, 50 and 150 µM IPTG). A strong growth defect was observed for PduA production when induced with 50 µM and 100 µM IPTG. **B** The coproduction of D18eYFP and P18eYFP with PduA showed the successful assembly of PduA filaments with the genome-based expression of *pduA* with 100 µM IPTG in MB001(DE3)::P_{T7}*pduA*.

3.3.3 C-terminal targeting to PduA is possible by using PDZ and GBD interactions

To test if C-terminal targeting to PduA filaments is possible, one of the three ligands (GBD, SH3 or PDZ) were C-terminally fused to *pduA* and coexpressed with the cognate interaction domain-tagged to eYFP in the *C. glutamicum* strain MB001(DE3). With the coproduction of PduA-GBD_{lig} together with eYFP-GBD_{dom}, and PduA-PDZ_{lig} together with eYFP-PDZ_{dom} in MB001(DE3) the targeting to the filaments was successfully proven with the visualization of the filaments *via* fluorescence microscopy (Figure 29). However, for the combination of *PduA*$_{SH3lig}$ and *eYFP-SH3*$_{dom}$, the fluorescence signal was evenly distributed in the cytosol. To examine whether the SH3 ligand impairs filament assembly,

$PduA_{SH3lig}$ was also coproduced with D18eYFP. Since no filamentous structures or loci were visible, it can be concluded that the SH3 ligand is interfering the proper assembly of $PduA_{SH3lig}$. As the fluorescence signal from D18eYFP coproduced with either $PduA_{PDZlig}$ or $PduA_{GBDlig}$ localizes to filaments, it can be assumed that they are not restricted in their ability to assemble.

$PduA_{PDZlig}$ and $PduA_{GBDlig}$ offer the possibility to either C-terminally (with proteins fused to PDZ/GBD domain) or N-terminally (with the native P18 and D18 peptide) target proteins of interest to the filaments.

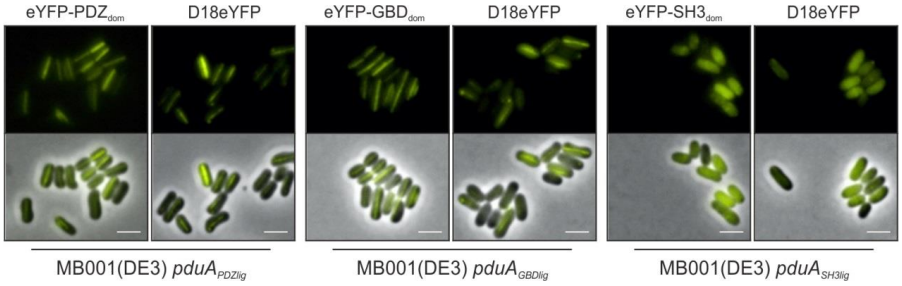

Figure 29: Distribution of $eYFP_{dom}$ with coproduction of the cognate $PduA_{lig}$ version. eYFP-PDZ_{dom} and eYFP-GBD_{dom} localize to the respective $PduA_{lig}$ filaments. $PduA_{SH3lig}$ seemed not to form filaments, as neither eYFP-$SH3_{dom}$ nor D18eYFP showed a distinct localization within the cytosol. The images were taken 4 h after induction of Pdu_{lig} production with 50 µM IPTG. Scale bar is 2 µm.

3.4 Towards a biotechnological application of BMCs

In nature, the production of BMCs allows the respective organism to catabolize substrates, whose conversion lead to the formation of toxic or volatile intermediates. Furthermore, BMCs can enhance ineffective reactions of enzymes with low turnover rates or suppress competing reactions by intermediate sequestration (Chen and Silver, 2012). In the same way, the utilization of synthetic BMCs in heterologous organisms, like the industrially important platform strain *C. glutamicum*, could be of great advantage for certain metabolic pathways.

In the following, three pathways which have the potential to be optimized by the usage of BMCs, and which were established before in *C. glutamicum*, were further evaluated with regard to an application in BMCs:

i. *C. glutamicum* was engineered to produce ethanol by the introduction of a pyruvate decarboxylase and an alcohol dehydrogenase from *Z. mobilis* and a recent publication showed the synthetic application of BMCs for ethanol production in *E. coli* (Lawrence *et al.*, 2014).
ii. Witthoff *et al.* engineered *C. glutamicum* to utilize methanol as a carbon source which involves the toxic metabolite formaldehyde (Witthoff *et al.*, 2015). Hence, using this pathway in BMCs, may minimize toxic effects of the intermediate formaldehyde.
iii. Itaconic acid is a reactive compound with a broad spectrum of applications and itaconate production was established in *C. glutamicum* (Otten *et al.,* 2015). With the usage of BMCs and the encapsulation of the two enzymes Acn and Cad, it is assumed that the itaconate production, which is limited by the supply of cis-aconitate for the Cad reaction, may be enhanced.

3.4.1 Ethanol production within BMCs in *C. glutamicum*

The ethanol production pathway was chosen as a target for encapsulation into BMCs to circumvent acetaldehyde toxicity occurring when pyruvate is converted to acetaldehyde catalyzed by the pyruvate decarboxylase (Figure 4). Ethanol was already successfully produced within BMCs in the heterologous host *E. coli* (Lawrence *et al.*, 2014), which emphasized this pathway as an appropriate proof-of-principle approach for implementation into BMCs in *C. glutamicum*. With this aim, a master thesis was performed by Kira Natascha Ludwig and the main results are described in the following, as they are the basis of the study pursued during this work (Ludwig, 2016). In order to localize the two enzymes for ethanol production from pyruvate (AdhB and Pdc from *Z. mobilis*) into BMCs, the two genes were fused with either the D18 or the P18 EP to

determine the influence of the EPs on the enzymatic activity. For the native AdhB, which was produced under control of the constitutive P_{tuf} promoter in *C. glutamicum* MB001(DE3), the highest enzymatic activity was determined showing an activity of 0.795 ± 0.017 U mg^{-1} protein within crude cell extract (Ludwig, 2016). Five D18 peptide versions using different linker sequences were tagged to AdhB and activity assays demonstrated an at least six times lower enzyme activity. D18-GSGS-AdhB had the highest activity with 0.131 ± 0.024 U mg^{-1} protein (Ludwig, 2016). The activity measurements of the native Pdc and three P18 peptide tagged versions revealed no noticeable negative influences of the targeting peptides (Ludwig, 2016).

Based on these results, an ethanol production plasmid with the untagged enzyme variants P_{tuf}*adhB_pdc* and two plasmids with the EP-tagged enzyme variants P_{tuf}*D18-GSGS-adhB_P18pdc* and P_{tuf}*D18-10aa-adhB_P18pdc* were constructed and evaluated in the MB001(DE3) *pduABJKNUT* production strains (Ludwig, 2016). However, in the course of this study, the prodction of BMCs with *pduABJKNUT* was disconfirmed. For this reason, the enzyme production plasmids were further used in the present work in the BMC production strain MB001(DE3)::P_{T7}*pduABJknt* for which compartment-like structures were observed with TEM analysis (Figure 19C). Additionally, the PduA production strain MB001(DE3)::P_{T7}*pduA* was evaluated on its potential to use the assembled PduA filaments as scaffolds to colocalize the ethanol production enzymes. MB001(DE3) strains containing the respective ethanol production plasmids served as controls.

First, the growth performance of all strains was examined by aerobic cultivations in standard CGXII with 2% (w/v) glucose in the BioLector® microbioreactor device for 24 h (Figure 30). In the respective strains, ethanol production enzymes were produced constitutively under control of P_{tuf} and the production of PduA and PduABJknt was induced with the addition of 50 µM IPTG. In all MB001(DE3) and MB001D(E3)::P_{T7}*pduABJknt* strains, the constitutive production of the different AdhB/Pdc enzyme variants caused only a minimal negative effect on growth (0.457-0.460 h^{-1}, 0 µM IPTG) in comparison to MB001(DE3) wild type with a growth rate of ~0.510 h^{-1} (Table S9). Furthermore, for all MB001(DE3)::P_{T7}*pduA* containing the different AdhB/Pdc enzyme variants, the growth rates were slightly reduced (0.413-0.415 h^{-1},) without IPTG supplementation and further declined with PduA coproduction (0.276-0.280 h^{-1}). The induction of PduABJknt production in MB001(DE3)::P_{T7}*pduABJknt* strains containing the ethanol production modules led to a less pronounced decrease in growth rates within a range of 0.351-0.362 h^{-1}. The amount of ethanol that was produced during this experiment was not calculated because it was known from experiments performed by

Kira Ludwig that the aerobic cultivation of the ethanol production strains led to ethanol contents below the quantification limit of the HPLC.

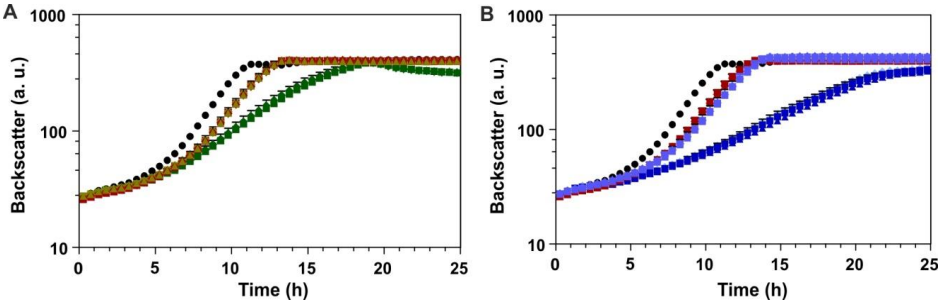

Figure 30: Aerobic cultivation of ethanol production strains. MB001(DE3) (black) was used as control for optimal growth. MB001(DE3) (red, squares), **A** MB001(DE3)::P_{T7}*pduABJknt* (green) and **B** MB001(DE3)::P_{T7}*pduA* (blue) produced AdhB/Pdc, D18-GGSG-AdhB/P18Pdc or D18-GGSG-AdhB/P18Pdc and showed very similar growth performances. Induction of PduABJknt (50 µM, dark green) and PduA (50 µM, dark blue) production resulted in declined growth, whereby strains producing PduA were more influenced.

To determine ethanol production titers, the strains used for the growth studies were cultivated in 50 mL CGXII medium with 2% (w/v) glucose in 100 mL shaking flasks at 30 °C and 140 rpm for 60 h. With the filling height of the flasks and no aeration, a reduction of O_2 supply should be achieved (adapted from Inui *et al.*, 2004). Therefore, this approach is referred as 'semi-anaerobic' cultivation. The ethanol content within the culture supernatants was measured after 24 h, 30 h, 48 h and 60 h of cultivation using HPLC. The summarized results with all ethanol titers are listed in Table S10 and Table S11 in the Appendix. The peak in ethanol production was reached after 48 h for all strains in the presence and absence of IPTG and the results are presented in Figure 31.
The strains MB001(DE3)::P_{T7}*pduA adhB_pdc* and MB001(DE3)::P_{T7}*pduA D18-GSGS-adhB_P18pdc* reached the highest ethanol titers, however, without the production of PduA (129.07 mM and 135.46 mM ethanol; 0 µM IPTG). The strains coproducing PduA or PduABJknt (induced with 50 µM IPTG) had consistently lower titers than the uninduced strains. An interesting exception was shown by the strain MB001(DE3)::P_{T7}*pduABJknt D18-10aa-adhB_P18pdc* which produced 126.29 mM ethanol when PduABJknt was coproduced in comparison to the 85.23 mM ethanol without induction of the operon. This result indicates a positive effect of tagged enzymes and BMC coproduction on ethanol titers since the ethanogenic control strain MB001(DE3), containing untagged enzyme variants AdhB/Pdc, showed slightly lower ethanol titers with 104.6 mM ethanol. The production of PduABJknt in MB001(DE3)::P_{T7}*pduABJknt D18-GGSG-adhB/P18pdc*, a strain with a lower AdhB

activity (Figure 25), did not show an enhanced ethanol production (85.84 mM ethanol if induced with IPTG and 89.14 mM ethanol without *pduABJknt* induction).

Concluding, even though PduABJknt coproduction had an positive effect in MB001(DE3)::P_{T7}*pduABJknt* D18-10aa-AdhB/P18Pdc, the ethanol production data collected here are preliminary work and the influence of different factors besides BMC production requires further investigations.

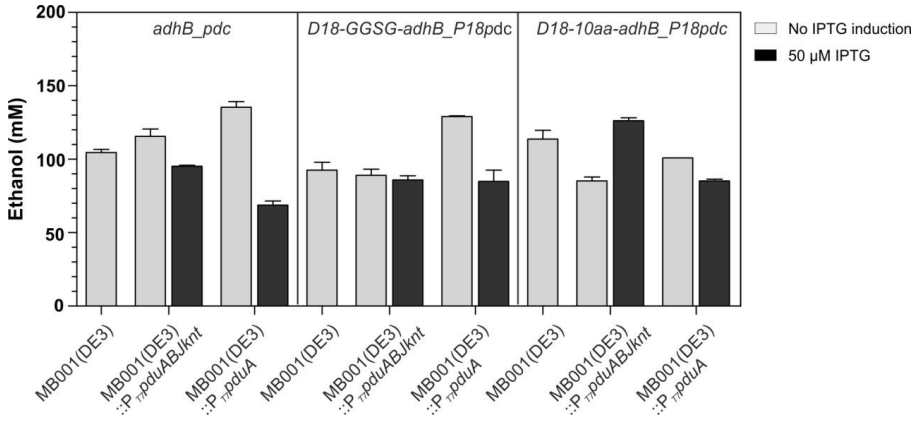

Figure 31: Application of optimized Pdu compartments and PduA filaments for ethanol production in *C. glutamicum*. The strains MB001(DE3), MB001(DE3)::P_{T7}*pduABJknt* and MB001(DE3)::P_{T7}*pduA* were analyzed with the enzyme combinations Pdc/AdhB, D18-10aa-AdhB/P18Pdc and D18-GGSG-AdhB/Pdc on their performance to produce ethanol. Ethanol production was assayed after 48 h of cultivation under 'semi-anaerobic' conditions with and without the coproduction of BMCs by HPLC analysis. The ethanol content was measured within sample supernatants of two biological replicates. Error bars represent the range of the two measured samples. Dark grey: 50 µM IPTG; light grey: 0 µM IPTG;

Another consideration, which should be further investigated, is whether there is an influence of the growth performance of a strain on the final ethanol production titers. For example, the control strain MB001(DE3)::P_{T7}*pduABJknt adhB_pdc* produced a final ethanol titer of 115.6 mM ethanol without PduABJknt production and a reduced titer of 95.3 mM ethanol when BMCs were coproduced. Concurrently, there was a moderate growth decline upon Pdu production under aerobic conditions (Figure 30A). A similar result was obtained for MB001(DE3)::P_{T7}*pduA adhB_pdc*, whose ethanol production was even lower with 68.67 mM ethanol when PduA was coproduced in comparison to 135.46 mM ethanol without PduA coproduction. Looking at the growth under aerobic cultivation conditions, PduA production had a drastic negative effect on growth performance (Figure 30), which might explain the lowered ethanol production titers upon Pdu induction.

3.4.2 Methanol consumption within BMCs

There are recent advances in the metabolic engineering of *C. glutamicum* to utilize methanol as a cheap and renewable carbon source in industrial production processes (Witthoff *et al.*, 2015). In *C. glutamicum*, the consumption of methanol was enabled *via* the ribulose monophosphate pathway with the introduction of four crucial enzymes from *B. methanolicus* (Mdh and Act) and *B. subtilis* (Hps and Phi) (Witthoff *et al.,* 2015). The two main bottlenecks of methanol consumption are on the one hand the accumulation of the toxic intermediate formaldehyde and on the other hand a competing endogenous pathway for formaldehyde detoxification by oxidation of methanol to carbon dioxide which cannot be used as a carbon source (Witthoff *et al.*, 2015).

The studies performed in this work aimed at the encapsulation of the heterologous methanol consumption pathway into the synthetic BMCs in the important industrial platform organism *C. glutamicum*. The assumption was that this approach can be used to overcome the stated limitations of methanol consumption and toxic aldehyde levels. This objective should be reached by production of BMCs and the integration of the critical enzymes for the metabolization of methanol to a C_6-sugar in the microcompartment lumen.

Two existing modules for methanol oxidation and formaldehyde assimilation located on the plasmids pEKEx2-P_{tuf}Bm(*mdh_act*) and pVWEx2-P_{tuf}Bs(*hps_phi*) (Witthoff *et al.*, 2015), respectively, were modified with the D18 an P18 EPs for a subsequent localization of those enzymes within BMCs. First, the plasmid variants listed in Table 24 were constructed, transferred into *C. glutamicum* MB001(DE3) and tested on their enzymatic activity.

Table 24: Plasmid variants for the methanol metabolism in *C. glutamicum.* The volumetric enzyme activity was baseline-corrected by the activity of *C. glutamicum* MB001(DE3) wild type.

Methanol oxidation module	Volumetric enzyme activity	Formaldehyde assimilation module	Volumetric enzyme activity
P_{tuf}Bm(*mdh_act*)	0.08 U µL^{-1}	P_{tuf}Bs(*hps_phi*)	0.10 U µL^{-1}
P_{tuf}Bm(*mdh*)	No specific activity	P_{tuf}Bs(*D18hps_P18phi*)	No specific activity
P_{tuf}Bm(*D18mdh*)		P_{tuf}Bs(*D18hps_phi*)	
		P_{tuf}Bs(*D18-GS-hps_phi*)	
		P_{tuf}Bs(*D18-GGSG-hps_phi*)	
		P_{tuf}Bs(*D18-10aa-hps_phi*)	

The extent of the impact of the activator protein (Act) on the methanol dehydrogenase activity *in vivo* is unknown. In *in vitro* experiments, Act showed a positive effect on the Mdh activity, however, Mdh activity was also measurable without Act (Ochsner *et al.*, 2014). Because it would be of advantage to reduce the number of enzymes which have to be targeted to BMCs, the activity of Mdh without the activator protein was determined

with and without the addition of the D18 targeting peptide to Mdh. The enzyme activity of crude extracts of those strains were assayed, but no specific activity could be determined for Mdh and D18Mdh. Importantly, the results shown here point out that the Act protein is required in *in vitro* assays for Mdh activity.

To determine the activity of the modified formaldehyde assimilation module variants of pVWEx2_Bs(*hps_phi*), shown in Table 24, *in vitro* assays with crude cell extracts were performed in a coupled Hps-Phi assay. For the tagged enzyme versions produced by MB001(DE3) P_{tuf}Bs(*D18hps_P18phi*), no specific activity was determined. Because of that, four plasmid variants containing *hps* tagged to the D18 targeting peptide with different linker sequences (no linker; GS; GGSG; GENLYFQSGG(10 aa)) and the untagged *phi* version were created and tested. However, neither the addition of linker sequences nor the usage of the untagged Phi version could restore the enzyme activity. From these results, it can be concluded that Hps is not active with the N-terminal addition of the D18 encapsulation peptide independent from the used linker. A reason for that might be that the targeting peptide disturbed the enzyme activity and/or the proper protein folding. This suggestion is supported by the finding that a direct fusion of *phi* to the N-terminus of *hps* also led to no enzyme activity (Orita *et al.*, 2007).

The functionality of the C-terminal targeting peptide versions (described in chapter 3.2.1) was validated in the end of this work and, therefore, the peptides were not tested whether they have an influence on the activity of *hps*. However, future work is planned with enzymatic activity assays of C-terminally tagged Hps versions.

3.4.3 Establishing itaconate production within Pdu shells

Besides the chemical synthesis of the industrially relevant compound itaconic acid, it is also produced by fungi like *Aspergillus terreus*, *Ustilago maydis* or *Candida sp*. (Okabe *et al.*, 2009). So far, there are no bacteria known which are natively able to produce itaconic acid. In former studies, *C. glutamicum* was engineered to produce itaconate by the overproduction of a codon optimized cis-aconitate decarboxylase from *A. terreus* (Otten *et al.*, 2015). Itaconate is build up from the intermediate cis-aconitate *via* Cad. In *C. glutamicum*, cis-aconitate is formed through the aconitase reaction within the citrate cycle which catalyzes the reversible isomerization of citrate to isocitrate over cis-aconitate (Figure 5).

The aim of this research was to produce the unsaturated dicarboxylic acid itaconate within the Pdu compartments from *C. freundii* in the heterologous host *C. glutamicum.* It was assumed that the targeting of the enzymes Acn and Cad into the BMCs can provide a better supply of cis-aconitate for the Cad reaction and, therefore, enhance the final

titers. Since the TCA cycle is a central metabolic pathway with a high flux, it seems likely that cis-aconitate availability is the major bottleneck of itaconate production. With the conversion of citrate within the compartments, the competing reaction from isocitrate to 2-oxoglutarate *via* the isocitrate dehydrogenase (Icd) within the TCA cycle might be circumvented.

The following sections focus on the determination of enzymatic activities of Acn and Cad with N-terminal targeting peptides and the influence of the enzymes Acn, Cad and Icd on the final itaconate production. The last part presents the results that were obtained with different *C. glutamicum* strains, in which the Pdu shell proteins were coproduced with the itaconate production enzymes.

Activity assays of Acn and Cad variants with the encapsulation peptides

The first step for the establishment of an itaconate production pathway within BMCs was to modify the enzymes Cad (*cad1*, *Aspergillus terreus*) and Acn (cg1737, *C. glutamicum*) to allow their targeting into the BMCs. The two enzymes were chosen on the basis of the work from Andreas Otten (Otten, 2013; Otten *et al.*, 2015). In his studies, a codon optimized version of Cad was fused to a maltose binding protein (*malEcad*) for stabilization and showed the highest activity. Different heterologous aconitase genes were tested by exchanging the native aconitase from *C. glutamicum* but the highest itaconate titer was achieved with the native one (Otten, 2013).

To determine the influence of the encapsulation peptides P18 and D18 on MalECad and Acn activities, the genes encoding the two enzymes were cloned separately with and without the targeting peptides under control of an IPTG inducible P_{tac} promoter in a pEKEx2 vector. *C. glutamicum* MB001(DE3) strains were transformed with the plasmids, resulting in the strains MB001(DE3) *malEcad*, MB001(DE3) *P18malEcad*, MB001(DE3) *acn* and MB001(DE3) *D18acn.*

Table 25: Determination of enzyme activity of MalECad and Acn variants in crude cell extracts. One unit (U) of Cad activity corresponds to the conversion of 1 µmol cis-aconitate to itaconate within 1 min. For the aconitase reaction, one unit is defined as the formation of 1 µmol cis-aconitate within 1 min.

Strain	Cad activity (mU mg^{-1} protein)	Strain	Acn activity (mU mg^{-1} protein)
MB001(DE3) *malEcad*	4.85 ± 0.12	MB001(DE3) *acn*	0.74 ± 0.16
MB001(DE3) *P18malEcad*	1.68 ± 0.20	MB001(DE3) *D18acn*	0.66 ± 0.18
MB001(DE3) pEKEx2	0.00 ± 0.00	MB001(DE3) pEKEx2	0.23 ±0.04

The strains MB001(DE3) *P18malEcad*, MB001(DE3) *malEcad* and MB001(DE3) pEKEx2 were grown for 24 h in CGXII with 2% (w/v) glucose and 0.5 mM IPTG. The formation of itaconate was determined *via* HPLC measurements afterwards. *In vitro* assays of the Cad enzyme were performed with crude cell extracts. The specific activities were

calculated to be 4.85 ± 0.12 mU mg^{-1} protein for MB001(DE3) *malEcad* and 1.68 ± 0.20 mU mg^{-1} protein for MB001(DE3) *P18malEcad* (Table 25). For the negative control MB001(DE3) pEKEx2, no itaconate production was detected.

The aconitase activity assay was conducted with crude cell extracts of MB001(DE3) *acn*, MB001(DE3) *D18acn* and MB001(DE3) pEKEx2 grown to a final OD_{600} of 5 in CGXII medium supplemented with 2% glucose. Isocitrate was used as substrate and the formation of cis-aconitate was determined with the increase in absorption at 240 nm. The activity measurements of MB001(DE3) pEKEx2 revealed a background activity of the native aconitase of 0.23 ± 0.04 mU mg^{-1} crude extract (Table 25). The overexpression of the native aconitase in MB001(DE3) *acn* resulted in a specific activity 0.74 ± 0.16 mU mg^{-1} protein and the D18 tagged version of the aconitase in MB001(DE3) *D18acn* reached an activity of 0.66 ± 0.18 mU mg^{-1} crude cell extract.

In conclusion, the performed enzyme activity assays revealed that the addition of the D18 peptide had a minor effect on the aconitase with a 10% decrease in activity in comparison to the untagged aconitase version. For MalECad, the addition of the P18 peptide led to more pronounced effect with an activity reduced to 35%.

Growth and itaconate production of MB001(DE3) acn_malECad and MB001(DE3) acn_malECad (without BMCs)

With regard to an application of itaconate production within BMCs, the genes of the two enzymes were cloned into the same operon under the control of the constitutive P_{tuf} promoter. As the activities of the tagged enzyme versions were successfully verified, two plasmids containing either the tagged (pVWEx2-P_{tuf}*D18acn_P18malEcad*) or the untagged (pVWEx2-P_{tuf}*acn_malEcad*) enzyme variants were constructed. The resulting strains MB001(DE3) *acn_malEcad*, MB001(DE3) D18*acn_P18malEcad* and the control strain MB001(DE3) pVWEx2 were analyzed regarding growth and itaconate production using the BioLector® microbioreactor system. Two different growth conditions were applied: (i) growth under standard conditions in CGXII supplemented with 2% (w/v) glucose and (ii) growth under nitrogen-limited conditions in N-limited CGXII supplemented with 2% (w/v) glucose. N-limited media were prepared by the addition of only 1 g L^{-1} urea (instead of 5 g L^{-1}) and the depletion of ammonium sulfate (20 g L^{-1} in standard CGXII medium). It was shown before that nitrogen-limitation drastically enhanced the itaconate production in *C. glutamicum* ATTC13032 *malEcad* (Otten *et al.*, 2015).

In standard CGXII medium, the empty vector control MB001(DE3) pVWEx2 had a growth rate of 0.49 ± 0.01 h^{-1}. MB001(DE3) *acn_malEcad*, constitutively producing Acn and MalECad, showed only a slightly impaired growth (0.43 ± 0.01 h^{-1}), whereby

MB001(DE3) *D18acn_P18malEcad* showed a stronger impairment (0.36 ± 0.01 h^{-1}) (Figure 32A and Table 26). Under nitrogen-limited conditions, all strains had a ~50% decreased final backscatter signal but the growth rates were less influenced by the enzyme production (growth rates: 5.0 ± 0.01 h^{-1} for MB001(DE3) pVWEx2, 4.93 ± 0.02 h^{-1} for MB001(DE3) *acn_malEcad* and 0.45 ± 0.01 h^{-1} for MB001(DE3) *D18acn_P18malEcad*, Figure 32B and Table 26).

The production of itaconate was measured within the culture supernatants of two biological replicates after 25 h of cultivation by HPLC analysis. The harvesting time point was chosen on basis of the work from Andreas Otten, showing that the main itaconate production started in the stationary phase (Otten *et al.*, 2015).

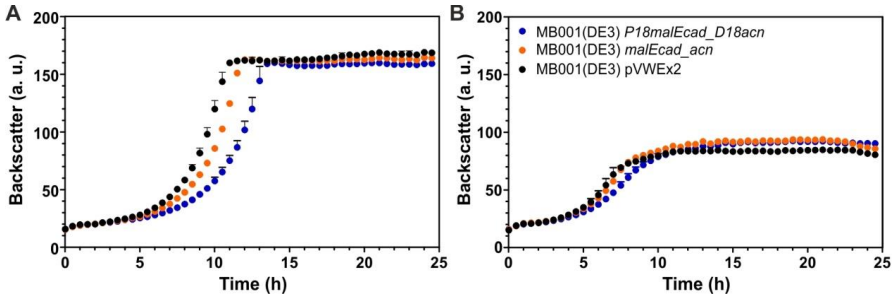

Figure 32: Growth of Acn/MalECad and D18Acn/P18MalECad production strains under different conditions in the BioLector®. The enzymes were constitutively expressed under the control of the P_{tuf} promoter. **A** Growth of MB001(DE3) pVWEx2, MB001(DE3) *acn_malEcad* and MB001(DE3) D18*acn_P18malEcad* in standard CGXII + 2% (w/v) glucose. **B** Growth of MB001(DE3) pVWEx2, MB001(DE3) *acn_malEcad* and MB001(DE3) D18*acn_P18malEcad* nitrogen-limited CGXII + 2% (w/v) glucose.

The negative control strain MB001(DE3) pVWEx2 revealed no itaconate production (Table 26). The final itaconate titers for MB001(DE3) *acn_malEcad* and MB001(DE3) *D18acn_P18malEcad* were drastically enhanced by the usage of N-limited CGXII medium in comparison to standard CGXII medium. For MB001(DE3) *acn_malEcad*, the final titer increased from 0.010 ± 0.00 mM to 1.25 ± 0.04 mM itaconate and for MB001(DE3) *D18acn_P18malEcad* from 0.02 ± 0.01 mM to a titer of 1.28 ± 0.01 mM itaconate (Table 26). The drastic enhancement of itaconate titers under N-limited conditions is in accordance with the data from Otten *et al.* (Otten *et al.*, 2015). Nevertheless, MB001(DE3) *acn_malEcad* and MB001(DE3) D18*acn*_P18*malEcad* produced significantly less itaconate (Table 26) than the published strain *C. glutamicum* ATCC13032 P_{tac}*malEcad* with 1.6 mM itaconate after 24 h of cultivation in CGXII with 4% glucose and 17 ± 5 mM itaconate after 24 h of cultivation in N-limited CGXII + 4% glucose (Otten *et al.*, 2015). To explain this, the most significant differences to the study from Otten *et al.* in the experimental design are summarized in Table 27.

Performing the growth studies and the itaconate production experiments in the BioLector® device has some great advantages in terms of parallel cultivation and the handling of samples. To ensure, that the microbioreactor is an appropriate cultivation device for itaconate production studies, MB001(DE3) D18*acn*_P18*malEcad* and MB001(DE3) *acn_malEcad* were also cultivated within shaking flasks in 50 mL N-limited CGXII medium with 2% (w/v) glucose for 25 h and the titers were compared to those obtained in the BioLector® microbioreactor.

Table 26: Growth and itaconate production of MB001(DE3) *acn_malEcad* and MB001(DE3) *D18acn_P18malEcad* under different conditions. The enzymes were constitutively expressed under control of P_{tuf}. The itaconate production was determined after 25 h of cultivation by HPLC.

Condition	Strain	Itaconate (mM)	Growth rate (h^{-1})
BioLector, CGXII	MB001(DE3) *acn_malEcad*	0.01 ± 0.00	0.43 ± 0.01
	MB001(DE3) *D18acn_P18malEcad*	0.02 ± 0.01	0.36 ± 0.01
	MB001(DE3) pVWEx2	ND	0.49 ± 0.01
BioLector, N-limitation	MB001(DE3) *acn_malEcad*	1.25 ± 0.04	0.50 ± 0.01
	MB001(DE3) *D18acn_P18malEcad*	1.28 ± 0.01	0.45 ± 0.01
	MB001(DE3) pVWEx2	ND	0.49 ± 0.02
Shaking flask, N-limitation	MB001(DE3) *acn_malEcad*	0.45 ± 0.04	
	MB001(DE3) *D18acn_P18malEcad*	0.51 ± 0.01	

With 0.45 ± 0.04 mM and 0.51 ± 0.01 mM itaconate, the final titers were approximately 40-60% lower than those from the BioLector® samples. These differenced might be explained with differences in the oxygen level within BioLector® wells and shaking flasks. In a previous study, especially the oxygen availability was demonstrated to influence the itaconate titers (Otten *et al.*, 2015).

Table 27: Summary of the major differences in the conditions used to produce itaconate between the study from Otten *et al.* and this work.

		This work	Otten *et al.*
i.	**Promoter system**	Constitutive P_{tuf}	IPTG inducible P_{tac}
ii.	**Enzymes**	*Acn* and *malEcad* or *D18acn and P18malEcad*	*malEcad*
iii.	**Cultivation**	750 µL in BioLector® microbioreactor	60 mL in 500 mL shaking flasks
iv.	**Cultivation medium**	CGXII + 2% glucose N-limited CGXII + 2% glucose	CGXII + 4% glucose N-limited CGXII + 4% glucose

The differences described in Table 27 (i) and (ii) are variances in protein abundances of MalECad and whether Acn was overproduced or not. Therefore, the next step was to determine the influence of MalECad levels and Acn overproduction on the itaconate titers.

Influence of Cad abundance on final itaconate titers

In order to determine the influence of MalECad on the itaconate production in MB001(DE3), the overexpression of the MalECad enzyme encoded from pEKEx2 was achieved using the IPTG inducible P_{tac} promoter (Otten *et al.*, 2015) or the pVWEx2 vector that contains a constitutive P_{tuf} promoter. MB001(DE3) P_{tac}*malEcad*, MB001(DE3) P_{tac}*P18malEcad* as well as MB001(DE3) P_{tuf}*malEcad* and MB001(DE3) P_{tuf}*P18malEcad* were compared under N-limited conditions regarding their itaconate production.

To induce the overexpression of the genes under control of P_{tac}, 0, 25, 50 and 250 µM IPTG were added to the cultivation medium. The results showed that the samples induced with 250 µM IPTG contained the highest itaconate titers in the supernatants with 5.91 ± 0.01 mM itaconate measured for the MB001(DE3) P_{tac}*malEcad* and 3.92 ± 0.12 mM itaconate for MB001(DE3) P_{tac}*P18malEcad* (Table 28). These values are almost threefold lower than the titer of 17 ± 5 mM itaconate published by Otten *et al.*, who used the same production plasmid P_{tac}*malEcad* in *C. glutamicum* ATCC13032. The constitutive Cad producers MB001(DE3) P_{tuf}*malEcad* and MB001(DE3) P_{tuf}P18*malEcad* reached itaconate titers of 2.20 ± 0.07 mM and 0.67 ± 0.02 mM itaconate, respectively, which is in a similar range to the IPTG induced production with 25 to 50 µM IPTG.

Table 28: Growth and itaconate production parameters of MalECad and P18malECad production strains. Itaconate titers were determined after 25 h of cultivation under N-limitation conditions with 2% glucose supplemented.

IPTG	Strain	Itaconate (mM)	Growth rate (h^{-1})
	MB001(DE3) pVWEx2	-	0.51 ± 0.06
-	MB001(DE3) P_{tuf}*malEcad*	2.20 ± 0.07	0.55 ± 0.02
-	MB001(DE3)P_{tuf}*P18malEcad*	0.67 ± 0.02	0.53 ± 0.02
-	MB001(DE3) pEKEx2	-	0.53± 0.04
-	MB001(DE3) P_{tac}*malEcad*	-	0.51 ± 0.02
25 µM	MB001(DE3) P_{tac}*malEcad*	1.39 ± 0.05	0.49 ± 0.02
50 µM	MB001(DE3) P_{tac}*malEcad*	3.40 ± 0.10	0.48 ± 0.02
250 µM	MB001(DE3) P_{tac}*malEcad*	5.91 ± 0.01	0.39 ± 0.02
0 µM	MB001(DE3) P_{tac}*P18malEcad*	-	0.50 ± 0.02
25 µM	MB001(DE3) P_{tac}*P18malEcad*	0.62 ± 0.03	0.50 ± 0.02
50 µM	MB001(DE3) P_{tac}*P18malEcad*	1.86 ± 0.04	0.46± 0.02
250 µM	MB001(DE3) P_{tac}*P18malEcad*	3.92 ± 0.12	0.37 ± 0.02

Interestingly, the constitutive overproduction of Acn and MalECad yielded in lower itaconate titers of 1.25 ± 0.04 mM itaconate (Table 26) compared to the production of MalECad alone with 2.20 ± 0.07 mM itaconate (Table 28). However, using the targeting peptide tagged enzyme variants, MB001(DE3) *D18acn_P18malEcad* produced more

itaconate than MB001(DE3) P_{tuf}*P18malEcad*, which did not overproduce D18Acn (1.28 ± 0.01 mM (Table 26) compared to 0.67 ± 0.02 mM (Table 28)).
Concluding, the obtained data emphasize a strong impact of MalECad and P18MalECad production levels on itaconate production, as shown by the different IPTG inducer concentrations and the constitutive expression strains. Furthermore, with the same expression strength of the enzymes, P18MalECad production strains reached 34-70% reduced titers in comparison to MalECad production strains. Furthermore, not only a high Cad activity, but also the balance of Acn and Cad activity seems to be important for high itaconate titers.

Influence of reduced Icd activity on the final itaconate titers

The current working hypothesis is that the overproduction of the aconitase leads to an enhanced flux of citrate over the intermediate cis-aconitate to isocitrate. However, the intended increase in precursor supply was not reflected by the final itaconate titers. A reason for that could be the high flux from isocitrate to α-ketoglutarate by the subsequent enzyme of the citrate cycle, the isocitrate dehydrogenase. The enzyme has a high specific activity (0.9-1.1 U mg^{-1} protein (Eikmanns *et al.*, 1995)) and, therefore, might limit the reverse reaction of the aconitase from isocitrate to citrate.
In previous work, a reduced *icd* expression led to a positive impact on the itaconate production and was achieved by modification of the start codon of *icd* from ATG to GTG and TTG (Otten *et al.*, 2015). In this work, the strains MB001(DE3)::*icd*(A1G) and MB001(DE3)::*icd*(A1T) were constructed and transformed with the itaconate production plasmids. The strains were cultivated for 25 h under N-limitation conditions in the BioLector® microbioreactor and the itaconate titers were measured in the supernatants by HPLC. The growth rates of the strains were not significantly influenced by the exchanges of the start codon. The control strain MB001(DE3) pVWEX2 revealed a growth rate of 0.47 ± 0.01 h^{-1} and all strains shown in Figure 33 had a growth rate between 0.42 h^{-1} and 0.48 h^{-1} (data not shown).
MB001(DE3), MB001(DE3)::*icd*(A1G) and MB001(DE3)::*icd*(A1T) containing *malEcad* or *P18malEcad* showed an enhancement in itaconate production with a concurrently lowered Icd activity (Figure 33 and Table S12). MB001(DE3)::*icd*(A1T) P_{tuf}*malEcad* produced the highest amount of itaconate with 4.98 ± 0.10 mM after 25 h of cultivation. The corresponding MB001(DE3)::*icd*(A1T) P_{tuf}*P18malEcad* strain produced only about half the amount of itaconate. The overexpression of the aconitase, which was shown before to negatively influence itaconate production, was almost negligible in MB001(DE3)::*icd*(A1T) *acn_malEcad* (4.56 ± 0.12 mM) as the itaconate production was nearly similar to MB001(DE3)::*icd*(A1T) *malEcad.* The most significant influence of Icd

decrease on the itaconate titers was obtained with MB001(DE3)::*icd*(A1T) *D18acn_P18malEcad.* The titer of 4.48 ± 0.04 mM itaconate almost reached those of the best producer strain MB001(DE3)::*icd*(A1T) P_{tuf}*malEcad.* Therefore, MB001(DE3)::*icd*(A1T) *D18acn_P18malEcad* is a promising candidate strain for BMC production as it shows no negative effects of the targeting peptides.

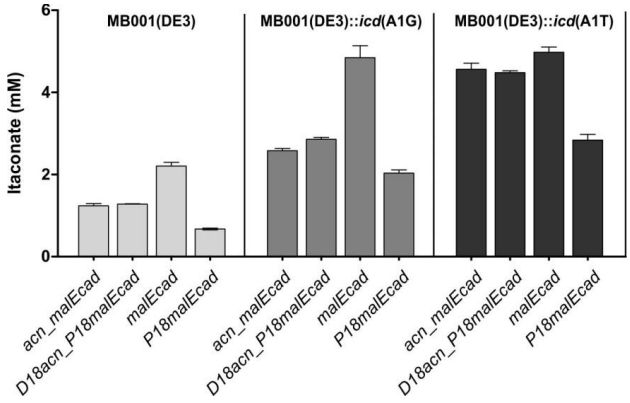

Figure 33: Influence of Icd activity on itaconate production. The Icd activity was lowered by the modification of the start codon from ATG to GTG in MB001(DE3)::*icd*(A1G) or TTG in MB001(DE3)::*icd*(A1T). Itaconate titers were determined after 25 h of cultivation under N-limitation conditions. With a lower Icd abundance, the itaconate titers were enhanced for all strains.

Itaconate production strains coproducing PduABJKNUT

The first experiments for the production of itaconate within BMCs in *C. glutamicum* were performed by plasmid-based expression of the operon *pduABJKNUT* together with the itaconate production enzymes. Unfortunately, during the process of this work the production of BMCs with this operon in *C. glutamicum* was disproved (Section 3.1.3). Nevertheless, also with the declaration of strains containing this operon as a negative control, some starting points regarding the optimization of itaconate production could be identified.

MB001(DE3) *pduABJKNUT acn_malEcad* and MB001(DE3) *pduABJKNUT D18acn_P18malEcad* were cultivated for 25 h in the BioLector® microbioreactor device under N-limitation conditions. The two strains were grown either with or without the induction of the *pduABJKNUT* operon by the addition of 20 µM IPTG. In comparison to MB001(DE3) *acn_malEcad* and MB001(DE3) *pduABJKNUT D18acn_P18malEcad*, the final titers within the supernatants of MB001(DE3) *pduABJKNUT acn_malEcad* and MB001(DE3) *pduABJKNUT D18acn_P18malEcad* were substantially reduced even without IPTG induction (Figure 34 and Table S13). With induction of the *pduABJKNUT* operon, the production of itaconate further declined below the detection limit. The

production of PduABJKNUT also drastically reduced the growth rate of the respective strains (Table S13). It was rather unexpected that this dramatic drop in itaconate titer was also found for the empty vector control MB001(DE3) pMKEx1 containing the respective itaconate production plasmids.

In an attempt to circumvent the usage of a second plasmid, the *pduABJKNUT* operon was integrated into the CGP1 region of MB001(DE3) controlled by the P_{T7} promoter revealing MB001(DE3)::P_{T7}*pduABJKNUT*. Even though the genomic integration of the operon had a positive effect on the growth and the itaconate production, the titers were still far below those revealed before with the control strains MB001(DE3) *acn_malEcad* and MB001(DE3) *malEcad* (Figure 34). Similar to the plasmid-based expression, also the induction of the genomically integrated *pduABJKNUT* operon with 50 µM IPTG further reduced the itaconate production in the respective strains.

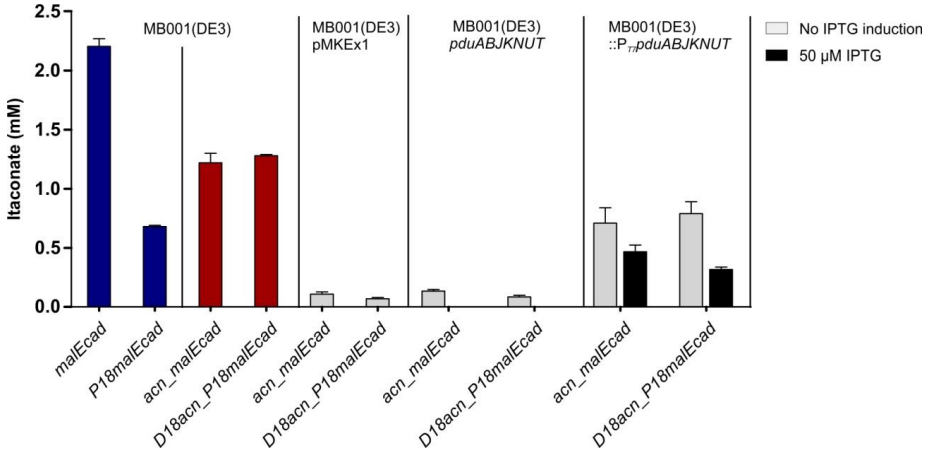

Figure 34: Application of PduABJKNUT for itaconate production in *C. glutamicum*. The strains MB001(DE3), MB001(DE3) pMKEx1, MB001(DE3) *pduABJKNUT* and MB001(DE3)::P_{T7}*pduABJKNUT* were compared and tested with the enzyme combinations Acn/MalECad and D18Acn/P18MalECad. Itaconate production was determined by HPLC analysis after 25 h of cultivation under N-limited conditions with and without coproduction of BMCs. There was a dramatic decrease in itaconate production with the usage of two plasmids, but also in a strain producing PduABJKNUT genomically. Itaconate was measured within the supernatants of three biological replicates. Dark grey: 50 µM IPTG; light grey: 0 µM IPTG; blue: control strains producing MalECad variants; red: control strains coproducing MalECad/Acn variants;

With the knowledge that PduABJKNUT is unable to form BMCs, the reduced itaconate titers with *pduABJKNUT* coproduction are not unexpected. Nevertheless, it was unanticipated that the strain background MB001(DE3)::P_{T7}*pduABJKNUT* attenuated itaconate production in comparison to MB001(DE3).

Itaconate production strains coproducing BMC shell or PduA scaffolds

An optimized BMC operon for compartment production was developed within this work (Section 3.1.4) and was proven to form compartment-like structures upon expression in *C. glutamicum*. The MB001(DE3)::*icd*(A1G) strain background was used to profit from the reduction of Icd activity as presented before. To circumvent the issues occurring with the usage of two plasmids, the operons *pduABJknt* and *pduA* were integrated into the CGP1 region of this strain under control of the promoter P_{T7}. Both strains were cotransformed with *acn_malEcad* and *D18acn_P18malEcad*. The itaconate production of those strains was determined after 25 h cultivation under N-limited conditions (Figure 35 and Table S14).

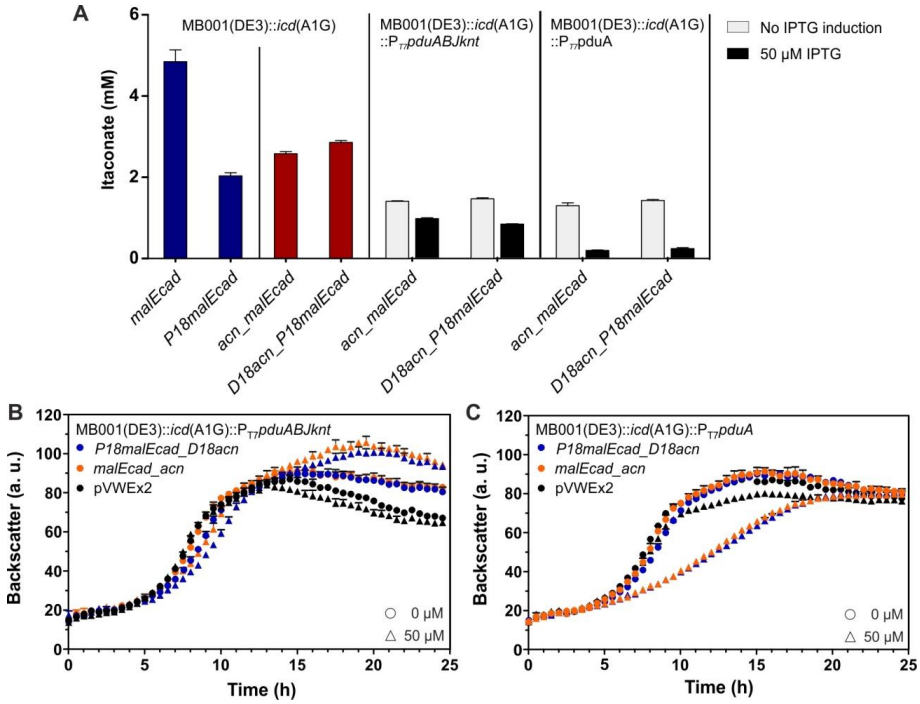

Figure 35: Application of PduABJknt BMCs and PduA filaments for itaconate production in *C. glutamicum*. A The strains MB001(DE3), MB001(DE3) pMKEx1, MB001(DE3)::P_{T7}*pduA* and MB001(DE3)::P_{T7}*pduABJknt* were containing the enzyme combinations Acn/MalECad and D18Acn/P18MalECad were cultivated for 25 h under N-limited conditions with and without the coproduction of BMCs. Itaconate production was determined by HPLC analysis within the supernatants of three biological replicates. Dark grey: 50 µM IPTG; light grey: 0 µM IPTG; blue: control strains producing MalECad variants; red: control strains coproducing MalECad/Acn variants; **B** Growth of MB001(DE3)::*icd*(A1G)::P_{T7}*pduABJknt* and **C** MB001(DE3)::*icd*(A1G)::P_{T7}*pduA* itaconate production strains in nitrogen-limited CGXII supplemented with 2% (w/v) glucose. The enzymes were constitutively expressed under the control of the P_{tuf} promoter and *pduA* or *pdABJknt* expression was induced with 50 µM IPTG (triangles). With the production of PduA, a strong growth defect was observed.

With the BMC production operon *pduABJknt* and the EP-tagged itaconate production enzyme variants, the strain MB001(DE3)::*icd*(A1G)::P_{T7}*pduABJknt D18acn_P18malEcad* contains the genetic requirements to target the enzymes into the PduABJknt BMCs. For this strain, the itaconate titers revealed 1.45 ± 0.02 mM itaconate without BMC induction. Similar to what was observed in the MB001(DE3)::P_{T7}*pduABJKNUT* background, the titer reached only half the titer of MB001(DE3)::*icd*(A1G) *D18acn_P18malEcad* even without the induction of *pduABJknt*. Furthermore, the production of PduABJknt affected the itaconate production negatively (0.831 ± 0.01 mM itaconate).

PduA was shown to assemble to large bundles of regular filaments with the overproduction in *C. glutamicum* (Section 3.3.1). Within this study, a potential benefit of those structures as scaffolds for P18MalECad and D18Acn was investigated. MB001(DE3)::*icd*(A1G)::P_{T7}*pduA D18acn_P18malEcad* was examined on its itaconate production in the absence and presence of IPTG (Figure 35). The experiments revealed that the itaconate titers dropped significantly from 1.413 ± 0.02 mM itaconate without PduA production to 0.23 ± 0.02 mM itaconate with the production of PduA filaments and a strong growth defect was observed with PduA overproduction.

Based on these data, it is evident, that no enhancement in the itaconate production could be achieved under the tested conditions. This might be related to the experimental configurations like a too high IPTG induction and/or the significant growth decline of the strains upon Pdu production (Figure 35). However, it may also be explained with a general missing of some prerequisites, which could not be investigated experimentally in this study. A very obvious drawback for the evaluation of the itaconate production was the drastic decrease in the final titer if two plasmids were used (Figure 34). Itaconate production was also sensitive to the chromosomal integration of *pduA* and *pduABJknt* even without the induction of the BMC operon (Table 29). This became apparent when the titers from MalECad producer strains, with and without the integrated *pduA* or *pduABJknt*, were directly compared. However, the reasons for that remain to be identified.

Table 29: Influence of chromosomal integration of PduA or PduABJknt on itaconate production.

Strain	Plasmid	Itaconate (mM)
MB001(DE3)::*icd*(A1G)	P_{tuf}*malEcad*	4.85 ± 0.06
MB001(DE3)::*icd*(A1G)::P_{T7}*pduA*	P_{tuf}*malEcad*	2.83 ± 0.08
MB001(DE3)::*icd*(A1G)::P_{T7}*pduABJknt*	P_{tuf}*malEcad*	2.17 ± 0.13

4 DISCUSSION

The Gram-positive Actinobacterium *C. glutamicum* is known as an important platform species for bioproduction processes. More than 5 million tons of amino acids (mainly L-glutamate and L-lysine) are produced with this host annually (Ajinomoto, 2016; Ajinomoto, 2017). Furthermore, *C. glutamicum* was successfully engineered towards the production of further value-added products, including diamines, dicarboxylic acids, polymer precursors or bio-based fuels like ethanol (Becker and Wittmann, 2015). The utilization of synthetic BMCs could expand the application range of *C. glutamicum* for derived products. Consequently, the primary aim of this work was the verification of BMC shell assembly in *C. glutamicum* by the heterologous expression of Pdu shell genes from the γ-Proteobacterium *C. freundii*.

4.1 Assembly of Pdu metabolosome shells

4.1.1 Optimization of the operon shell design

Prior work has documented the heterologous Pdu BMC production in *E. coli* by the usage of the native Pdu operon *pduA-X* (Parsons *et al.*, 2008). In the present study, two of the initially chosen operon designs, *pduA-X* (Parsons *et al.*, 2008) and a synthetic shell operon with native upstream regions (*pduABJKNTU*$_{native}$), led to aberrant structures like laminar filaments in combination with adjacent round structures in *C. glutamicum* cells (Figure 11) and, in order to that, the assembly of BMC structures could not be confirmed. These results show the limitations of the direct transfer of a 21 gene operon from *C. freundii* into *C. glutamicum*. It could be assumed that not all open reading frames present on the polycistronic mRNA were appropriately translated into protein in the heterologous host, resulting in imbalances in protein stoichiometry. This assumption is in good agreement with several publications documenting that the overproduction or deletion of a single or multiple shell genes from the operon can result in diversely shaped structures like regular lined structures, large homogenous aggregates or clumping BMCs (Parsons *et al.*, 2008; Parsons *et al.*, 2010; Cheng *et al.*, 2011).

The synthetic shell operon *pduABJKNUT* contains the BMC shell genes separated by 40 bp RBS regions (Parsons *et al.*, 2010). The fluorescence pattern observed in *C. glutamicum pduABJKNUT* strains showed distinct eYFP localizations different to PduA-X and PduABJKNTU$_{native}$ (Figure 11). Nonetheless, TEM analysis revealed the accumulation of proteins without detached structures and no compartment formation. It may be reasonable to assume that with the same RBS in front of each gene, each shell gene was translated with a similar rate. Therefore, it was reasoned, that the protein

abundancies were suboptimal within *C. glutamicum pduABJKNUT*. Hence, further experiments focusing on the differential protein production were performed.

Lassila *et al*. adapted the operon expression of a compartment of unknown function from *H. ochraceum* to mimic typical BMC shell protein ratios. This was implemented by the utilization of RBSs with different predicted translation initiation rates. However, in their study no comparison of the adapted operon version with an operon containing the same RBSs was done (Lassila *et al.*, 2014) and it cannot be concluded, if the adaption of the RBSs had an influence on BMC formation. In the present work, a similar approach was followed. The protein ratios produced from the BMC shell operon *pduABJKNUT* were modified by modifications of the start codons to match the protein stoichiometries determined from purified BMCs (Havemann and Bobik, 2003; Mayer *et al.*, 2016). The effects of 8 modified operons were individually analyzed by TEM. It was found that in all operons using $PduK_{GTG}$, the reduction of PduK levels was associated with the successful assembly of BMC-like structures as visualized by TEM (Figure 15). This result provides compelling evidence that the operon design has a major influence on the BMC assembly in *C. glutamicum*.

In *E. coli,* PduK is known to be essential for compartment assembly (Parsons *et al.*, 2010) and the overexpression of *pduK* in addition to *pduA-X* led to large aggregates with delimiting boundaries (Parsons *et al.*, 2008). The 'fluffy' phenotype of the shell proteins observed in this study appeared to be exclusive for *C. glutamicum* and revealed significant differences to the structures observed with PduK overproduction in *E. coli* (Parsons *et al*., 2008). One can speculate that a direct effect of the high protein abundance with the overproduction of $PduK_{ATG}$ led to unwanted interactions with other shell proteins. Furthermore, the *pduK* sequence contains three most rarely used codons in *C. glutamicum* (2x ATA, AGA). For heterologous genes, the codon usage was identified as the most important factor for appropriate translation (Boel *et al.*, 2016) and is furthermore considered to have significant effects on RNA processing, protein translation and protein folding (Plotkin and Kudla, 2011). From that, it can be assumed that the observed 'fluffy' phenotype could also be caused by the agglomeration of misfolded PduK and other shell proteins.

The data obtained in this study on the modulation of PduN levels are in good agreement with previous *E. coli* studies where no significant impact was observed with PduN overproduction (Parsons *et al.*, 2008). PduU and PduT were demonstrated to be dispensable for the successful compartment formation (Parsons *et al.*, 2010; Cheng *et al.*, 2011), a result, which could be revalidated in this study. However, the BMC operons encoding *pduT* (*e.g.* the constructs *pduABJknt*, *pduABJkNut*, *pduABJkNt*) revealed to have more distinct borders upon expression in *C. glutamicum* than compartment operons

lacking *pduT* (Figure 15). It could be therefore concluded that PduT has an important role in shaping and closure of the compartments. This assumption is substantiated by the hypothesis from Lassila *et al.* that BMC-T proteins, which PduT belongs to, are present around pentameric proteins and the edges of hexameric facets, where the curvature of the BMCs is provided (Lassila *et al.*, 2014).

The deletion of *pduU* did not result in any visible differences during TEM studies and BMC-like structures were also observed in strains containing operons lacking *pduU* (*e.g. pduABJknt, pduABJkn*). The yellow phenotype of the cells might be a result of carotenoid accumulation within the cell membrane (Heider *et al.*, 2012) but if this is, for example, caused by a stress response directly triggered by PduU remains unclear.

To conclude, this study provides evidence that heterologous BMC formation is possible in *C. glutamicum.* The BMC assembly was validated by TEM analyses (Figure 15 and Figure S1) for several operon versions (*pduABJkNut*, *pduABJknt*, *pduABJkN* and *pduABJkn*). It has to be noted that with all operons also misshaped structures and protein aggregates appeared in a considerable fraction of cells: However, it is suggested that the further optimization of protein stoichiometries provides the potential to reduce the formation of misshaped structures.

4.1.2 Growth of *C. glutamicum* during BMC formation

Numerous studies dealt with heterologous BMC production in *E. coli*, but the growth of the production strains was not discussed (Choudhary *et al.*, 2012; Lassila *et al.*, 2014; Held *et al.*, 2016). However, to establish BMCs as a profitable technology, it is important to evaluate and understand the influence of compartment production on cell growth performance and to optimize the system to minimize its influence. In a publication focusing on the application of 1,2-PD production, it was shown that there is no difference in growth between an *E. coli* control strain and an *E. coli* strain producing the PduABJKNUT shells under control of P_{T7}. However, the tested conditions were at reduced cultivation temperature at 28 °C and glycerol was used as sole carbon source. This limited the growth of the cells and a maximum OD_{600} of ~0.6 was achieved (Lee *et al.*, 2016). In another study, the same strains were grown in LB medium supplemented with 4% glucose at 28 °C. Here, *E. coli pduABJKNUT* showed a minor growth rate reduction but reached a final OD_{600} of ~10 (Lawrence *et al.*, 2014).

Against this, in *C. glutamicum* the production of BMCs seem to have a major impact on biomass formation kinetics. Growth experiments of the 8 different *C. glutamicum* Pdu production strains revealed drastic impacts on growth of those strains upon plasmid-based overexpression with 50 µM IPTG (Figure 17A). However, a slightly improved

growth was observed for strains with Pdu operons (i) not containing *pduU*, (ii) containing *pduK*$_{GTG}$ instead of *pduK*$_{ATG}$ and (iii) with a decreased number of genes. The adverse effect of *pduU* might be accounted to the hypothetic stress response in *C. glutamicum*, causing the production of carotenoids in those strains. The aggregation of proteins in strains using *pduK*$_{ATG}$ also influenced their overall fitness.

With a decreased number of genes, for example in *C. glutamicum pduABJkn*, there might be lower energy cost for the organism because fewer proteins need to be produced. This is probably also the reason for the less drastic growth rate reduction of the strains when being cultivated in the presence of only 25 µM IPTG (Figure 17B and C). Therefore, it is not surprising that the best growth performance was observed with the production strain *C. glutamicum* MB001(DE3)::P$_{T7}$*pduABJknt,* containing the *pdu* operon genomically integrated. However, other successfully validated operons have not been integrated into the genome yet and could be target of further investigations.

In published work, heterologous BMC production in *E. coli* was performed under control of a constitutive P$_{lac}$ promoter (Choudhary *et al.*, 2012; Held *et al.*, 2016) or of the *T7* promoter (Parsons *et al.*, 2010; Lassila *et al.*, 2014). For TEM analysis during the present work, the BMCs produced in *C. glutamicum* were expressed under control of P$_{T7}$ with induction of cells with 50 µM IPTG, which is ~80% of the maximal promoter output (Kortmann *et al.*, 2015). Those BMCs were found as agglomerations within the cell rather than as detached structures (Figure 15 and Figure S1) and also the chromosomal integration strain MB001(DE3)::P$_{T7}$*pduABJknt* (50 µM IPTG) showed the agglomerated BMCs (Figure 19). This is in accordance to other studies heterologously producing Pdu BMCs in *E. coli,* which also observed BMCs arranged together in the mid part of the cell, rather than being distributed across the cytoplasm (Parsons *et al.*, 2010; Lee *et al.*, 2016; Mayer *et al.*, 2016). This may be a consequence of the high expression levels in heterologous systems, whereas BMC production in native hosts is more tightly regulated (Kim *et al.*, 2014). For example, in the native Pdu production strain *S. enterica*, the transcription factor PocR positively regulates *pdu* gene induction in the presence of 1,2-PD (Chowdhury *et al.*, 2014). The transcription of *pocR* is, in turn, only produced during the growth on energy-poor carbon sources. This circumvents high maintenance energy in the absence of the substrate 1,2-PD and when the metabolism is optimized towards other preferred carbon sources (Kim *et al.*, 2014).

For the optimization of the heterologous BMCs production in *C. glutamicum*, the reduction of BMC protein production to the minimal amounts necessary would be favorable to reduce the growth implications of Pdu shell production and to circumvent the agglomeration of BMCs. This could be achieved with the reduction of IPTG inducer concentration or a constitutive promoter system like P$_{tuf}$ or another moderate promoter.

4.1.3 Methodical limitations concerning the validation of BMC assembly

Implications of cell lysis to BMC purification

With regard to a further application of BMCs for pathway enhancement, the possibility to purify the Pdu assemblies would provide the opportunity to validate the encapsulation of EP-targeted enzymes (Fan *et al.*, 2010; Choudhary *et al.*, 2012; Lassila *et al.*, 2014; Jakobson *et al.*, 2015) and to determine enzymatic activities within the compartment bioreactors (Lawrence *et al.*, 2014).

A number of different purification protocols has been described (Reviewed in (Lassila, 2015) since the first successful purifications of metabolosomes *via* sucrose density gradient centrifugation (Havemann and Bobik, 2003). The cell lysis steps used in these protocols include lysozyme digest, sonication cycles, protein extraction reagents as well as various combinations of these options. Pdu and Eut BMCs were isolated from the heterologous host *E. coli* (Parsons *et al.*, 2010; Choudhary *et al.*, 2012; Laslo *et al.*, 2012; Lawrence *et al.*, 2014; Mayer *et al.*, 2016), from native producers like *S. enterica* (Havemann and Bobik, 2003; Fan and Bobik, 2011; Sinha *et al.*, 2012) or *C. freundii* (Mayer *et al.*, 2016). As all of those organisms are Gram-negative, the cell lysis typically does not constitute a major challenge. In contrast, *C. glutamicum* is Gram-positive and additional to the thick peptidoglycan layer, the cell wall contains an arabinogalactan and mycolic acids layer typical for Mycobacteria (Bayan *et al.*, 2003). Thereby, the cell wall is highly resistant to lysozymic digestion (Figure 22A) and protein extraction reagent treatment (B-PER™ II and Y-PER™ Plus, data not shown). French Press treatment can efficiently lyse *C. glutamicum* MB001(DE3) (Figure 22C), however, is an intrusive method and was stated to interfere with compartment purification by the entrapment of compartments within membrane vesicles (Havemann and Bobik, 2003). Also, the disruption of the large ~100 nm BMC structures may be also assumed as a consequence of this treatment. Another mechanical cell lysis method, sonication, was used for the compartment purifications from *E. coli* (Havemann and Bobik, 2003; Parsons *et al.*, 2010; Lassila *et al.*, 2014). The longest application of sonication was found with 4x 45 sec (Output 10, 5 mm diameter disrupter horn, SoniPrep 150) but isolated BMCs were found to yield in poor quality (Parsons *et al.*, 2008). Even more, sonication was also used as method of choice to break BMCs (Fan and Bobik, 2011; Choudhary *et al.*, 2012). For *C. glutamicum* MB001(DE3), the protein release by sonication treatment was relatively ineffective if no further treatment was applied (Figure 22B). The analysis of two mutant strains with a reduced cell surface integrity, *C. glutamicum* ATCC13032 Δ*ipsA* (Baumgart *et al.*, 2013) and *C. glutamicum* ATCC13032::P_{cg2732}*lcpA* (Baumgart *et al.*, 2016), confirmed a drastically enhanced

susceptibility to sonication and French Press treatment of both strains (Figure 22B and C). These results are encouraging further investigations with those strains for the purification of BMC shells. As the strains were not available soon enough to be seriously taken into consideration, this may be a promising path to follow in upcoming experiments.

Furthermore, some compounds which are known to weaken cell wall or membrane structure could be tested on their performance. Isonicotinic acid hydrazide (INH) is an antibiotic that inhibits mycolic acid synthesis in Mycobacteria (Takayama *et al.*, 1975) and is used to weaken the cell wall for subsequent transformation of *C. glutamicum via* electroporation (Ruan *et al.*, 2015). Concentrations ranging from 2-10 mg mL^{-1} INH (Jang *et al.*, 1997) could be applied for one or more hours prior to cell harvesting. Further compounds enhancing the transformation efficiencies by the manipulation of membrane or cell wall structure are glycine, Tween80 (Haynes and Britz, 1989) and ampicillin (Bonnassie *et al.*, 1990). Furthermore, the growth of *C. glutamicum* cells in glycine-containing medium enhanced its susceptibility to lysozyme treatment (Yoshihama *et al.*, 1985). Some DNA purification protocols include a combined step of lysozyme/mutanolysin treatment (Björkroth *et al.*, 1999). Both enzymes catalyze the endolytic cleavage of peptidoglycans and could therefore be applied in combination for a more efficient and gentle cell lysis of *C. glutamicum*. Furthermore, an achromopeptidase from *Achromobacter lyticus* was stated to be effective for the lysis of Gram-positive bacteria, which are resistant to lysozyme (Ezaki and Suzuki, 1982) and was used for the preparation of *C. glutamicum* protoplasts in combination with lysozyme before (Thierbach *et al.*, 1988).

During this work, the BMC purification approaches performed were often accompanied with the copurification of ribosomal proteins (Figure 20A). As a possible solution, RNase I could be used during the purification for the destabilization of ribosome complexes (Mehta *et al.*, 2012). In general, a high abundance of ribosomes can be found in fast-growing cells in the mid-log phase, at optimal growth temperatures and with the usage of rich medium (Rivera *et al.*, 2015). These conditions, known to be favorable for high-yield ribosome purification, could be avoided during the cultivation of *C. glutamicum* cells for BMC purification.

In any case, different parameters like cultivation temperature, expression strength and cultivation time have to be considered carefully. The cultivation procedures which can be found in literature are quite diverse, ranging from low temperature cultivation over night at 16 °C (Parsons *et al.*, 2010) or 18 °C (Lawrence *et al.*, 2014) to the optimal growth temperature of *E. coli* at 37 °C for 4 h (Lassila *et al.*, 2014) or until late-log phase (Parsons *et al.*, 2008). It would be beneficial to verify the assembly of BMCs under

various conditions *via* TEM analysis as preparatory work. Within this study, the investigation of *C. glutamicum* BMC production strains *via* TEM was only performed after 4 h cultivation at 30 °C and revealed BMC-like structures. However, due to time limitations no purification approach was performed under these conditions, yet.

Limitations of fluorescence microscopy to determine BMC assembly

Fluorescence microscopy is a common technique to visualize BMC structures within the production host by targeting fluorescent reporter proteins into the compartment lumen. BMCs are often visible as punctate fluorescence signal or bright fluorescent foci (Choudhary *et al.*, 2012; Jakobson *et al.*, 2015; Held *et al.*, 2016) but also occur as less distinctly localized patches (Fan *et al.*, 2010; Parsons *et al.*, 2010). However, in none of those studies the fluorescence microscopy results were used to validate successful BMC assembly as the resolution limit is too high to distinctly constitute single compartment structures. This study further confirms this limitation, as fluorescence microscopy alone was unsuitable to prove the formation of BMCs. The appearance of distinct foci within the cells did not necessarily hint to successful BMC formation. Furthermore, the *C. glutamicum* BMC production strains, for which the assembly of BMC-like structures was proven by TEM images, showed fluorescent localizations in large clusters in the mid of the cells (Figure 15 and Figure 18).

Concluding, the BMC formation of a respective strain should be proven by TEM analysis of whole cells and/or purified compartments. However, fluorescence microscopy is still an appropriate tool for *e.g.* localization studies of EP-targeted fluorescence reporter.

4.2 Targeting of proteins of interest to the Pdu shell protein

To further direct the work towards an application of the heterologously produced BMC shells, the encapsulation of relevant pathway enzymes into the Pdu BMCs is a necessary prerequisite. The choice of the targeting peptide can be important for the enzymatic activity of the tagged enzyme (Lee *et al.*, 2016) (Table 31). Therefore, an enhanced selection of different C- and N-terminal encapsulation peptides will increase the possible fusion partners of the enzymes. These variants can then be individually tested on their enzymatic activity, revealing targeting peptide/enzyme fusions with a preferably minimal loss of function.

4.2.1 Evaluation of native BMC-derived encapsulation peptides

N-terminal targeting sequences are frequently used within native BMCs to encapsulate target proteins into BMCs (Aussignargues *et al.*, 2015). Prior work showed that the N-terminal targeting peptide of PduP interacts with the C-terminal extensions of the shell proteins PduA and PduJ (Fan *et al.*, 2012) and targets PduP into the compartment lumen. Additionally, Lawrence *et al.* confirmed the binding of the P18 peptide to the shell protein PduK with a pull-down assay (Lawrence *et al.*, 2014). A very recent study revealed that PduP and also the multi-enzyme complex PduCDE interact with the N-terminus of the shell protein PduB (Lehman *et al.*, 2017).

This data is consistent with the results obtained during this work with *C. glutamicum*. The localization of eYFP by the D18 and P18 EPs to BMCs was confirmed by fluorescence microscopy (Figure 14). Furthermore, a direct interaction of PduA with both targeting peptides was confirmed (Figure 27). This result provides support for earlier studies confirming the interaction of PduA to P18. Even more, to the knowledge of the author, the interaction of the D18 peptide with PduA was experimentally proven for the first time.

Due to the high similarity of PduA and PduJ, PduJ was also suspected to have a role in binding of different targeting peptides, but due to the missing structural data on PduJ this could not be confirmed yet (Jorda *et al.*, 2015). PduJ forms linear filaments and rolled up filamentous structures when overproduced in *C. glutamicum* (Figure 26). Fluorescence microscopy revealed a huge number of cells with fluorescent foci, which hint to an interaction of PduJ and D18eYFP/P18eYFP (Figure 27). However, this interaction could also be explained by the production of inclusion bodies due to the accumulation of misfolded protein. The filamentous structures observed via TEM could not be confirmed with fluorescence microscopy, even though some cell (<1%) showed some really weakly visible filaments (data not shown). The confirmation with for example pull-down assays,

as it was performed for the interaction of PduK and PduP (Lawrence *et al.*, 2014), would be necessary to have further proof.
However, there must be another binding partner of D18/P18 besides PduA, because the strain MB001(DE3) *pduBJKN*, which was not forming BMCs because of the lack of PduA, showed localizations of D18eYFP/P18eYFP to the aberrant structures formed (Figure 27). According to literature, this interaction partners could be PduK, PduB and PduJ (Fan *et al.*, 2012; Lawrence *et al.*, 2014; Jorda *et al.*, 2015; Lehman *et al.*, 2017).

4.2.2 Evaluation of C-terminal BMC-derived encapsulation peptides

The bioinformatic evaluation of more than 1000 EPs revealed that the *α*-helical amphipathic encapsulation peptides have conserved sequence properties and can be found at the C- or N-termini of proteins (Aussignargues *et al.*, 2015). However, to the best of the knowledge of the author, no experimental work has been done before on the utilization of C-terminal encapsulation peptides in Pdu BMCs.
The first hypothesis was that a targeting peptide natively present at the C-terminus of an enzyme is able to target a fluorescence reporter into the non-native Pdu BMCs. This is assumption is based on previous publications, demonstrating that different predicted encapsulation peptides were able to localize GFP to the non-native *S. enterica* Pdu compartment (Choudhary *et al.*, 2012; Sargent *et al.*, 2013; Jakobson *et al.*, 2015). The second hypothesis was that targeting peptides are transferable from the N- to C-terminus of a protein and remain their function. The main prerequisite would be that the sequence is still able to fold the *α*-helical structure and that the C-terminal addition is not structurally hindered to target the shell protein. Both assumptions were tested with the addition of two proposed C-terminal targeting sequences from *K. pneumonia* and *P. mirabilis* (Aussignargues *et al.*, 2015) and the C-terminal addition of P18 to *eyfp*. Subsequent fluorescence microscopy studies in MB001(DE3) *pduABJknt* (Figure 23) could indeed show that eYFP-P18 was targeted to PduABJknt BMCs, and therefore, the function of the P18 peptide was independent from its location at the protein and seems to function as isolated functional unit. Similarly, the $C17_{K.p.}$ peptide from *K. pneumonia*, natively present at the C-terminus of AdhDH, was also functional in the heterologous system. Interestingly, even though both C-terminal peptide sequences are very similar in their distribution of hydrophilic and hydrophobic amino acids to the D18 and P18 peptides (Table 30), the $C17_{P.m.}$ peptide from *P. mirabilis* was unable to localize eYFP to the BMCs. For future work, it would be very interesting to elucidate why the $C17_{P.m.}$ peptide was not functional and also to also test more diverse encapsulation sequences.

Table 30: Distribution of aliphatic (red), hydrophilic (blue) and tiny (green) amino acids in different encapsulation peptides.

$C17_{K.p}$		N	E	Q	N	V	E	R	V	I	R	Q	V	L	E	R	L	A
$C17_{P.m}$		T	E	E	N	V	E	R	I	I	K	E	V	L	G	R	L	G
D18	M	N	E	K	L	L	R	Q	I	I	E	D	V	L	S	E	M	Q
P18	M	N	T	S	E	L	E	T	L	I	R	N	I	L	S	E	Q	L

In this study, the assessment of reporter protein targeting to BMCs was solely based on fluorescence microscopy as the purification of BMCs from *C. glutamicum* was not possible. With fluorescence microscopy, a quantitative evaluation of the efficiency of the newly provided C-terminal targeting peptides in comparison to the native ones is almost impossible. Quantitative data, however, could provide knowledge to maximize or individually adjust the enzyme levels for the respective pathway within BMCs. Interesting in this context might be that there is a high-throughput method available which can quantify the relative amounts of fluorescence reporter incorporation into BMCs (Kim and Tullman-Ercek, 2014; Jakobson *et al.*, 2015). For that, the overall fluorescence of cells containing BMCs and tagged GFP molecules with a C-terminal SsrA degradation tag is measured by flow cytometry relative to a wildtype not containing BMCs. However, the drawback of this method is that it can only be applied for the investigation of N-terminal targeting peptides as the addition of the C-terminal SsrA tag would probably inhibit the function of the C-terminal targeting peptide. In these cases, the quantitative analysis of those peptides with the more time-consuming BMCs purification and subsequent Western Blot analysis (Jakobson *et al.*, 2015) probably remains the only suitable method.

4.2.3 Implementation of protein scaffolds for BMC targeting

In parallel to the targeting approach with BMC-derived encapsulation peptides, as discussed in the section before, another C-terminal targeting approach was taken based on synthetic scaffolding proteins (Dueber *et al.*, 2009). The hypothesis is that the self-assembly of a scaffolding domain to its ligand can provide synthetic interactions between BMC shell proteins and an enzyme of interest. The major benefit is that a ligand peptide and the cognate domain can be added to the C-terminus of the respective proteins and therefore allow C-terminal targeting, which can be beneficial for the enzymatic activity of the respective enzyme in comparison to an N-terminal targeting.

PduA is a major BMC shell component with ~30% abundance in assembled compartments (Mayer *et al.*, 2016). The C-terminus of the protein is known to interact with N-terminal targeting peptides (Fan *et al.*, 2012) and is therefore suggested to be localized to the luminal site of the assembled compartment shell. Because of that and

the high availability of PduA, the protein was used as a target for the C-terminal addition of the 7–32 aa interaction ligands. The operon *pduABJknt* was chosen for the evaluation of the synthetic scaffolds, as the operon was proven to form BMC-like structures. However, also the usage of the operons *pduABJkNut* or *PduABJkn* would have been possible. The influence of the ligand addition was tested *via* TEM analysis and the production of $PduA_{lig}$BJknt versions revealed BMC-like structures (Figure 24A). However, the fusion of the interaction ligand seemed to slightly interfere with BMC assembly, as also a high amount of misshaped structures were observed (Figure 24B). The most stable production with the highest number of cells producing BMC-like structures (58%) was accomplished with $PduA_{PDZlig}$BJknt containing the smallest interaction ligand with 7 aa. An interference of the interaction ligands with the compartment assembly is not unexpected, as PduA is a major shell protein and maintains interactions with five other shell proteins: PduB, PduJ, PduK, PduN and PduU (Parsons *et al.*, 2010; Jorda *et al.*, 2015). Future approaches could focus on the optimization of the operon, for example by the addition of the ligand peptide to PduJ instead of PduA, because PduJ is highly similar to PduA and present within the shells with ~15% (Mayer *et al.*, 2016) but only interacts with PduA (Parsons *et al.*, 2010).

The fluorescence reporter $eYFP_{dom}$ as well as D18eYFP/P18CFP were successfully targeted to the respective $PduA_{lig}$BJknt BMCs in separate approaches (Figure 24). However, it is likely that C- and N-terminal tagged versions can also be targeted to BMCs at the same, as the D18 and P18 peptides can also interact with other shell proteins (Figure 27). The importance of a quantitative analysis of encapsulation efficiencies was discussed in the section before, and should be performed for the scaffolding approaches, as well.

4.2.4 Issues with the N-terminal targeting of pathway enzymes

In an approach from Lee *et al.* to produce 1,2-PD from glycerol within BMCs, the effect of the N-terminal targeting peptides D18 and P18 on the enzymatic activity of the targeted enzymes was investigated (Lee *et al.*, 2016). Following a similar strategy, the evaluation of enzymatic activities of utilized pathway enzymes was performed during this work. In Table 31, an overview of the influence of targeting peptides on enzymatic activities, provided from different studies, is given.

It becomes obvious that the effects of the targeting peptides are highly variable depending on the enzyme and the used targeting peptide. Reasons for the lowered activity of targeted enzymes could be the formation of inclusion bodies and a lower protein abundancy of the targeted enzymes (Lee *et al.*, 2016), but also issues in protein

folding are possible. Future work should include the time-consuming nevertheless important screening of the available targeting peptide versions for each enzyme individually to obtain the most active enzyme combination. Additionally, to test whether the encapsulation peptides are also functional in combination with the corresponding enzyme, the purification of BMCs and subsequent Western Blot analysis can prove the enzyme incorporation (Lawrence *et al.*, 2014; Jakobson *et al.*, 2015).

Table 31: The influence of different targeting peptides on enzymatic activities. The reduction of enzymatic activity of targeted enzyme versions in comparison to untargeted enzymes is given in %. ND, not determined;

Pathway	Enzyme	D18 peptide	P18 peptide	C-terminal scaffold$_{dom}$	Reference
1,2-PD production	MgsA	- 15%.	- 18%	ND	(Lee *et al.*, 2016)
	DhaK	No reduction	No reduction	ND	
	GldA	- 90%	- 55%	ND	
	FucO	- 58%	- 76%	ND	
Ethanol production	AdhB	- 85%	ND	- 70%	(Ludwig, 2016) and this work
	Pdc	ND	No reduction	ND	
Itaconate production	Acn	- 10%	ND	ND	This work
	Cad	ND	- 65%	ND	
	Acn	ND	ND	No reduction (PDZ_{dom})	(Yang *et al.*, 2017)
	Cad	ND	ND	- 20% (PDZ_{lig})	
Methanol consumption	Hps	No activity	ND	ND	This work
	Details of Phi, Act and Phi see Discussion Section 4.3.5.				
	Mdh	ND	ND	works ($SH3_{lig}$)	(Price *et al.*, 2016)
	Hps	ND	ND	works (N-term. $SH3_{dom}$)	

In this work, a first evaluation of the C-terminal targeting peptides PDZ_{dom}, $SH3_{dom}$ and GBD_{dom} revealed a ~15% less significant influence of those peptides on AdhB activity than the D18 peptide (Table 31). Furthermore, Yang *et al.* used the scaffolding technique without the involvement of BMCs and found no reduced activity for Acn-PDZ_{dom} and a 20% reduced activity for Cad_{PDZlig} (Yang *et al.*, 2017). Similarly, Price *et al.* successfully used the interaction of Mdh_{SH3lig} and $SH3_{dom}$-Hps, amongst other modifications, to enhance methanol consumption, but did not quantify the enzymatic activities (Price *et al.*, 2016). These studies provide evidence that some enzymes, which were also target of this investigation, remain their activity with C-terminal scaffold domains or ligands. This is highly relevant in the light of a future use of the different $PduA_{lig}$BJknt versions and also underlines the potential of the established C-terminal encapsulation peptides with pathways containing enzymes which are inactive when carrying an N-terminal encapsulation peptides.

4.3 Pathway enhancement with Pdu BMCs

Within the following section, some general findings and issues using the Pdu BMCs in a heterologous organism with a non-native pathway will be summarized. Three different metabolic pathways were investigated during this study to different extents. The major difficulties and challenges will be discussed in the subsequent sections as each pathway contains some specific characteristics (Table 32).

Table 32: Summary of certain characteristics of the ethanol and itaconate production pathways and the methanol consumption pathway.

	Ethanol production	Methanol consumption	Itaconate production
Enzymes	AdhB, Pdc	Mdh, Act, Hps, Phi	Cad, Acn
Toxic intermediate	Acetaldehyde	Formaldehyde	-
Competing reaction	TCA cycle	Formaldehyde detoxification reaction	TCA cycle
Cofactors required	$NADH_2$	NAD^+	-
Substrates	Pyruvate	Ribulose-5-phosphate, methanol	Citrate
Product	Ethanol	Fructose-6-phosphate	Itaconate

4.3.1 Transport mechanisms through the BMC shells

A key challenge for the introduction of heterologous pathways into empty BMC shells is the understanding of influx and efflux mechanisms of substrates, products and cofactors. Besides the native substrates and products of the respective class of BMCs, it is difficult to predict if the non-native substrates, products and cofactors are able to pass the compartment shell.

It is known that the central PduA pore of the Pdu BMC provides an environment allowing the mostly polar 1,2-PD to pass but retains the less polar propionaldehyde (Crowley *et al.*, 2010). But even though it is possible to alter the substrate specificity of this pore (Chowdhury *et al.*, 2015), a directed modification of the pore region towards the transport of a specific substrate remains a challenging future task.

Concerning the pathways chosen for this study, the alcohols ethanol and methanol are assumed to pass the Pdu pores as the Pdu compartment was already successfully used for ethanol production in *E. coli* (Lawrence *et al.*, 2014). Furthermore, the BMC shells are known to be permeable for the alcohol 1-propanol, a product during 1,2-PD utilization (Chowdhury *et al.*, 2015). However, it remains to be elucidated if all other substrates and products (Table 32) are able to pass the shells.

Cofactors like NAD/NADH and CoA can be exchanged across BMC shells by allosterically regulated pores of BMC-T proteins. In absence of the respective BMC

substrate, the pores are mainly open, with the binding of the substrate the pore opening is prevented (Tanaka *et al.*, 2010; Pang *et al.*, 2012; Thompson *et al.*, 2015). For the Pdu BMC from *Lactobacillus reuteri*, the PduB shell protein was shown to interact with 1,2-PD (Pang *et al.*, 2012) and therefore, it seems likely that also in *C. freundii* 1,2-PD regulates the pore opening of PduB. This implies that the pores are rather open than closed in a heterologous system in the absence of 1,2-PD. If this is the case, substrates, intermediates and products could rather freely pass the compartment shell as they are smaller than cofactors. Additional to the complete exchange of cofactors through the pores, in the native system the cofactors can also be internally recycled within the Pdu compartments (Cheng *et al.*, 2012; Huseby and Roth, 2013).

To further investigate those issues, two prerequisites must be given: (i) the possibility to target all enzymes of interest of a respective pathway into BMCs and (ii) to purify the BMCs from the host organism. Having the purified BMCs containing the pathway enzymes at hand, activity assays can provide information about the permeability of the shells for the respective compounds (Lawrence *et al.*, 2014; Chowdhury *et al.*, 2015).

4.3.2 Growth of BMC strains coproducing pathway enzymes

As mentioned earlier, the production of Pdu BMC shells had almost no influence on growth of *E. coli* under the tested conditions (Lawrence *et al.*, 2014; Lee *et al.*, 2016). The coproduction of D1AdhB/P18pdc and the BMC shells slightly decreased the growth (Lawrence *et al.*, 2014). A stronger effect on growth was found for the coproduction of the Pdu shells with the tagged 1,2-PD production enzymes (Lee *et al.*, 2016).

Contrary to the production of Pdu shells in *E. coli*, this study revealed declined the growth rates for MB001(DE3)::P_{T7}*pduABJknt* due to the production of PduABJknt alone. The production of untargeted and targeted AdhB and Pdc versions in MB001(DE3)*::*P_{T7}*pduABJknt* had slide effects on growth rates and with additional PduABJknt coproduction, the growth defects were more pronounced (Figure 30). However, the growth studies were performed in CGXII supplemented with 2% glucose under aerobic conditions and not under the actual ethanol production conditions.

The production of Acn/Cad and P18MalECad/Acn had almost no effect on growth under N-limited conditions in MB001(DE3)::*icd*(A1G)*::*P_{T7}*pduABJknt* and also with the coproduction of PduABJknt, the growth performance was not further reduced (Figure 35). This raises the question if the BMC shells are produced properly under N-limited conditions, which was not tested during this study. A further optimization of the production conditions of the respective pathway and the influence of the growth on final product titers was so far not investigated, but should be included in future work.

4.3.3 Difficulties and directions for ethanol production in BMCs

The first successful application of Pdu BMCs for small molecule production was the incorporation of the ethanol fermentation pathway in *E. coli* (Lawrence *et al.*, 2014). From that, it can be concluded that the prerequisites of substrate transport into and product transport out of the compartment shells should be given for the Pdu BMCs. The ethanol production within Pdu BMCs in *C. glutamicum* is not competitive with established processes in high cell density, which already provided a theoretical maximum yield of 95% (Jojima *et al.*, 2015). Even though not being economically successful, this pathway has the intention to serve as a proof-of-principle for the utilization of BMCs in *C. glutamicum*.

In a preliminary experiment with *C. glutamicum* MB001(DE3)::P_{T7}*pduABJknt* containing the different ethanol production modules *adhB_pdc*, *D18-GGSG-adhB_P18pdc* and *D18-10aa-adhB_P18pdc*, the ethanol production was investigated. One major outcome was that the wildtype MB001(DE3) and MB001(DE3)::P_{T7}*pduABJknt* without PduABJknt production revealed ethanol titers within a similar range of 85-115 mM ethanol (Figure 31). This indicated that the lower AdhB activity of D18AdhB was no bottleneck for the ethanol production in these strains.

Furthermore, MB001(DE3)::P_{T7}*pduABJknt D18-10aa-adhB_P18pdc* exhibited a higher ethanol titer with compartment coproduction (126.29 mM) than without BMC production (85.23 mM ethanol) (Figure 31), which could hint to the functional compartment application. However, validation of this result will be a crucial future task, as the experiment was only performed once in two biological replicates.

Nevertheless, this finding is very promising and should be further explored as the optimization possibilities for the ethanol production pathway are still huge. One target could be to yield for ethanol production under anaerobic conditions and high cell density, as it was performed in other studies before (Inui *et al.*, 2004; Jojima *et al.*, 2015). Another important factor might be the protein abundance of the respective enzymes or even further, the ratio between AdhB and Pdc within the cells. In *E. coli*, the ethanol enzymes were under control of the *tac* promoter in the presence of 400 µM IPTG (Lawrence *et al.*, 2014). In the present study, the enzymes were presumably produced to a lower extent under control of the P_{tuf} promoter. Future studies in *C. glutamicum* could also focus on the enhancement of enzyme production, for example with the P_{T7} promoter system or the *ldhA* promoter, which was used in former ethanol production approaches (Inui *et al.*, 2004; Jojima *et al.*, 2015).

4.3.4 Difficulties and directions for itaconate production in BMCs

The itaconate production pathway was used as an example to prevent the loss of the intermediate cis-aconitate to the competitive TCA cycle by relocating itaconate production into BMCs. However, this work provides several arguments that itaconate production within BMCs in C. *glutamicum* is probably not a suitable approach to enhance product titers. It became apparent, that the MalECad production level is of major importance for the final itaconate titers. This might be trivial as it is expected that higher product titers can be achieved with higher enzyme abundancies. However, all changes which are necessary for BMC production, like the targeting of MalECad, drastically lowered itaconate titers. Also, the coproduction of Acn which is necessary for the subsequent usage in BMCs, resulted in drastically lower itaconate titers than the production of MalCad alone. The negative effect of Acn overproduction was assumed to be a result of a higher flux to isocitrate, the product of the aconitase reaction through the TCA cycle (Figure 5). This is plausible as the Icd has a high specific activity of 0.9-1.1 U mg^{-1} protein for isocitrate under standard conditions (Eikmanns *et al.*, 1995). This effect could be partly counteracted by reduction of the Icd activity. For the lowest Icd activity in the strain MB001(DE3)::*icd*(A1T), the Acn overproduction did not extensively influence itaconate production, presumably because the flux from isocitrate to *α*-ketoglutarate was almost abolished (Otten *et al.*, 2015).

During this work, the best itaconate titers were achieved with the prophage-free *C. glutamicum* MB001(DE3) P_{tac}*malEcad* producing 5.91 ± 0.01 mM itaconate within 25 h. An almost identical strain, *C. glutamicum* ATCC13032 P_{tac}*malEcad,* produced almost threefold more itaconate with 17 ± 5 mM, however, was cultivated differently (Otten, 2013). Similarly, in the present work MB001(DE3)::*icd*(A1T) P_{tuf}*malEcad* produced 4.98 ± 0.10 mM itaconate within 25 h, the published production strain *C. glutamicum* ATCC13032::*icd*(A1T) P_{tac}*malEcad* produced a titer of ~27 mM itaconate during 25 h (Otten *et al.*, 2015). These variances in itaconate titers are probably primary caused by differences in the promoter system (P_{tuf} or P_{tac}) and cultivation conditions including the medium composition (differences summarized in Table 27 in Section 3.4.3).

A further and rather unexpected observation was made with the usage of the Pdu production plasmid together with itaconate production plasmid. This led to dramatically declined itaconate production titers in *C. glutamicum* (Figure 34), even though Pdu production was not induced. In future, it could be further analyzed if the co-occurrence of two plasmids lowers the copy numbers of each plasmid. Possible copy number changes could be analyzed by quantitative real-time PCR (Plotka *et al.*, 2017). A lowered copy number of the MalECad production plasmid could explain the reduced itaconate titers.

The integration of the BMC operon into the genome, resulting in MB001(DE3)::P_{T7}*pduABJknt*, circumvented the usage of a second plasmid but the strain MB001(DE3)::P_{T7}*pduABJknt* P_{tuf}*malEcad* produced only half of the amount of itaconate which was produced with MB001(DE3) P_{tuf}*malEcad* (Table 30). For this phenomenon, no satisfying explanation can be named. Compared to the production of ethanol, which was performed in the same strain background, no such negative effect on final titers was observed.

Finally, the potential itaconate production strain MB001(DE3)::*icd*(A1G)::P_{T7}*pduABJknt D18acn_P18malEcad* revealed that with *pdu* induction, the itaconate production further declined. The most obvious argumentation is that, the MalECad enzyme production is reduced due to the concurrent coproduction of PduABJknt.

Concluding, even when omitting the negative effects of the P_{T7}*pduABJknt* integration into *C. glutamicum*, itaconate titers were highly sensitive to the coproduction of Acn and the Pdu proteins. Furthermore, there are many open questions like if citrate does enter the Pdu BMCs and if itaconate is released. Furthermore, a very recent study published the assembly of a Cad_{PDZlig}/Acn-PDZ_{dom} complex provided by the PDZ scaffold in *E. coli*. With that, an almost twofold increase in itaconate production after 48 h of fermentation was achieved in comparison to the unlinked enzymes (Yang *et al.*, 2017). It would be interesting if a direct scaffolding approach, as described before, could enhance the itaconate production in *C. glutamicum.*

In general, the itaconate titers achieved in bacteria are significantly lower than the maximum titers which can be achieved in yeasts. In *E. coli*, the maximum yield of 1.7 mM itaconate was produced within 48 h fermentation (Yang *et al.*, 2017), the maximum itaconate titer reached with *C. glutamicum* was 60 mM itaconate within 2 days (Otten *et al.*, 2015). In comparison, with the native itaconate production strain *A. terreus* a final itaconate titer of 660 mM was achieved after 7 days cultivation (Kuenz *et al.*, 2012).

4.3.5 Difficulties and directions for methanol utilization in BMCs

The establishment of methanol as an alternative carbon source in industrial production processes could contribute to a more sustainable bioeconomy. Methanol is a non-food raw material and the production from renewable feedstocks is possible (Law *et al.*, 2013). The methanol consumption pathway was established in *C. glutamicum* with the introduction of four crucial enzymes (Witthoff *et al.,* 2015). However, the main bottlenecks stated were the accumulation of the toxic intermediate formaldehyde and a

competing endogenous pathway for formaldehyde detoxification (Witthoff *et al.*, 2015). BMCs therefore constitute a promising idea to circumvent those limitations.

The first aim was to target the enzymes used in Witthoff *et al.* from *B. methanolicus* (Mdh and Act, methanol oxidation module) and *B. subtilis* (Hps and Phi, formaldehyde assimilation module) with N-terminal encapsulation peptides to be able to relocate their activity into the BMC lumen. However, activity assays with the formaldehyde module Bs(*P18hps_phi*) showed that the main restriction was the complete loss of function of N-terminally targeted Hps variants (Figure 32). It could be assumed, that the N-terminal addition of 18 amino acids, necessary for the targeting, prevented the dimerization (Orita *et al.*, 2010) or the proper folding of the protein. The second assumption is underlined by the fact that crystal structures of Hps revealed an important active site (Asp8) for Mg^{2+} binding near the N-terminus and a ß-strand secondary structure for the first seven amino acids (Orita *et al.*, 2010). Furthermore, this finding is in accordance with an approach to enhance the Hps and Phi reaction by direct fusion of both enzymes showing that the N-terminal addition of *phi* to *hps* (Phi-Hps) did not retain any activity (Orita *et al.*, 2007). However, it was also shown that the Hps-Phi fusion with the C-terminal addition of Phi remains activity and is even more active than both enzymes in a mixture (Orita *et al.*, 2007). This result gives an indication that it might be possible to restore the Hps activity with the new to C-terminally targeting peptides established towards the end of the present work.

To reduce the number of enzymes which need to be targeted to BMCs, the activity of Mdh and D18Mdh were investigated without the activator protein Act (Figure 32). However, the Act protein seemed to be essential in *in vitro* assays in *C. glutamicum* as both Mdh versions did not examine any activity. This is in contrast to a study from Ochsner *et al.* which could determine the activity of Mdh alone even though the activity of Mdh was reduced to half without the presence of Act (Ochsner *et al.*, 2014). Up to now, no further studies to re-activate Mdh were performed, but literature provides a promising option to circumvent the usage of Act: Mdh from *B. methanolicus* was modified by site directed mutagenesis to gain Mdh^{S98G} (Ochsner *et al.*, 2014). The introduced mutation mimics the effect of Act by destroying the NAD^+-binding capacity of Mdh (Hektor *et al.*, 2002). The modified Mdh^{S98G} enzyme achieved a 3.4 times higher activity than Mdh alone and a 1.7 times higher activity than Mdh/Act (Ochsner *et al.*, 2014).

An alternative approach for methanol production in *E. coli* was recently published by Price *et al.* and could be also tested in *C. glutamicum*. The authors used $Mdh3_{SH3lig}$ and $SH3_{dom}$-Hps-Phi for the assembly of large protein complexes and the subsequent enhanced formation of the product fructose-6-phosphate (Price *et al.*, 2016).

4.4 Pathway enhancement with enzyme scaffolds

The central idea of the scaffold-mediated pathway optimization is to enhance the local concentrations of pathway intermediates and enzymes and, therefore, reduce the interaction of intermediates with competing pathway enzymes or, if the intermediate is toxic, with cellular components (Siu *et al.*, 2015). There are several possible ways for pathway enhancement (Figure 36).

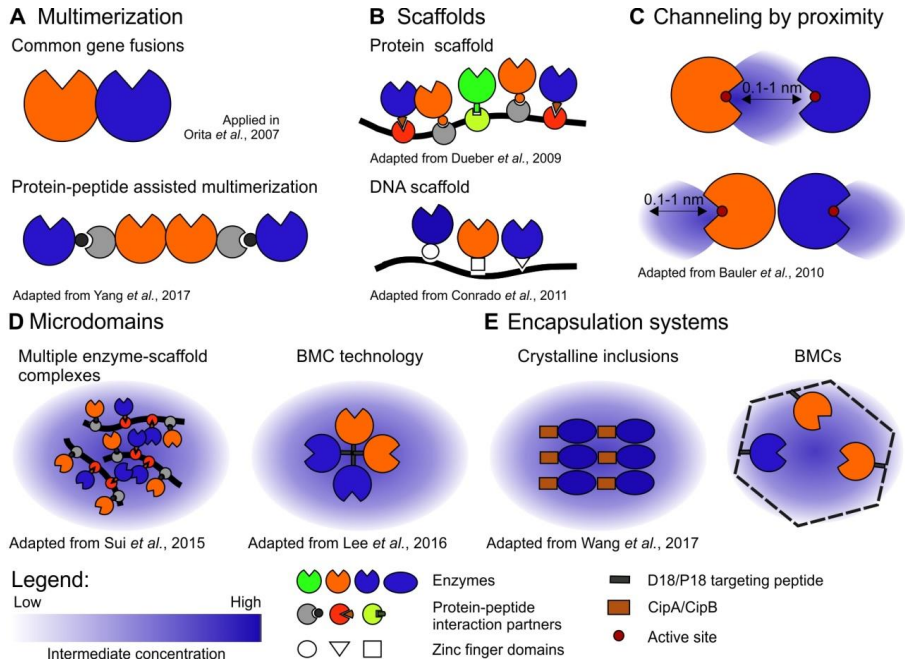

Figure 36: Overview of approaches for pathway enhancement. A Synthetic multimeric enzyme complexes can be achieved with gene fusions or by protein-peptide interaction partners. **B** Target enzymes can be targeted onto synthetic DNA or protein scaffolds. **C** Active sites of enzymes need to be within 0.1-1 nm distance to each other to directly channel the intermediate between the two enzymes. **D** and **E** Within microdomains and BMCs, the local concentrations of substrates and intermediates are elevated and the probability to be converted is higher than outside the system.

One way to achieve that is the multimerization of enzymes (Figure 36A), which can be done by common gene fusions (Orita *et al.*, 2007). Another possibility is to initiate enzyme interactions by synthetic protein-peptide interaction partners (PDZ, SH3, GBD; initially established by Dueber *et al.,* 2009), which can be fused to the respective genes. With this strategy, a synthetic interaction of the natively dimeric Cad and Acn was achieved and itaconate production titers were doubled in *E. coli* (Yang *et al.*, 2017).

These protein-peptide interactions can also be used to target enzymes onto a protein scaffold (Figure 36B). With that, a 77-fold enhanced mevalonate production (Dueber *et*

al., 2009) and a 5-fold improved glucaric acid production could be achieved in *E. coli* (Moon *et al.*, 2010). Similarly, zinc finger domains were used to provide an interaction of enzymes and cognate DNA sequences to achieve scaffolds (Figure 36B), which significantly improved 1,2-PD and mevalonate production (Conrado *et al.*, 2012).

The functionality of the described strategies can be mainly explained by the close proximity of the enzymes, whereby an intermediate can be channeled between the enzymes. However, the direct proximity channeling requires the diffusion of the substrate from one active site to another within a range of 0.1-1 nm to effectively prevent diffusion (Figure 36C) (Bauler *et al.*, 2010). As this distance is relatively small, another proposed mechanism for the scaffold-mediated pathway enhancement is the microdomain hypothesis. This hypothesis describes that with the accumulation of proteins within a microdomain, the probability of an intermediate to be catalyzed by any of the present downstream enzymes is higher than outside of the microdomain (Siu *et al.*, 2015). Interestingly, this theory is not in contrast to the previously-described approaches as microdomains can also assemble when the actual scaffold is one-dimensional but one or more targeted enzymes are naturally in an oligomeric state and trigger the aggregation of multiple scaffolds (Figure 36D) (Siu *et al.*, 2015).

The formation of microdomains was also achieved with the so-called microcompartment technology. The authors demonstrated that the P18 and D18 peptides can cause the formation of enzyme aggregates yielding in an increased 1,2-PD production (Figure 36D) (Lee *et al.*, 2016). Furthermore, there are other encapsulation systems besides BMCs, for example crystalline inclusions, which were used to enhance the violacein biosynthesis in *E. coli* (Figure 36E) (Wang *et al.*, 2017).

During this work, another potential scaffolding approach was investigated. With their ability to form higher-order assemblies, PduA and $PduA_{lig}$*s* offer the possibility to be used as scaffolds onto which pathway enzymes can be targeted. In two preliminary experiments, PduA scaffolds were tested for ethanol and itaconate production. In both approaches, the strains MB001(DE3)::P_{T7}*pduA* coproducing PduA and the targeted ethanol or itaconate production enzymes revealed decreased product titers in comparison to the lack of PduA filaments (Figure 31 and Figure 35). However, it should be noted that PduA production led to a significantly declined growth which is less than ideal for the production process and could have caused the low titers. In future work, PduA production should be optimized to levels where growth rates are less influenced. More general questions are, whether the enzymes targeted onto a PduA scaffold are close enough for proximity channeling and whether the filaments are able to aggregate to each other similar to the enzyme-scaffold complexes (Figure 36D) or if they are too static.

4.5 Future prospects for the Pdu application in *C. glutamicum*

It would be of great advantage to make synthetic BMCs accessible for the usage in industrially relevant production strains like *C. glutamicum*. In the present work, the synthetic *pduABJKNUT* operon (Parsons *et al.*, 2010) with genes derived from *C. freundii* was established in *C. glutamicum* by altering protein production levels. Even though the formation of BMC structures by *C. glutamicum* was validated, the study also strongly emphasizes further optimization of the BMC production process to reduce effects on growth and the occurrence of misshaped assemblies. The evaluation of synthetic interaction peptides localized at the C-terminus of enzymes enlarged the targeting toolbox for enzymes which can be utilized within BMCs without loss of function and expands the modularity of the system.

The production of ethanol remains to be an interesting proof-of-principle example and should be further optimized, for example concerning cultivation conditions. As top-down approach this pathway could reveal further bottlenecks also with regard to other pathways. Even though the activity of the methanol consumption enzymes could not be restored during this work, this pathway remains a promising strategy for the optimization of methanol utilization.

However, besides the potential benefits of BMCs, the complexity of the system remains a major issue. The incorporation of whole pathways cannot be done without further fundamental research on the shell permeability to understand the transport mechanisms of substrates, products and cofactors and, going a step further, to modulate the system towards the desired application.

BMCs will have to compete with other strategies (Figure 36), which were also designed to contribute to advancements in metabolic engineering of pathways with toxic or volatile intermediates or pathways with competing reactions.

5 REFERENCES

Ajinomoto Co. Inc. (2016). "Food Product Business." 21.03.2017, [https://www.ajinomoto.com/jp/ir/pdf/fact/Food-Oct2016.pdf].

Ajinomoto Co. Inc. (2017). "Ajinomoto Co., Inc. Consolidated Results FY2016 ended periodended March 31, 2017." 07.06.2017, [https://www.ajinomoto.com/en/ir/main/07/teaserItems1/0/linkList/01/link/FY16_Results_E.pdf].

Arfman N., Watling E. M., Clement W.*, et al.* (1989). "Methanol metabolism in thermotolerant methylotrophic *Bacillus* strains involving a novel catabolic NAD-dependent methanol dehydrogenase as a key enzyme." Arch. Microbiol. **152**(3): 280-288.

Arfman N., Bystrykh L., Govorukhina N. I.*, et al.* (1990). "3-Hexulose-6-phosphate synthase from thermotolerant methylotroph *Bacillus* C1." Methods Enzymol. **188**: 391-397.

Arndt A. and Eikmanns B. J. (2007). "The alcohol dehydrogenase gene *adhA* in *Corynebacterium glutamicum* is subject to carbon catabolite repression." J. Bacteriol. **189**(20): 7408-7416.

Aussignargues C., Paasch B. C., Gonzalez-Esquer R.*, et al.* (2015). "Bacterial microcompartment assembly: The key role of encapsulation peptides." Commun. Integr. Biol. **8**(3): e1039755.

Axen S. D., Erbilgin O. and Kerfeld C. A. (2014). "A taxonomy of bacterial microcompartment loci constructed by a novel scoring method." PLoS Comput. Biol. **10**(10): e1003898.

Bauler P., Huber G., Leyh T.*, et al.* (2010). "Channeling by proximity: The catalytic advantages of active site colocalization using brownian dynamics." J.of Physic. Chem. Lett. **1**(9): 1332-1335.

Baumgart M. and Bott M. (2011). "Biochemical characterisation of aconitase from *Corynebacterium glutamicum*." J. Biotechnol. **154**(2-3): 163-170.

Baumgart M., Luder K., Grover S.*, et al.* (2013). "IpsA, a novel LacI-type regulator, is required for inositol-derived lipid formation in Corynebacteria and Mycobacteria." BMC Biol. **11**: 122.

Baumgart M., Unthan S., Ruckert C.*, et al.* (2013). "Construction of a prophage-free variant of *Corynebacterium glutamicum* ATCC 13032 for use as a platform strain for basic research and industrial biotechnology." Appl. Environ. Microbiol. **79**(19): 6006-6015.

Baumgart M., Schubert K., Bramkamp M.*, et al.* (2016). "Impact of LytR-CpsA-Psr proteins on cell wall biosynthesis in *Corynebacterium glutamicum*." J. Bacteriol. **198**(22): 3045-3059.

Baumgart M., Huber I., Abdollahzadeh I.*, et al.* (2017). "Heterologous expression of the *Halothiobacillus neapolitanus* carboxysomal gene cluster in *Corynebacterium glutamicum*." J. Biotechnol. **27**(17): 30124-30124.

Bayan N., Houssin C., Chami M.*, et al.* (2003). "Mycomembrane and S-layer: two important structures of Corynebacterium glutamicum cell envelope with promising biotechnology applications." J. Biotechnol. **104**(1–3): 55-67.

Becker J. and Wittmann C. (2015). "Advanced biotechnology: metabolically engineered cells for the bio-based production of chemicals and fuels, materials, and health-care products." Angew. Chem., Int. Ed. Engl. **54**(11): 3328-3350.

Bentley R. and Thiessen C. P. (1957). "Biosynthesis of itaconic acid in *Aspergillus terreus*. I. Tracer studies with C14-labeled substrates." J. Biol. Chem. **226**(2): 673-687.

Birnboim H. C. and Doly J. (1979). "A rapid alkaline extraction procedure for screening recombinant plasmid DNA." Nucl. Acids Res. **7**(6): 1513-1523.

Björkroth J., Korkeala H. and Funke G. (1999). "rRNA gene RFLP as an identification tool for *Corynebacterium* species." Int. J. Syst. Evol. Microbiol. **49**(3): 983-989.

Bobik T. A., Lehman B. P. and Yeates T. O. (2015). "Bacterial microcompartments: widespread prokaryotic organelles for isolation and optimization of metabolic pathways." Mol. Microbiol. **98**(2): 193-207.

Boel G., Letso R., Neely H.*, et al.* (2016). "Codon influence on protein expression in *E. coli* correlates with mRNA levels." Nature **529**(7586): 358-363.

Bonnassie S., Burini J. F., Oreglia J.*, et al.* (1990). "Transfer of plasmid DNA to *Brevibacterium lactofermentum* by electrotransformation." J. Gen. Microbiol. **136**(10): 2107-2112.

Cai F., Sutter M., Bernstein S. L.*, et al.* (2015). "Engineering bacterial microcompartment shells: chimeric shell proteins and chimeric carboxysome shells." ACS Synth. Biol. **4**(4): 444-453.

Chen A. H. and Silver P. A. (2012). "Designing biological compartmentalization." Trends Cell Biol. **22**(12): 662-670.

Cheng S., Sinha S., Fan C., *et al.* (2011). "Genetic analysis of the protein shell of the microcompartments involved in coenzyme B12-dependent 1,2-propanediol degradation by *Salmonella*." J. Bacteriol. **193**(6): 1385-1392.

Cheng S., Fan C., Sinha S., *et al.* (2012). "The PduQ enzyme is an alcohol dehydrogenase used to recycle NAD^+ internally within the Pdu microcompartment of *Salmonella enterica*." PLoS One **7**(10): e47144.

Chistoserdova L. (2011). "Modularity of methylotrophy, revisited." Environ. Microbiol. **13**(10): 2603-2622.

Choudhary S., Quin M. B., Sanders M. A., *et al.* (2012). "Engineered protein nano-compartments for targeted enzyme localization." PLoS One **7**(3): e33342.

Chowdhury C., Sinha S., Chun S., *et al.* (2014). "Diverse bacterial microcompartment organelles." Microbiol. Mol. Biol. Rev. **78**(3): 438-468.

Chowdhury C., Chun S., Pang A., *et al.* (2015). "Selective molecular transport through the protein shell of a bacterial microcompartment organelle." PNAS **112**(10): 2990-2995.

Conrado R. J., Wu G. C., Boock J. T., *et al.* (2012). "DNA-guided assembly of biosynthetic pathways promotes improved catalytic efficiency." Nucl. Acids Res. **40**(4): 1879-1889.

Craciun S. and Balskus E. P. (2012). "Microbial conversion of choline to trimethylamine requires a glycyl radical enzyme." PNAS **109**(52): 21307-21312.

Crowley C. S., Sawaya M. R., Bobik T. A., *et al.* (2008). "Structure of the PduU shell protein from the Pdu microcompartment of *Salmonella*." Structure **16**(9): 1324-1332.

Crowley C. S., Cascio D., Sawaya M. R., *et al.* (2010). "Structural insight into the mechanisms of transport across the *Salmonella enterica* Pdu microcompartment shell." J. Biol. Chem. **285**(48): 37838-37846.

Drews G. and Niklowitz W. (1956). "Beiträge zur Cytologie der Blaualgen." Arch. Microbiol. **24**(2): 147-162.

Dueber J. E., Wu G. C., Malmirchegini G. R., *et al.* (2009). "Synthetic protein scaffolds provide modular control over metabolic flux." Nat. Biotechnol. **27**(8): 753-759.

Eggeling L. and Bott M. (2005). Handbook of *Corynebacterium glutamicum*, CRC press.

Eikmanns B. J., Kleinertz E., Liebl W., *et al.* (1991). "A family of *Corynebacterium glutamicum*/*Escherichia coli* shuttle vectors for cloning, controlled gene expression, and promoter probing." Gene **102**(1): 93-98.

Eikmanns B. J., Rittmann D. and Sahm H. (1995). "Cloning, sequence analysis, expression, and inactivation of the *Corynebacterium glutamicum icd* gene encoding isocitrate dehydrogenase and biochemical characterization of the enzyme." J. Bacteriol. **177**(3): 774-782.

Ezaki T. and Suzuki S. (1982). "Achromopeptidase for lysis of anaerobic gram-positive cocci." J. Clin. Microbiol. **16**(5): 844-846.

Fan C., Cheng S., Liu Y., *et al.* (2010). "Short N-terminal sequences package proteins into bacterial microcompartments." PNAS **107**(16): 7509-7514.

Fan C. and Bobik T. A. (2011). "The N-terminal region of the medium subunit (PduD) packages adenosylcobalamin-dependent diol dehydratase (PduCDE) into the Pdu microcompartment." J. Bacteriol. **193**(20): 5623-5628.

Fan C., Cheng S., Sinha S., *et al.* (2012). "Interactions between the termini of lumen enzymes and shell proteins mediate enzyme encapsulation into bacterial microcompartments." PNAS **109**(37): 14995-15000.

Frunzke J., Engels V., Hasenbein S., *et al.* (2008). "Co-ordinated regulation of gluconate catabolism and glucose uptake in *Corynebacterium glutamicum* by two functionally equivalent transcriptional regulators, GntR1 and GntR2." Mol. Microbiol. **67**(2): 305-322.

Gibson D. G., Young L., Chuang R. Y., *et al.* (2009). "Enzymatic assembly of DNA molecules up to several hundred kilobases." Nat. Methods **6**(5): 343-345.

Giessen T. W. and Silver P. A. (2016). "Encapsulation as a strategy for the design of biological compartmentalization." J. Mol. Biol. **428**(5 Pt B): 916-927.

Hahn-Hagerdal B., Karhumaa K., Jeppsson M., *et al.* (2007). "Metabolic engineering for pentose utilization in *Saccharomyces cerevisiae*." Adv. Biochem. Eng. Biotechnol. **108**: 147-177.

Hanahan D. (1983). "Studies on transformation of *Escherichia coli* with plasmids." J. Mol. Biol. **166**(4): 557-580.

Havemann G. D., Sampson E. M. and Bobik T. A. (2002). "PduA is a shell protein of polyhedral organelles involved in coenzyme B-12-dependent degradation of 1,2-propanediol in *Salmonella enterica* serovar typhimurium LT2." J. Bacteriol. **184**(5): 1253-1261.

Havemann G. D. and Bobik T. A. (2003). "Protein content of polyhedral organelles involved in coenzyme B12-dependent degradation of 1,2-propanediol in *Salmonella enterica* serovar Typhimurium LT2." J. Bacteriol. **185**(17): 5086-5095.

Haynes J. A. and Britz M. L. (1989). "Electrotransformation of Brevibacterium lactofermentum and Corynebacterium glutamicum: growth in tween 80 increases transformation frequencies." FEMS Microbiol. Lett. **61**(3): 329-333.

Heck d. H. A., Casanova M. and Starr T. B. (1990). "Formaldehyde toxicity—New understanding." Critical Reviews in Toxicology **20**(6): 397-426.

Heider S. A., Peters-Wendisch P. and Wendisch V. F. (2012). "Carotenoid biosynthesis and overproduction in *Corynebacterium glutamicum*." BMC Microbiol. **12**: 198.

Hektor H. J., Kloosterman H. and Dijkhuizen L. (2002). "Identification of a magnesium-dependent NAD(P)(H)-binding domain in the nicotinoprotein methanol dehydrogenase from *Bacillus methanolicus*." J. Biol. Chem. **277**(49): 46966-46973.

Held M., Kolb A., Perdue S.*, et al.* (2016). "Engineering formation of multiple recombinant Eut protein nanocompartments in *E. coli*." Sci. Rep. **6**: 24359.

Heldt D., Frank S., Seyedarabi A.*, et al.* (2009). "Structure of a trimeric bacterial microcompartment shell protein, EtuB, associated with ethanol utilization in *Clostridium kluyveri*." Biochem. J. **423**(2): 199-207.

Hentschel E., Will C., Mustafi N.*, et al.* (2013). "Destabilized eYFP variants for dynamic gene expression studies in *Corynebacterium glutamicum*." Microb. Biotechnol. **6**(2): 196-201.

Herman C., Thevenet D., Bouloc P.*, et al.* (1998). "Degradation of carboxy-terminal-tagged cytoplasmic proteins by the *Escherichia co*li protease HflB (FtsH)." Genes Dev. **12**(9): 1348-1355.

Huseby D. L. and Roth J. R. (2013). "Evidence that a metabolic microcompartment contains and recycles private cofactor pools." J. Bacteriol. **195**(12): 2864-2879.

Inui M., Kawaguchi H., Murakami S.*, et al.* (2004). "Metabolic engineering of *Corynebacterium glutamicum* for fuel ethanol production under oxygen-deprivation conditions." J. Mol. Microbiol. Biotechnol. **8**(4): 243-254.

Jakobson C. M., Kim E. Y., Slininger M. F.*, et al.* (2015). "Localization of proteins to the 1,2-propanediol utilization microcompartment by non-native signal sequences is mediated by a common hydrophobic motif." J. Biol. Chem. **290**(40): 24519-24533.

James C. L. and Viola R. E. (2002). "Production and characterization of bifunctional enzymes. Substrate channeling in the aspartate pathway." Biochemistry **41**(11): 3726-3731.

Jang K.-H., Pierotti D., Kemp G. W.*, et al.* (1997). "Mycotic acid composition of *Corynebacterium glutamicum* and its cell surface mutants: effects of growth with glycine and isonicotinic acid hydrazide." Microbiology **143**(10): 3209-3221.

Jojima T., Noburyu R., Sasaki M.*, et al.* (2015). "Metabolic engineering for improved production of ethanol by *Corynebacterium glutamicum*." Appl. Microbiol. Biotechnol. **99**(3): 1165-1172.

Jorda J., Liu Y., Bobik T. A.*, et al.* (2015). "Exploring bacterial organelle interactomes: a model of the protein-protein interaction network in the Pdu microcompartment." PLoS Comput. Biol. **11**(2): e1004067.

Kataoka M., Nakamura Y., Urano N.*, et al.* (2006). "A novel $NADP^+$-dependent L-1-amino-2-propanol dehydrogenase from *Rhodococcus erythropolis* MAK154: a promising enzyme for the production of double chiral aminoalcohols." Lett. Appl. Microbiol. **43**(4): 430-435.

Kato O., Youn J. W., Stansen K. C.*, et al.* (2010). "Quinone-dependent D-lactate dehydrogenase Dld (Cg1027) is essential for growth of *Corynebacterium glutamicum* on D-lactate." BMC Microbiol. **10**: 321.

Keilhauer C., Eggeling L. and Sahm H. (1993). "Isoleucine synthesis in *Corynebacterium glutamicum* - Molecular analysis of the *ilvB-ilvN-ilvC* operon." J. Bacteriol. **175**(17): 5595-5603.

Kerfeld C. A., Sawaya M. R., Tanaka S.*, et al.* (2005). "Protein structures forming the shell of primitive bacterial organelles." Science **309**(5736): 936-938.

Kerfeld C. A., Heinhorst S. and Cannon G. C. (2010). "Bacterial microcompartments." Annual Review of Microbiol. **64**: 391-408.

Kerfeld C. A. and Erbilgin O. (2015). "Bacterial microcompartments and the modular construction of microbial metabolism." Trends Microbiol. **23**(1): 22-34.

Kerfeld C. A. and Melnicki M. R. (2016). "Assembly, function and evolution of cyanobacterial carboxysomes." Curr. Opin. Plant Biol. **31**: 66-75.
Kim E. Y., Jakobson C. M. and Tullman-Ercek D. (2014). "Engineering transcriptional regulation to control Pdu microcompartment formation." PLoS One **9**(11): e113814.
Kim E. Y. and Tullman-Ercek D. (2014). "A rapid flow cytometry assay for the relative quantification of protein encapsulation into bacterial microcompartments." Biotechnol. J. **9**(3): 348-354.
Kinney J. N., Salmeen A., Cai F.*, et al.* (2012). "Elucidating essential role of conserved carboxysomal protein CcmN reveals common feature of bacterial microcompartment assembly." J. Biol. Chem. **287**(21): 17729-17736.
Kinoshita S., Kakizono T., Kadota K.*, et al.* (1985). "Purification of two alcohol dehydrogenases from *Zymomonas mobilis* and their properties." Appl. Microbiol. Biotechnol. **22**(4): 249-254.
Kirchner O. and Tauch A. (2003). "Tools for genetic engineering in the amino acid-producing bacterium *Corynebacterium glutamicum*." J. Biotechnol. **104**(1-3): 287-299.
Klein M. G., Zwart P., Bagby S. C.*, et al.* (2009). "Identification and structural analysis of a novel carboxysome shell protein with implications for metabolite transport." J. Mol. Biol. **392**(2): 319-333.
Kortmann M., Kuhl V., Klaffl S.*, et al.* (2015). "A chromosomally encoded T7 RNA polymerase-dependent gene expression system for *Corynebacterium glutamicum*: construction and comparative evaluation at the single-cell level." Microb. Biotechnol. **8**(2): 253-265.
Kuenz A., Gallenmuller Y., Willke T.*, et al.* (2012). "Microbial production of itaconic acid: developing a stable platform for high product concentrations." Appl. Microbiol. Biotechnol. **96**(5): 1209-1216.
Laslo T., von Zaluskowski P., Gabris C.*, et al.* (2012). "Arabitol metabolism of *Corynebacterium glutamicum* and its regulation by AtlR." J. Bacteriol. **194**(5): 941-955.
Lassila J. K., Bernstein S. L., Kinney J. N.*, et al.* (2014). "Assembly of robust bacterial microcompartment shells using building blocks from an organelle of unknown function." J. Mol. Biol. **426**(11): 2217-2228.
Lassila J. K. (2015). Production of bacterial microcompartments. Protein Cages - Methods and Protocols. B. P. Orner, Springer Protocols.
Law K., Rosenfeld J. and Jackson M. (2013). White Paper, "Methanol as renewable carbon source". Alexandria, Methanol Institute.
Lawrence A. D., Frank S., Newnham S.*, et al.* (2014). "Solution structure of a bacterial microcompartment targeting peptide and its application in the construction of an ethanol bioreactor." ACS Synth. Biol. **3**(7): 454-465.
Lee H., DeLoache W. C. and Dueber J. E. (2012). "Spatial organization of enzymes for metabolic engineering." Metab. Eng. **14**(3): 242-251.
Lee J. Y., Na Y. A., Kim E.*, et al.* (2016). "The Actinobacterium *Corynebacterium glutamicum*, an Industrial Workhorse." J. Microbiol. Biotechnol. **26**(5): 807-822.
Lee M. J., Brown I. R., Juodeikis R.*, et al.* (2016). "Employing bacterial microcompartment technology to engineer a shell-free enzyme-aggregate for enhanced 1,2-propanediol production in *Escherichia coli*." Metab. Eng. **36**: 48-56.
Lehman B. P., Chowdhury C. and Bobik T. A. (2017). "The N-terminus of the PduB protein binds the protein shell of the Pdu microcompartment to Its enzymatic core." J. Bacteriol. **199**(8): 00785-00716.
Liu F., Banta S. and Chen W. (2013). "Functional assembly of a multi-enzyme methanol oxidation cascade on a surface-displayed trifunctional scaffold for enhanced NADH production." Chem. Commun. **49**(36): 3766-3768.
Ludwig K. (2016). Master thesis, Ethanol production in *Corynebacterium glutamicum* using bacterial microcompartments." Faculty of Nature and Technology, City University of Applied Sciences Bremen.
Maity B., Fujita K. and Ueno T. (2015). "Use of the confined spaces of apo-ferritin and virus capsids as nanoreactors for catalytic reactions." Curr. Opin. Chem. Biol. **25**: 88-97.
Mallette E. and Kimber M. S. (2017). "A complete structural inventory of the mycobacterial microcompartment shell proteins constrains models of global architecture and transport." J. Biol. Chem. **292**(4): 1197-1210.
Mayer M. J., Juodeikis R., Brown I. R.*, et al.* (2016). "Effect of bio-engineering on size, shape, composition and rigidity of bacterial microcompartments." Sci. Rep. **6**: 36899.

Mehta P., Woo P., Venkataraman K., *et al.* (2012). "Ribosome purification approaches for studying interactions of regulatory proteins and RNAs with the ribosome." Methods in molecular biology **905**: 273-289.

Moon T. S., Dueber J. E., Shiue E., *et al.* (2010). "Use of modular, synthetic scaffolds for improved production of glucaric acid in engineered *E. coli*." Metab. Eng. **12**(3): 298-305.

Muller J. E., Heggeset T. M., Wendisch V. F., *et al.* (2015). "Methylotrophy in the thermophilic *Bacillus methanolicus*, basic insights and application for commodity production from methanol." Appl. Microbiol. Biotechnol. **99**(2): 535-551.

Nakagawa T., Mitsui R., Tani A., *et al.* (2012). "A catalytic role of XoxF1 as La^{3+}-dependent methanol dehydrogenase in *Methylobacterium* extorquens strain AM1." PLoS One **7**(11): e50480.

Niebisch A. and Bott M. (2001). "Molecular analysis of the cytochrome bc1-aa3 branch of the *Corynebacterium glutamicum* respiratory chain containing an unusual diheme cytochrome c1." Arch. Microbiol. **175**(4): 282-294.

Obradors N., Badia J., Baldoma L., *et al.* (1988). "Anaerobic metabolism of the L-rhamnose fermentation product 1,2-propanediol in *Salmonella typhimurium*." J. Bacteriol. **170**(5): 2159-2162.

Ochsner A. M., Muller J. E., Mora C. A., *et al.* (2014). "In vitro activation of NAD-dependent alcohol dehydrogenases by Nudix hydrolases is more widespread than assumed." FEBS Lett. **588**(17): 2993-2999.

Ohta K., Beall D. S., Mejia J. P., *et al.* (1991). "Genetic improvement of *Escherichia coli* for ethanol production: chromosomal integration of *Zymomonas mobilis* genes encoding pyruvate decarboxylase and alcohol dehydrogenase II." Appl. Environ. Microbiol. **57**(4): 893-900.

Okabe M., Lies D., Kanamasa S., *et al.* (2009). "Biotechnological production of itaconic acid and its biosynthesis in *Aspergillus terreus*." Appl. Microbiol. Biotechnol. **84**(4): 597-606.

Oreb M., Dietz H., Farwick A., *et al.* (2012). "Novel strategies to improve co-fermentation of pentoses with D-glucose by recombinant yeast strains in lignocellulosic hydrolysates." Bioengineered **3**(6): 347-351.

Orita I., Sakamoto N., Kato N., *et al.* (2007). "Bifunctional enzyme fusion of 3-hexulose-6-phosphate synthase and 6-phospho-3-hexuloisomerase." Appl. Microbiol. Biotechnol. **76**(2): 439-445.

Orita I., Kita A., Yurimoto H., *et al.* (2010). "Crystal structure of 3-hexulose-6-phosphate synthase, a member of the orotidine 5'-monophosphate decarboxylase suprafamily." Proteins **78**(16): 3488-3492.

Otten A. (2013). PhD thesis, Metabolic Engineering von *Corynebacterium glutamicum* für die Produktion einer Dicarbonsäure." Institute of Bio- and Geosciences (IBG): Biotechnology (IBG-1), University Düsseldorf

Otten A., Brocker M. and Bott M. (2015). "Metabolic engineering of *Corynebacterium glutamicum* for the production of itaconate." Metab. Eng. **30**: 156-165.

Pallerla S. R., Knebel S., Polen T., *et al.* (2005). "Formation of volutin granules in *Corynebacterium glutamicum*." FEMS Microbiol. Lett. **243**(1): 133-140.

Pang A., Warren M. J. and Pickersgill R. W. (2011). "Structure of PduT, a trimeric bacterial microcompartment protein with a 4Fe-4S cluster-binding site." Acta Crystallogr. D. Biol. Crystallogr. **67**(Pt 2): 91-96.

Pang A., Liang M., Prentice M. B., *et al.* (2012). "Substrate channels revealed in the trimeric *Lactobacillus reuteri* bacterial microcompartment shell protein PduB." Acta Crystallogr. D. Biol. Crystallogr. **68**(Pt 12): 1642-1652.

Pang A., Frank S., Brown I., *et al.* (2014). "Structural insights into higher order assembly and function of the bacterial microcompartment protein PduA." J Biol Chem **289**(32): 22377-22384.

Parsons J. B., Dinesh S. D., Deery E., *et al.* (2008). "Biochemical and structural insights into bacterial organelle form and biogenesis." J. Biol. Chem. **283**(21): 14366-14375.

Parsons J. B., Frank S., Bhella D., *et al.* (2010). "Synthesis of empty bacterial microcompartments, directed organelle protein incorporation, and evidence of filament-associated organelle movement." Mol. Cell **38**(2): 305-315.

Peters-Wendisch P. G., Schiel B., Wendisch V. F., *et al.* (2001). "Pyruvate carboxylase is a major bottleneck for glutamate and lysine production by *Corynebacterium glutamicum*." J. Mol. Microbiol. Biotechnol. **3**(2): 295-300.

Petit E., LaTouf W. G., Coppi M. V., *et al.* (2013). "Involvement of a bacterial microcompartment in the metabolism of fucose and rhamnose by *Clostridium phytofermentans*." PLoS One **8**(1): e54337.

Plotka M., Wozniak M. and Kaczorowski T. (2017). "Quantification of plasmid copy number with single colour droplet digital PCR." PLoS One **12**(1).

Plotkin J. B. and Kudla G. (2011). "Synonymous but not the same: the causes and consequences of codon bias." Nature Reviews Genetics **12**(1): 32-42.

Price J. V., Chen L., Whitaker W. B., *et al.* (2016). "Scaffoldless engineered enzyme assembly for enhanced methanol utilization." PNAS **113**(45): 12691-12696.

Rae B. D., Long B. M., Badger M. R., *et al.* (2013). "Functions, compositions, and evolution of the two types of carboxysomes: polyhedral microcompartments that facilitate CO2 fixation in cyanobacteria and some proteobacteria." Microbiol. Mol. Biol. Rev. **77**(3): 357-379.

Rittmann D., Lindner S. N. and Wendisch V. F. (2008). "Engineering of a glycerol utilization pathway for amino acid production by *Corynebacterium glutamicum*." Appl. Environ. Microbiol. **74**(20): 6216-6222.

Rivera M. C., Maguire B. and Lake J. A. (2015). "Isolation of ribosomes and polysomes." Cold Spring Harbor Protocols **2015**(3): pdb.prot081331.

Ruan Y., Zhu L. and Li Q. (2015). "Improving the electro-transformation efficiency of *Corynebacterium glutamicum* by weakening its cell wall and increasing the cytoplasmic membrane fluidity." Biotechnol. Lett. **37**(12): 2445-2452.

Sambrook J. and Russell D. W. (2001). Molecular cloning: A laboratory manual. NY, Cold Spring Harbor Laboratory Press.

Sargent F., Davidson F. A., Kelly C. L., *et al.* (2013). "A synthetic system for expression of components of a bacterial microcompartment." Microbiology **159**(Pt 11): 2427-2436.

Sasaki M., Jojima T., Kawaguchi H., *et al.* (2009). "Engineering of pentose transport in *Corynebacterium glutamicum* to improve simultaneous utilization of mixed sugars." Appl. Microbiol. Biotechnol. **85**(1): 105-115.

Sauer M., Porro D., Mattanovich D., *et al.* (2008). "Microbial production of organic acids: expanding the markets." Trends Biotechnol. **26**(2): 100-108.

Schäfer A., Tauch A., Jäger W., *et al.* (1994). "Small mobilizable multi-purpose cloning vectors derived from the *Escherichia coli* plasmids pK18 and pK19: selection of defined deletions in the chromosome of *Corynebacterium glutamicum*." Gene **145**(1): 69-73.

Seibold G., Auchter M., Berens S., *et al.* (2006). "Utilization of soluble starch by a recombinant *Corynebacterium glutamicum* strain: growth and lysine production." J. Biotechnol. **124**(2): 381-391.

Shen X.-H., Zhou N.-Y. and Liu S.-J. (2012). "Degradation and assimilation of aromatic compounds by *Corynebacterium glutamicum*: another potential for applications for this bacterium?" Appl. Microbiol. Biotechnol. **95**(1): 77-89.

Sinha S., Cheng S., Fan C., *et al.* (2012). "The PduM protein is a structural component of the microcompartments involved in coenzyme B12-dependent 1,2-propanediol degradation by *Salmonella enterica*." J. Bacteriol. **194**(8): 1912-1918.

Sinha S., Cheng S., Sung Y. W., *et al.* (2014). "Alanine scanning mutagenesis identifies an asparagine-arginine-lysine triad essential to assembly of the shell of the Pdu microcompartment." J. Mol. Biol. **426**(12): 2328-2345.

Siu K. H., Chen R. P., Sun Q., *et al.* (2015). "Synthetic scaffolds for pathway enhancement." Curr. Opin. Biotechnol. **36**: 98-106.

Snijder J., Kononova O., Barbu I. M., *et al.* (2016). "Assembly and mechanical properties of the cargo-free and cargo-loaded bacterial nanocompartment encapsulin." Biomacromolecules **17**(8): 2522-2529.

Steiger M. G., Blumhoff M. L., Mattanovich D., *et al.* (2013). "Biochemistry of microbial itaconic acid production." Front Microbiol. **4**: 23.

Sutter M., Boehringer D., Gutmann S., *et al.* (2008). "Structural basis of enzyme encapsulation into a bacterial nanocompartment." Nat. Struct. Mol. Biol. **15**(9): 939-947.

Takayama K., Schnoes H. K., Armstrong E. L., *et al.* (1975). "Site of inhibitory action of isoniazid in the synthesis of mycolic acids in Mycobacterium tuberculosis." J. Lipid Res. **16**(4): 308-317.

Tanaka S., Sawaya M. R. and Yeates T. O. (2010). "Structure and mechanisms of a protein-based organelle in *Escherichia coli*." Science **327**(5961): 81-84.

Thierbach G., Schwarzer A. and Pühler A. (1988). "Transformation of spheroplasts and protoplasts of *Corynebacterium glutamicum*." Appl. Microbiol. Biotechnol. **29**(4): 356-362.

Thompson M. C., Cascio D., Leibly D. J., *et al.* (2015). "An allosteric model for control of pore opening by substrate binding in the EutL microcompartment shell protein." Protein Sci. **24**(6): 956-975.

Tobimatsu T., Kawata M. and Toraya T. (2005). "The N-terminal regions of β and γ subunits lower the solubility of adenosylcobalamin-dependent diol dehydratase." Bioscience, Biotechnology, and Biochemistry **69**(3): 455-462.

Tsoy O., Ravcheev D. and Mushegian A. (2009). "Comparative genomics of ethanolamine utilization." J. Bacteriol. **191**(23): 7157-7164.

Urano N., Kataoka M., Ishige T., *et al.* (2011). "Genetic analysis around aminoalcohol dehydrogenase gene of *Rhodococcus erythropolis* MAK154: a putative GntR transcription factor in transcriptional regulation." Appl. Microbiol. Biotechnol. **89**(3): 739-746.

van der Rest M. E., Lange C. and Molenaar D. (1999). "A heat shock following electroporation induces highly efficient transformation of *Corynebacterium glutamicum* with xenogeneic plasmid DNA." Appl. Microbiol. Biotechnol. **52**(4): 541-545.

Wang Y., Heermann R. and Jung K. (2017). "CipA and CipB as scaffolds to organize proteins into crystalline inclusions." ACS Synth. Biol.

Werpy T., Petersen G., Aden A., *et al.* (2004). Technical report, "Top value added chemicals from biomass.", US Department of Energy (US).

Witthoff S., Muhlroth A., Marienhagen J., *et al.* (2013). "C1 metabolism in *Corynebacterium glutamicum*: an endogenous pathway for oxidation of methanol to carbon dioxide." Appl. Environ. Microbiol. **79**(22): 6974-6983.

Witthoff S., Schmitz K., Niedenfuhr S., *et al.* (2015). "Metabolic engineering of *Corynebacterium glutamicum* for methanol metabolism." Appl. Environ. Microbiol. **81**(6): 2215-2225.

Yamamoto S., Suda M., Niimi S., *et al.* (2013). "Strain optimization for efficient isobutanol production using *Corynebacterium glutamicum* under oxygen deprivation." Biotechnol. Bioeng. **110**(11): 2938-2948.

Yang Z., Gao X., Xie H., *et al.* (2017). "Enhanced itaconic acid production by self-assembly of two biosynthetic enzymes in *Escherichia coli*." Biotechnol. Bioeng. **114**(2): 457-462.

Yeates T. O., Jorda J. and Bobik T. A. (2013). "The shells of BMC-type microcompartment organelles in bacteria." J. Mol. Microbiol. Biotechnol. **23**(4-5): 290-299.

Yoshihama M., Higashiro K., Rao E. A., *et al.* (1985). "Cloning vector system for *Corynebacterium glutamicum*." J. Bacteriol. **162**(2): 591-597.

Zahoor A., Lindner S. N. and Wendisch V. F. (2012). "Metabolic engineering of *Corynebacterium glutamicum* aimed at alternative carbon sources and new products." Comput. Struct. Biotechnol. J. **3**: e201210004.

6 APPENDIX

6.1 Supplemental material – Construction of plasmids

For the construction of the Pdu production and integration plasmids, the plasmids pJP063 containing *pduABJKNUT* (Parsons *et al.*, 2010) and pED460 containing *pduA-X* (Parsons *et al.*, 2008) were used as initial PCR templates. All constructs derived from those plasmids are listed and construction procedures are described in Table S1.

Table S1: Construction of Pdu production plasmids. The numbers represent oligonucleotide pairs used for PCR (Table S4). The DNA template used for amplification is given in brackets behind the oligonucleotides, followed by the information on the plasmid backbone and the restriction enzymes used for linearization.

Plasmid	Construction
pAN6_*pduA-X*	Gibson assembly: 725/726 and 727/728 (pED460) and pED460 *AscI *KpnI into pAN6 *NdeI *EcoRI
pAN6_*pduABJKNUT*	Gibson assembly: 725/729 (pET3a_*pduABJKNUT*) into pAN6 *NdeI *EcoRI
pMKEx1_*pduABJKNUT*	Gibson assembly: 036/028 (pAN6_*pduABJKNUT*) into pMKEx1 *BamHI *NcoI
pMKEx1_*mcherrypduABJKNUT*	Gibson assembly: 030/029 (pK19_*alpC-mcherry*) and 027/028 (pAN6_*pduABJKNUT*) into pMKEx1 *BamHI *NcoI
pMKEx1_*pduA*	Gibson assembly: 140/159 (pMKEx1_*pduABJKNUT*) into pMKEx1 *BamHI * XbaI
pMKEx1_*mcherrypduA*	Gibson assembly: 140/159 (pMKEx1_*mcherrypduABJKNUT*) into pMKEx1 *BamHI * XbaI
pMKEx1_*pduABJKNTU*$_{native}$	Gibson assembly: 140/178 (pMKEx1_*pduABJKNUT*), 179/180, 181/182 and 183/174 (pAN6_*pduA-X*) into pMKEx1 *XbaI *BamHI
pMKEx1_*pduABJkN*	Gibson assembly: 140/168 and 167/176 (pMKEx1_*pduABJKNUT*) into pMKEx1 *XbaI *BamHI
pMKEx1_*pduABJkNu*	Gibson assembly: 140/168, 167/170 and 169/174 (pMKEx1_*pduABJKNUT*) into pMKEx1 *XbaI *BamHI
pMKEx1_*pduABJkNut*	Gibson assembly: 140/168,167/170, 169/172, 171/028 (pMKEx1_*pduABJKNUT)* into pMKEx1 *XbaI *BamHI
pMKEx1_*pduABJkn*	Gibson assembly: 140/168neu 167neu/200 199/176 (pMKEx1_*pduABJkNut*) into pMKEx1 *XbaI *BamHI
pMKEx1_*pduABJknt*	Gibson assembly: 140/168neu, 167neu/200, 199/202 and 201/028 (pMKEx1_*pduABJkNut*) into pMKEx1 *XbaI *BamHI
pMKEx1_*pduABJkNt*	Gibson assembly: 140/168neu, 167neu/202 and 201/028 (pMKEx1_*pduABJkNut*) into pMKEx1 *XbaI *BamHI
pMKEx1_*pduJ*	Gibson assembly: 232/184 (pMKEx1_*pduABJKNUT*) into pMKEx1 *XbaI *BamHI
pMKEx1_*pduABJKnut*	Gibson assembly: 140/200 (pMKEx1_*pduABJKNUT)* and 199/028 *(*pMKEx1_*pduABJkNut)* into pMKEx1 *XbaI *BamHI
pMKEx1_*pduABJKnt*	Gibson assembly: 140/200 (pMKEx1_*pduABJKNUT*) and 199/028 (pMKEx1_*pduABJknt)* into pMKEx1 *XbaI *BamHI
pMKEx1_*pduABJKN*	Gibson assembly: 140/176 (pMKEx1_*pduABJKNUT*) into pMKEx1

Plasmid	Construction
	*XbaI *BamHI
pMKEx1_*pduABJKNU*	Gibson assembly: 140/174 (pMKEx1_*pduABJKNUT*) into pMKEx1 *XbaI *BamHI
pMKEx1_*pduBJKN*	Gibson assembly: 233/176 (pMKEx1_*pduABJKNUT*); 140/176 (PCR product 233/176) into pMKEx1 *XbaI *BamHI
pMKEx1_*pduA*$_{GBDlig}$*BJKNUT*	Gibson assembly: 137/138 (Protein_scaffolds$_{opt}$), 136/726 and 139/140 (pMKEx1_*pduABJKNUT*) into pMKEx1_*PduABJKNUT* *AscI * XbaI
pMKEx1_*pduA*$_{SH3lig}$*BJKNUT*	Gibson assembly: 139/140 and 142/726 (pMKEx1_*pduABJKNUT*) into pMKEx1_*PduABJKNUT* *AscI *XbaI
pMKEx1_*pduA*$_{PDZlig}$*BJKNUT*	Gibson assembly: 139/140 and 141/726 (pMKEx1_*pduABJKNUT*) into pMKEx1_*PduABJKNUT* *AscI *XbaI
pMKEx1_*pduA*$_{PDZlig}$*BJknt*	Gibson assembly: 240/028 (pMKEx1_*pduABJknt*) and 140/242 (pMKEx1_*pduA*$_{PDZlig}$*BJKNUT*) into pMKEx1 *XbaI *BamHI
pMKEx1_*pduA*$_{SH3lig}$*BJknt*	Gibson assembly: 243/140 *pduA*$_{SH3lig}$*BJKNUT* and 240/028 (pMKEx1_*pduABJknt*) into pMKEx1 *XbaI *BamHI
pMKEx1_*pduA*$_{GBDlig}$*BJknt*	Gibson assembly: 241/140 (pMKEx1_*pduA*$_{GBDlig}$*BJKNUT)* and 240/028 (pMKEx1_*pduABJknt*) into pMKEx1 *XbaI *BamHI
pMKEx1_*pduA*$_{PDZlig}$	Gibson assembly: 140/156 (pMKEx1_*pduA*$_{PDZlig}$*BJknt*) into pMKEx1 *XbaI *BamHI
pMKEx1_*pduA*$_{SH3lig}$	Gibson assembly: 140/157 (pMKEx1_*pduA*$_{SH3Zlig}$*BJknt*) into pMKEx1 *XbaI *BamHI
pMKEx1_*pduA*$_{GBDlig}$	Gibson assembly: 140/158 (pMKEx1_*pduA*$_{GBDlig}$*BJknt*) into pMKEx1 *XbaI *BamHI
pK19_*pduABJKNUT*	Gibson assembly: 197/198 (pMKEx1_*pduABJKNUT*) into pK19_CGP1int_P$_{T7}$*eyfp* *XbaI *BlpI
pK19_*pduABJknt*	Gibson assembly: 197/198 (pMKEx1_*pduABJknt*) into pK19_CGP1int_P$_{T7}$*eyfp* *XbaI *BlpI
pK19_*pduA*	Gibson assembly: 197/198 (pMKEx1_*pduA*) into pK19_CGP1int_P$_{T7}$*eyfp* *XbaI *BlpI

The construction of different fluorescence reporter production plasmids is described in Table S2. The DNA template 'Protein_scaffolds$_{opt}$' was synthesized (Sequence S1) and used as described.

Sequence S1: Synthesized 'Protein_scaffolds$_{opt}$' sequences.

>GBD$_{lig}$

CTGGTGGGCGCACTGATGCACGTGATGCAGAAGCGCTCCCGCGCAATCCACTCCTCCGATGAAGGCG
AAGATCAGGCAGGCGATGAAGATGAAGAT

>SH3$_{dom}$

GCAGAGTATGTGCGTGCCCTCTTTGACTTTAATGGTAATGATGAAGAAGATCTTCCCTTTAAGAAAGGAG
ACATCCTGCGCATCCGCGATAAGCCTGAAGAGCAGTGGTGGAATGCAGAGGACAGCGAAGGAAAGCG
CGGTATGATTCCTGTCCCTTACGTGGAGAAGTATCGC

>PDZ$_{dom}$

CTCCAGCGTCGCCGCGTGACGGTGCGCAAGGCCGACGCCGGCGGTCTGGGCATCAGCATCAAGGGT
GGCCGTGAAAACAAGATGCCTATTCTCATTTCCAAGATCTTCAAGGGACTGGCAGCAGACCAGACGGA
GGCCCTTTTTGTTGGTGATGCCATCCTGTCTGTGAATGGTGAAGATTTGTCCTCTGCCACCCACGATGA

AGCGGTACAGGCCCTCAAGAAGACCGGCAAGGAGGTTGTGTTGGAGGTTAAGTACATGAAGGAGGTCT
CACCCTATTTCAAG

>GBD_{dom}

ACCAAGGCAGATATTGGAACTCCATCCAATTTCCAGCACATTGGACATGTTGGTTGGGATCCAAATACC
GGTTTTGATCTAAATAATTTGGATCCAGAATTGAAGAATCTTTTTGATATGTGTGGTATCTCTGAGGCCCA
GCTTAAAGACCGCGAAACTTCAAAAGTTATTTATGACTTTATTGAAAAAACTGGAGGTGTAGAAGCTGTT
AAAAATGAACTCCGTCGCCAAGCACCA

>$C17_{P.m.}$ with $(GGGS)_2GG$ linker

GGCGGTGGCTCCGGCGGCGGTTCCGGCGGTACCGAAGAAAACGTGGAACGCATCATCAAGGAAGTGC
TGGGCCGCCTGGGCAAG

Table S2: Construction of different fluorescence reporter production plasmids. Numbers represent oligonucleotide pairs used for PCR (Table S4). The DNA template used for amplification is given in brackets behind the oligonucleotides followed by the information on the plasmid backbone and the restriction enzymes used for linearization.

Plasmid	Construction
pEC-P_{tetR}	Gibson assembly: 780/012 (pCL-TON1) into pEC-XC99E *PstI *NdeI
pEC_*eyfp*	Cloning: 008/009 (pEKEx2_eyfp$_{ASV}$)*BcuI *EcoRI ligated into pEC-TetR *BcuI * EcoRI
pEC_*P18*	Cloning: 003/004 (pED460)*BglII *EcoRV ligated into pEC-TetR *BglII *EcoRV
pEC_*D18*	Cloning: 005/006 (pED460)*BglII *EcoRV ligated into pEC-TetR *BglII *EcoRV
pEC_*P18eyfp*	Cloning: 007/013 (pEKEx2_eyfp$_{ASV}$) *BglII *BcuI into pEC_*P18* *BglII *BcuI
pEC_*P18eyfp$_{ASV}$*	Cloning: 007/014 (pEKEx2_eyfp$_{ASV}$) *BglII *BcuI into pEC_*P18* *BglII *BcuI
pEC_*D18eyfp$_{AAV}$*	Cloning: 007/015 (pEKEx2_eyfp$_{AAV}$) *BglII *BcuI into pEC_*P18* *BglII *BcuI
pEC_*D18eyfp*	Cloning: 007/013 (pEKEx2_eyfp$_{ASV}$) *BglII *BcuI into pEC_*D18* *BglII *BcuI
pEC_*D18eyfp$_{ASV}$*	Cloning: 007/014 (pEKEx2_eyfp$_{ASV}$) *BglII *BcuI into pEC_*D18* *BglII *BcuI
pEC_*D18eyfp$_{AAV}$*	Cloning: 007/015 (pEKEx2_eyfp$_{AAV}$) *BglII *BcuI into pEC_*P18* *BglII *BcuI
pEC_*D18eyfp-P18cfp*	Gibson assembly: 215/217 (pEC_*D18eyfp),* 216/218 (*cfp*) into pEC_*P18eyfp* *BcuI
pEC_*eyfp-PDZ$_{dom}$*	Gibson assembly: 143/144 (Protein_scaffolds$_{opt}$) into pEC_eyfp *BcuI
pEC_*eyfp-SH3$_{dom}$*	Gibson assembly: 145/146 (Protein_scaffolds$_{opt}$) into pEC_eyfp *BcuI
pEC_*eyfp-GBD$_{dom}$*	Gibson assembly: 147/148 (Protein_scaffolds$_{opt}$) into pEC_eyfp *BcuI
pEC_*eyfp-P18*	Gibson assembly: 109/114 (pEC_*eyfp*) and 116/115 (pEC-*P18eyfp*) into pEC_TetR *EcoRV *BcuI
pEC_*eyfp-C17$_{K.p.}$*	Gibson assembly: 109/131 (pEC_*eyfp(GGGS)2GG_P18*) and 109/132 (PCR product 109/131) into pEC_TetR *EcoRV *BcuI
pEC_*eyfp-C17$_{P.m.}$*	Gibson assembly: 109/114 (pEC_*eyfp*) and 134/135 (Protein_scaffolds$_{opt}$) into pEC_TetR *EcoRV *BcuI

Genomic template DNA from *Zymomonas mobilis subsp. mobilis* ATCC 29191 was kindly provided by Stephanie Bringer-Meyer and used for the amplification of the enzymes alcohol dehydrogenase B (AdhB; GenBank: AFN57379.1) and the pyruvate decarboxylase (Pdc; GenBank: AFN57569.1). All derived plasmids are listed in Table S3.

Table S3: Construction of AdhB and Pdc production plasmids. The numbers represent oligonucleotide pairs used for PCR (Table S4). The DNA template used for amplification is given in brackets behind the oligonucleotides followed by the information on the plasmid backbone and the restriction enzymes used for linearization.

Plasmid	Construction
pVWEx2_Bm(*mdh*)	Gibson assembly: 081/086 (pVWEx2_Bm(*D18mdh_act*)) into 082/085 (pVWEx2_mdh_act)
pVWEx2_Bm(*D18mdh*)	Gibson assembly: 080/081 (pVWEx2_Bm(*D18mdh_act*)) into 079/082 (pVWEx2_Bm(*mdh_act*))
pVWEx2_Bm(*D18mdh_act*)	Gibson assembly: 080/103 (pVWEx2_Bm(*D18mdh_act*)) into 079/080 (pVWEx2_Bm(*mdh_act*))
pEKEx2_Bs(*D18hps_P18phi*)	Gibson assembly: 074/075 (pEKEx2_Bs(hps_phi)) into 073/077 (pEKEx2_Bs(*hps_phi*))
pEKEx2_Bs(*D18hps_phi*)	Gibson assembly: 074/076 (pEKEx2_Bs(*hps_phi*)) into 073/078 (pEKEx2_Bs(*hps_phi*))
pEKEx2_Bs(*D18-GS-hps_phi*)	Site directed mutagenesis: 094/095 on pEKEx2_Bs(*D18hps_phi*)
pEKEx2_Bs(*D18-GGSG-hps_phi*)	Gibson assembly: 076/096 (pEKEx2_Bs(*hps_phi*)) into 073/078 (pEKEx2_Bs(*hps_phi*))
pEKEx2_Bs(*D18-10aa-hps_phi*)	Gibson assembly: 076/101 pEKEx2_Bs(*hps_phi*)) into 078/102 (pEKEx2_Bs(*hps_phi*))
pVWEx2_*pdc*	Gibson assembly: K15/K16 (*Z. mobilis* genome) into pVWEx2 *XbaI *SalI
pVWEx2_*P18-NdeI-pdc*	Gibson assembly: K24/K16 (*Z. mobilis* genome) and K27/K28 (pEC_*P18eyfp*) into pVWEx2 *XbaI *SalI
pVWEx2_*P18-GS-pdc*	Gibson assembly: K26/K16 (*Z. mobilis* genome) and K30/K27 (pEC_*P18eyfp*) into pVWEx2 *XbaI *SalI
pVWEx2_*P18-GSGS-pdc*	Gibson assembly: K25/K16 (*Z. mobilis* genome) and K29/K27 (pEC_*P18eyfp*) into pVWEx2 *XbaI *SalI
pVWEx2_*adhB*	Gibson assembly: K14/K13 (*Z. mobilis* genome) into pVWEx2 *XbaI *SalI
pVWEx2_*D18-GSGS-adhB*	Gibson assembly: K14/K19 (*Z. mobilis* genome) and K34/K23 (pEC_*D18eyfp*) into pVWEx2 *XbaI *SalI
pVWEx2_*D18-10aa-adhB*	Gibson assembly: K35/K14 (*Z. mobilis* genome) and K20/K36 (pVWEx2_*D18-GSGS-adhB*) into pVWEx2 *XbaI *SalI
pVWEx2_*D60adhB*	Gibson assembly: K33/K14 (*Z. mobilis* genome) and K34/K32 (pET14b-pdu65) into pVWEx2 *XbaI *SalI
pVWEx2_*adhB-GBD*$_{dom}$	Gibson assembly: K13/257 (pVWEx2-*adhB*) and 258/260 (pEC_*eyfp-GBD*$_{dom}$) into pVWEx2 *SalI*XbaI
pVWEx2_*adhB-SH3*$_{dom}$	Gibson assembly: K13/257 (pVWEx2_*adhB*) and 258/261 (pEC_*eyfp-SH3*$_{dom}$) into pVWEx2 *SalI*XbaI
pVWEx2_*adhB-PDZ*$_{dom}$	Gibson assembly: K13/257 (pVWEx2_*adhB*) and 258/259 (pEC_*eyfp-PDZ*$_{dom}$) into pVWEx2 *SalI*XbaI
pVWEx2-*adhB_pdc*	Gibson assembly: K38/K16 (pVWEx2_*pdc)* and K13/K39 (pVWEx2-*adhB*) into pVWEx2 *SalI*XbaI
pVWEx2-*D18-GSGS-adhB_P18pdc*	Gibson assembly: K20/K39 (pVWEx2_*D18-GSGS-adhB*) and K37/K16 (pVWEx2_*P18-NdeI-pdc*) into pVWEx2 *SalI*XbaI
pVWEx2-*D18-10aa-adhB_P18pdc*	Gibson assembly: K20/K39 (pVWEx2-*D18-10aa-adhB*) and K37/K16 (pVWEx2_*P18-NdeI-pdc*) into pVWEx2 *SalI*XbaI
pEKEx2_P$_{tac}$*P18malEcad*	Gibson assembly: 110/111 (pEC-*P18eyfp*) and 112/113 (pEKEx2_P$_{tac}$*malEcad*) into pEKEx2_*malEcad* *PstI *EcoRI
pEKEx2_P$_{tac}$*acn*	Gibson assembly: 122/125 (*C. glutamicum* genome) into pEKEx2_P$_{tac}$*malEcad* *PstI *EcoRI
pEKEx2_P$_{tac}$*D18acn*	Gibson assembly: 119/120 (pEKEx2_Bs(*D18-GGSG-hps_phi*)) and 121/122 (*C. glutamicum* genome) into pEKEx2_P$_{tac}$*malEcad* *PstI *EcoRI

Plasmid	Construction
pVWEx2_*malEcad*	Gibson assembly: 204/161 (pEKEx2_P$_{tac}$*malEcad*) into pVWEx2 *SalI *XbaI
pVWEx2_*P18malEcad*	Gibson assembly: 203/161 (pEKEx2_P$_{tac}$*P18malEcad*) into pVWEx2 *SalI *XbaI
pVWEx2_*acn_malEcad*	Gibson assembly: 161/166 (pEKEx2_P$_{tac}$*malEcad*) and 163/165 (pEKEx2_P$_{tac}$*acn*) into pVWEx2 *SalI*XbaI
pVWEx2_*D18acn_P18malEcad*	Gibson assembly: 161/162 (pEKEx2_P$_{tac}$*P18malEcad*) and 163/164 (pEKEx2_P$_{tac}$*D18acn*) into pVWEx2 *SalI*XbaI
pK19_*D18acn*$_{ATG}$	Gibson assembly: 189/213 (*C. glutamicum* genome), 210/211 (pEKEx2_P$_{tac}$*D18acn*) and 194/212 (*C. glutamicum* genome) into pK19mobSacB *EcoRI *PstI
pK19_*D18acn*$_{GTG}$	Gibson assembly: 189/209 (*C. glutamicum* genome), 214/211 (pEKEx2_P$_{tac}$*D18acn*) and 194/212 (*C. glutamicum* genome) into pK19mobSacB *EcoRI *PstI

Table S4: Summary of oligonucleotides used in this work.

Oligonucleotide	Sequence (5' -> 3')
(003)EcoRV_P18_fw	ACGTGATATCCATATGAACACTTCAGAACTTGA
(004)P18_BglII_rv	ACGTAGATCTAAGTTGCTCACTCAAAATGT
(005)EcoRV_D18_fw	ACGTGATATCCATATGGAAATCAATGAAAAGCT
(006)D18_BglII_rv	ACGTAGATCTTTCAGACAGTACGTCTTCAA
(007)BglII_Venus_fw	ACGTAGATCTGTGAGCAAGGGCGAGGAGCT
(008)EcoRV_Venus_fw	ACGTGATATCCATATGGTGAGCAAGGGCGAGGA
(012)pEC-tetR_MCS_rv	CCAAGCTTGCATGCCTGCAGTTAACTAGTTCCAGATCTTCCCATATGGATATCTCCTTGTGTATCAACAAGCTGGGGATC
(013)eYFP_SpeI_rv	ACGTACTAGTTCTAGACTTGTACAGCTCGT
(014)eYFP_asv_SpeI_rv	ACGTACTAGTTTAAACTGATGCAGCGTAATCAC
(028)pduT_pMKEx1_rv	CGGAGCTCGAATTCGGATCCTTATCCCTCCACCATCTGTC
(036)pMKEx1_pduA_fw	CTTTAAGAAGGAGATATACCATGCAACAAGAAGCGTTAGG
(073)Vectoramp.D18rv	CGTCTTCAATAATCTGGCGCAGCAGCTTTTCATTGATTTCCATATCTATCCTCCTTTCGTCG
(074)D18_Hps_fw	GCTGCGCCAGATTATTGAAGACGTACTGTCTGAAAGATCTGAATTACAGCTTGCATTAGAC
(075)Hps_P18_rv	AAATGTTACGAATAAGGGTTTCAAGTTCTGAAGTGTTCATCGGAGTTATCCTTGGACAATC
(076)Hps_Phi_rv	TACGTATTCAGTCGTTTTCATCGGAGTTATCCTTGGACAATC
(077)P18_Phi_fw	AACCCTTATTCGTAACATTTTGAGTGAGCAACTTAGATCTAAAACGACTGAATACGTAGCGGAAATTC
(078)Hps_phi_fw	GATTGTCCAAGGATAACTCCGATGAAAACGACTGAATACGTAG
(079)pVWamp.D18_rv	GTCTTCAATAATCTGGCGCAGCAGCTTTTCATTGATTTCCATATAGACCTCCTTTCGTCG
(080)D18_mdh_fw	TGCGCCAGATTATTGAAGACGTACTGTCTGAAAGATCTACCAACTTCTTCATCCCTCC
(081)mdh_pVW_rev	GTACCCGGGGATCCTCTAGATTATTACAGTGCGTTCTTAATG
(082)mdh_pVW_fw	TCGCACAGATCATTAAGAACGCACTGTAATAATCTAGAGGATCCC
(083)Mdhaav_pVW_fw	GAAAAGAGCCAACGTGATTACGCAGCAGCTGTTTAATAATCTAGAGGATCCCCGGGTACC
(084)Mdh_aav_rv	TAATCACGTTGGCTCTTTTCTGCTGCCAGTGCGTTCTTAATGATCTGTG
(085)pVWamp_mdh_rv	CGGATGCTGGAGGGATGAAGAAGTTGGTCATATAGAC
(086)pVW_Mdh_fw	GTCTATATGACCAACTTCTTCATCCCTCCAG
(87)59longer	AGAGCGAGCTCTGCGGCCGCGTCGACTTGTACAGGATCCTTATCCCTCCACCATCT

Oligonucleotide	Sequence (5' -> 3')
	GTC
(88)58longer	CTAGAAATAATTTTGTTTAACTTTAAGAAGGAGATATCATATGCAACAAGAAGCGTTAGG
(94)GS-Linker_SDM	GACGTACTGTCTGAAAGATCTGGCTCCGAATTACAGCTTGCATTAGAC
(95)GS-Linker_SDM	GTCTAATGCAAGCTGTAATTCGGAGCCAGATCTTTCAGACAGTACGTC
(96)D18_GGSG	CGCCAGATTATTGAAGACGTACTGTCTGAAAGATCTGGCGGTTCCGGCGAATTACAGCTTGCATTAG
(99)Hps_fw	TCGACGAAAGGAGGATAGATATGGAATTACAGCTTGCATTAG
(100)Hps_rv	CGAGGTCTAATGCAAGCTGTAATTCCATATCTATCCTCCTTTCG
(101)10aahps_fw	TGGTGAAAATTTGTATTTTCAATCTGGTGGTGAATTACAGCTTGCATTAG
(102)10aahps_rv	GATTGAAAATACAAATTTTCACCAGATCTTTCAGACAGTACGTCTTC
(103)act_pVW_rv	AATTCGAGCTCGGTACCCGGGGATCCTCTAG
(104)MdhS97G_fw	TGCGGTATCGTGGGAACCGCCACCGCCGATGGA
(105)mdhS97G	TCCATCGGCGGTGGCGGTTCCCACGATACCGCA
(106)GS_D18_rv	GCTTGCATGCCTGCAGTTAACTAGTTTACATTTCGATATTTTCCTTC
(107)GS_D18rev_fw	GGACGAGCTGTACAAGTCTAGAGGCTCCTCTAGAGAATCTCTG
(108)eYFPGSD18_rv	GAGATTCTCTAGAGGAGCCTCTAGACTTGTACAGCTCGTCCATG
(109)pEC_eYFP_fw	GTTGATACACAAGGAGATATCCATATGGTGAGCAAGGGCGAGGAGC
(110)pEKEx2P18_fw	CGCCAAGCTTGCATGCCTGCAGAAGGAGATCAATGAACACTTCAGAACTTG
(111)P18GSMalE_rv	CTTCTTCAGTTTTGGAGCCAAGTTGCTCACTCAAAATGTTAC
(112)P18MalE_fw	ACTTGGCTCCAAAACTGAAGAAGGTAAACTG
(113)Cad_pEKEx2_rv	TGTAAAACGACGGCCAGTGAATTCTTACACCAGTGGGGACTTC
(114)eYFP3xGGGS	GCCGCCGGAGCCACCGCCTCTAGACTTGTACAGCTCGTCCATGC
(115)3xGGG3P18_pEC-fw	CGGTGGCTCCGGCGGCGGTTCCGGCGGTATGAACACTTCAGAACTTGAAACCC
(116)P18_pEC_rv	CATGCCTGCAGTTAACTAGTTTAAAGTTGCTCACTCAAAATG
(117)pTuf_P18	GCCACCACGAAGTCCGTCGACGAAAGGAGGATAGATATGAACACTTCAGAACTTGAAAC
(118)Ptuf_MalE_fw	TCGTAGCCACCACGAAGTCCGTCGACGAAAGGAGGATAGATATGAAAACTGAAGAAGGTA
(119)PTacD18_fw	CGCCAAGCTTGCATGCCTGCAGAAGGAGATCAATGGAAATCAATGAAAAGCTG
(120)D18GGSGAcn_rv	TCAGTCACAGTGAGCTCCAAGCCGGAACCGCCAGATCTTT
(121)D18GGSG_Acn_fw	GAAAGATCTGGCGGTTCCGGCTTGGAGCTCACTGTGACTG
(122)Acn_pEKEx2_rv	CTGTAAAACGACGGCCAGTGAATTCTTACTTAGAAGAAGCAGCCATC
(123)Ptuf_D18_fw	AAGTCGTAGCCACCACGAAGTCCGTCGACGAAAGGAGGATAGATATGGAAATCAATGAAAAGC
(124)Ptuf_Acn_fw	TCGTAGCCACCACGAAGTCCGTCGACGAAAGGAGGATAGATATGTTGGAGCTCACTGTGACTG
(125)Ptac_acn_fw	TACGCCAAGCTTGCATGCCTGCAGAAGGAGATCAATGTTGGAGCTCACTGTGACTGAAAGCAAG
(131)GGGS_C-termKp	GTTCCAGCACCTGGCGGATCACGCGTTCCACGTTCTGTTCGTTACCGCCGGAACCGCCGCCG
(132)C-termKp_rv	CTTGCATGCCTGCAGTTAACTAGTTTACTTTGCCAGGCGTTCCAGCACCTGGCGGATCACG
(134)Linker_Pmirab.C-term	GACGAGCTGTACAAGTCTAGAGGCGGTGGCTCCGGCGGCGGTTC
(135)Pmirab.C-term-pEC	AGCTTGCATGCCTGCAGTTAACTAGTTTACTTGCCCAGGCGGCCCAGCAC
(136)GBD_ligand_PduB	AGATGAAGATTAATGAGCAGCAATGAGCTGGTTG
(137)GBD_ligand_PduBrv	TCAACCAGCTCATTGCTGCTCATTAATCTTCATCTTCATCGC
(138)GS-LinkerGBDLig_fw	GGATCTGGTTCCGGCTCCGGTTCCGGCCTGGTGGGCGCACTGATGCAC

Oligonucleotide	Sequence (5' -> 3')
(139)PduA_9xGS_rv	GCCGGAACCGGAGCCGGAACCAGATCCGCTAATTCCCTTCGGTAAG
(140)pEKEx_PduA_fw	GTGAGCGGATAACAATTCCCCTCTAGAAATAATTTTGTTTAAC
(141)GsLinker_PDZligand	GTTCCGGCTCCGGTTCCGGCGGCGTGAAGGAATCCCTGGTGTAATGAGCAGCAATG AGCTGG
(142)GS_SH3ligand_PduB_fw	GTTCCGGCTCCGGTTCCGGCCCACCACCAGCACTGCCACCAAAGCGCCGCCGCTA ATGAGCAGCAATGAGCTG
(143)PDZ_domain_rv	TTGCATGCCTGCAGTTAACTAGTTTACTTGAAATAGGGTGAGACCTCCTTCATG
(144)eYFP9GSPDZfw	CGAGCTGTACAAGTCTAGAACTAGTGGATCTGGTTCCGGCTCCGGTTCCGGCCTCC AGCGTCGCCGCGTGAC
(145)SH3domain_rv	GCTTGCATGCCTGCAGTTAACTAGTTTAGCGATACTTCTCCACGTAAGGGACAG
(146)eYFP9GSSh3domain_fw	GAGCTGTACAAGTCTAGAACTAGTGGATCTGGTTCCGGCTCCGGTTCCGGCGCAGA GTATGTGCGTGCCCTC
(147)GBDdomain_rv	GCATGCCTGCAGTTAACTAGTTTATGGTGCTTGGCGACGGAGTTCATTTTTAAC
(148)eYFP9GSGBDdomain	ACGAGCTGTACAAGTCTAGAACTAGTGGATCTGGTTCCGGCTCCGGTTCCGGCACC AAGGCAGATATTGGAAC
(149)eYFP9GS-GBDdomain	CAAGTCTAGAGGATCTGGTTCCGGCTCCGGTTCCGGCACCAAGGCAGATATTGGAA C
(156)PdzLig_pMKEX1	CTTGTCGACGGAGCTCGAATTCGGATCCTTACACCAGGGATTCCTTCAC
(157)SH3lig_pMKEx1	GTCGACGGAGCTCGAATTCGGATCCTTAGCGGCGGCGCTTTGGTG
(158)GBDlig_pMKEx1	AGCTTGTCGACGGAGCTCGAATTCGGATCCTTAATCTTCATCTTCATCG
(159)PduA_pMKEx1	CTTGTCGACGGAGCTCGAATTCGGATCCTTAGCTAATTCCCTTCGGTAAG
(161)MalE_CAD_pVW	CGAGCTCGGTACCCGGGGATCCTCTAGACTACACCAGTGGGGACTTCACTG
(162)Acn-P18MalECAD	TGATTGATGCGGAAAGGAGGTCTATATGAACACTTCAGAACTTGA
(163)Acn-P18MalECAD	CCTCCTTTCCGCATCAATCATTACTTAGAAGAAGCAGCCATC
(164)pVW-D18-Acn	CGTAGCCACCACGAAGTCCGTCGACGAAAGGAGGTCTATATGGAAATCAATGAAAA GCTG
(165)Ptuf_acn	GTCGTAGCCACCACGAAGTCCGTCGACGAAAGGAGGTCTATATGTTGGAGCTCACT GTGAC
(166)Acn_MalECAD	ATTGATGCGGAAAGGAGGTCTATATGAAAACTGAAGAAGGTAAACTG
(167)GTG_PduK	ACAAGTGAAGCAATCACTGGGATTACTTGAAGTTAGTGGTC
(168)J_GTG_PduK	ACTTCAAGTAATCCCAGTGATTGCTTCACTTGTATATCTCCTTCTTAAAG
(169)GTG_PduU	AGTGGAAAGACAACCCACCACGGATCGTATGATTCAG
(170)N_GTG_PduU	GTGGTGGGTTGTCTTTCCACTTGTATATCTCCTTCTTAAAG
(171)GTG_PduT	AGTGTCTCAGGCTATAGGGATTTTAGAAC
(172)U_GTG_PduT	CCCTATAGCCTGAGACACTTTATGTATATCTCCTTCTTAAAG
(174)PduU_pMKEx1_rv	TCGACGGAGCTCGAATTCGGATCCTTATGTCCGGGTGATGGGAC
(176)PduN_pMKEx1_rv	TCGACGGAGCTCGAATTCGGATCCCTAACGAGAAAGCGTGTCGAC
(178)wholePduB_J_rv	ATACTGCTTTTCTCCTGTGGGTCAGATGTAGGACGGACGATC
(179)wholePduB_J_fw	ATCGTCCGTCCTACATCTGACCCACAGGAGAAAAGCAGTATG
(180)wholePduJK_N_rv	ACCCGTGCCAGATGCATAGCTCACGCTTCACCTCGTTTGC
(181)wholePduJK_N_fw	GCAAACGAGGTGAAGCGTGAGCTATGCATCTGGCACGGGTTAC
(182)wholePduN_TU_rv	CTATAGCCTGAGACATGACTAACGAGAAAGCGTGTCGACAATG
(183)wholePduN_TU_fw	CATTGTCGACACGCTTTCTCGTTAGTCATGTCTCAGGCTATAG
(184)PduJ_pMKEx1_rv	TGTCGACGGAGCTCGAATTCGGATCCTTATGCGGATTTAGGTAAAATG
(189)pK19_Cg1737_fw	TTACGCCAAGCTTGCATGCCTGCAGGAAAATCTGATTCCTTTGCATC
(194)Cg1737	TTGTAAAACGACGGCCAGTGAATTCAAGGACTCGGAACCCCAAC
(197)intCGP1_fw	GTGAGCGGATAACAATTCCCCTCTAG
(198)intCGP1_rv	GCCCCAAGGGGTTATGCTAGTTATTGCTCAG

Oligonucleotide	Sequence (5' -> 3')
(199)TTG_PduN_fw	CTTTAAGAAGGAGATATACATTTGCATCTGGCACGGGTTAC
(200)TTG_PduN_rv	GTAACCCGTGCCAGATGCAAATGTATATCTCCTTCTTAAA
(201)PduN_PduT_fw	TTAAGAAGGAGATATACAAGTGTCTCAGGCTATAGGGATT
(202)PduN_PduT_rv	AATCCCTATAGCCTGAGACACTTGTATATCTCCTTCTTAAAG
(209)newD18-Acnrv	AGCTTTTCATTGATTTCCATAGTGAGCTCCAATTCTAACTTT
(210)newD18-Acn-fw	GTTAGAATTGGAGCTCACTGTGGAAATCAATGAAAAGCTGCTG
(211)D18-Acn_rv2	GAAGGAGTTCTTGCTTTCAGTGCCGGAACCGCCAGATCTTTC
(212)D18-Acn_fw2	AAAGATCTGGCGGTTCCGGCACTGAAAGCAAGAACTCCTTC
(213)newD18-Acnrv	CAGCTTTTCATTGATTTCCACAGTGAGCTCCAATTCTAAC
(214)newATG-D18-Acn-fw	GTTAGAATTGGAGCTCACTATGGAAATCAATGAAAAGCTGCTG
(215)D18CFP_fw	CGAGCTGTACAAGTCTAGAACTAGTTAATTAAGATCCCCAGCTTGTTG
(216)D18-CFP_fw	TGAAGACGTACTGTCTGAAAGATCTGTGAGCAAGGGCGAGGAGCTG
(217)D18CFP_rv	ACAGCTCCTCGCCCTTGCTCACAGATCTTTCAGACAGTACGTCTTC
(218)CFP_pEC_rv	CTTGCATGCCTGCAGTTAACTAGTTTACTTGTACAGCTCGTCCATG
(222)P18-Acn-rv	CAGTCACAGTGAGCTCCAAGCCGGAACCGCCAAGTTGCTCACTCAAAATGTTAC
(223)P18Acn_fv	ACATTTTGAGTGAGCAACTTGGCGGTTCCGGCTTGGAGCTC
(224)D18-MalE_rv	CAGTTTACCTTCTTCAGTTTTGGAGCCAGATCTTTCAGACAGTACGTCTTCA
(225)D18-MalE-fw	ACTGTCTGAAAGATCTGGCTCCAAAACTGAAGAAGGTAAAC
(226)GS-PDZlig_PudB_fw	CGGCGTGAAGGAATCCCTGGTGTAATGAGCAGCAATGAGCTGG
(227)PduA-GS_PDZ_rv	ATTACACCAGGGATTCCTTCACGCCGGAGCCGCTAATTCCCTTCGGTAAGA
(232)p_PduJ_fw	GTGAGCGGATAACAATTCCCCTCTAGAAATAATTTTGTTTAAC
(240)scaf.PduB_fw	ATTTTGTTTAACTTTAAGAAGGAGATATACATATGAGCAGCAATGAGCTGGTTGATC
(241)GBD_PduB_fw	CTTCTTAAAGTTAAACAAAATTATTTCTAGTTTAATCTTCATCTTCATCGCCTG
(242)PDZ_PduB_rv	CTTCTTAAAGTTAAACAAAATTATTTCTAGTTACACCAGGGATTCCTTCAC
(243)SH3_PduB_rv	TTCTTAAAGTTAAACAAAATTATTTCTAGTTAGCGGCGGCGCTTTGGTGGC
(257)AdhB-9GS-rv	ACCGGAGCCGGAACCAGATCCGAAAGCGCTCAAGAAGAGTTC
(258)AdhB-9GS-fw	AAGAACTCTTCTTGAGCGCTTTCGGATCTGGTTCCGGCTCCG
(259)PDZdomain-rv	GTACCCGGGGATCCTCTAGATTACTTGAAATAGGGTGAGAC
(260)GBDdomain-rv	TACCCGGGGATCCTCTAGATTATGGTGCTTGGCGACGGAGTTC
(261)SH3domain	GTACCCGGGGATCCTCTAGATTAGCGATACTTCTCCACGTAAGG
725	CTGCAGAAGGAGATATACATATGCAACAAGAAGCGTTAGGAATGG
726	ATCAGGACACCAACGGATGCCGG
727	TTCGTCGTTATGGTTTTCATGGTACC
728	GTAAAACGACGGCCAGTGAATTCGACCCTTATTGCAGTTCGACC
729	GTAAAACGACGGCCAGTGAATTCTTATCCCTCCACCATCTGTCG
780	GTGCGGTATTTCACACCGCAGCTTTTAAGACCCACTTTCACATTTAAG
(K13)V_AdhB_fw	GTCGTAGCCACCACGAAGTCCGTCGACGAAAGGAGGTCTATATGGCTTCTTCAACTT TTTATATTC
(K14)V_AdhB_rv	GCTCGGTACCCGGGGATCCTCTAGATTAGAAAGCGCTCAAGAAGAGTTC
(K15)V_Pdc_fw	CGTAGCCACCACGAAGTCCGTCGACGAAAGGAGGTCTATATGAGTTATACTGTCGGT AC
(K16)V_Pdc_rv	TCGGTACCCGGGGATCCTCTAGACTAGAGGAGCTTGTTAACAGG
(K19)D18_GSGS_adhB_fw	CGTACTGTCTGAAGGTTCTGGCTCCGCTTCTTCAACTTTTTATATTCCTTTCG
(K20)V_SalI_D18_fw	CGTAGCCACCACGAAGTCCGTCGACGAAAGGAGGTCTATATGG

Oligonucleotide	Sequence (5' -> 3')
(K23)adhB_GSGS_D18_rv	GAATATAAAAAGTTGAAGAAGCGGAGCCAGAACCTTCAGACAGTACGTCTTCAATAATC
(K24)P18_NdeI_Pdc_fw	GCAACTTCATATGAGTTATACTGTCGGTACCTATTTAG
(K25)P18_GSGS_Pdc_fw	ACTTGGTTCTGGCTCCAGTTATACTGTCGGTACCTATTTAG
(K26)P18_GS_Pdc_fw	GCAACTTGGTTCTAGTTATACTGTCGGTACCTATTTAGC
(K27)V_SalI_P18_fw	GTCGTAGCCACCACGAAGTCCGTCGACGAAAGGAGGTCTATATGAACACTTCAGAACTTGAAACC
(K28)Pdc_NdeI_P18_rv	GTACCGACAGTATAACTCATATGAAGTTGCTCACTCAAAATGTTAC
(K29)Pdc_GSGS_P18_rv	GTACCGACAGTATAACTGGAGCCAGAACCAAGTTGCTCACTCAAAATGTTACG
(K30)Pdc_GS_P18_rv	ATAGGTACCGACAGTATAACTAGAACCAAGTTGCTCACTCAAAATG
(K32)adhB_D60_rv	AAGTTGAAGAAGCTTGCTGCTGGCCTTGTTTGGCTTCGCCAATC
(K33)D60_adhB_fw	GCCAAACAAGGCCAGCAGCAAGCTTCTTCAACTTTTTATATTCC
(K34)V_D60_adhB_fw_2	CGTAGCCACCACGAAGTCCGTCGACGAAAGGAGGTCTATATGGAAATCAATGAAAAGCTGCTG
(K35)10AS_L_adhB_fw	CTGGATCGACATCAGGCTCCGGTGCTTCTTCAACTTTTTATATTCCTTTCGTCAAC
(K36)10AS_L_D18_rv	GGAGCCTGATGTCGATCCAGAGCCCTTTTCAGACAGTACGTCTTCAATAATCTG
(K37)adhB_P18_pdc_fw2	ATTGATGCGGAAAGGAGGTCTATATGAACACTTCAGAACTTGAAACCCTTATTCG
(K38)adhB_RBS_pdc_fw	ATGCGGAAAGGAGGTCTATATGAGTTATACTGTCGGTACCTATTTAGC
(K39)pdc_RBS_adhB_rv	CATATAGACCTCCTTTCCGCATCAATCATTAGAAAGCGCTCAAGAAGAG

6.2 Supplemental material – pMKEx1 vector

An unexpected finding was that the empty vector control MB001(DE3) pMKEx1 showed a negative growth effect when IPTG was supplemented (Table S5). The growth rates declined from 0.500 ± 0.007 h^{-1} without IPTG to 0.315 ± 0.004 h^{-1} with 50 µM IPTG and to 0.154 ± 0.003 h^{-1} with the addition of 100 µM IPTG. The MB001(DE3) wild type strain is not impaired by the addition of IPTG (Table S7).

The first assumption was that this growth effect was a result of the production of a small peptide, which is presumably produced when no insert is introduced into the multiple cloning site, as there is a start codon following the promoter sequence and a stop codon after 62 amino acids. However, this cause was excluded with a control plasmid pMKEx1_new, which contained a stop codon two amino acids after the start codon and the potential coding gene sequence was deleted. The respective stain MB001(DE3) pMKEx1_new showed growth rates similar to MB001(DE3) pMKEx1 (Table S5).

Table S5: Growth rates of *C. glutamicum* MB001(DE3) containing pMKEx1 or pMKEx1_new.

Strain	Growth rate (h^{-1})			
MB001(DE3) pMKEx1	0.500 ± 0.007	0.501 ± 0.007	0.315 ± 0.004	0.154 ± 0.003
MB001(DE3) pMKEx1_new	0.499 ± 0.007	0.511 ± 0.006	0.277 ± 0.005	0.121 ± 0.008
	0 µM IPTG	**20 µM IPTG**	**50 µM IPTG**	**100 µM IPTG**

Another assumption was that the termination of the transcription upon IPTG induction was inefficient and some read-through transcription influenced the growth negatively. To evaluate that further, the plasmid pMKEx1 was compared to its sister plasmid of pMKEx2 (Kortmann *et al.*, 2015). Both plasmids only differ in their sequence between the RBS the T7 terminator sequence, however, pMKEx1 was not experimentally characterized in detail before this work. As MB001(DE3) pMKEx2 did not show any impairments upon IPTG induction (Kortmann *et al.*, 2015), it cannot be excluded that the sequence between the stop codon and T7 terminator also has an influence on transcription termination and the pMKEx1 plasmid is therefore not working correctly.

Unfortunately, as the reason for the influenced growth was not conclusively found, it cannot be differentiated if the growth effects observed for the Pdu production strains in the presence of 50 µM IPTG (Table S6) are additional effects of pMKEx1 impairment and Pdu production or the exclusive influence of Pdu production. This could be tested in future studies by the utilization of the pMKEx1 plasmid producing a protein, which is known to not influence the growth of *C. glutamicum*, like eYFP. Depending on the growth of *C. glutamicum* pMKEx1_*eYFP*, it could then be concluded if the growth defect is based on pMKEx1 plasmid or on the respective gene(s).

Table S6: Growth rates of different *C. glutamicum* MB001(DE3) Pdu production strains in presence and absence of IPTG. Given are some exemplary calculated growth rates of strains, whose growth curves are presented in Figure 17.

Plasmid	Growth rate (h^{-1})		Plasmid	Growth rate (h^{-1})	
pMKEx1	0.491 ± 0.004	0.354 ± 0.009	*pduABJkNu*	0.448 ± 0.003	0.288 ± 0.007
pduABJknt	0.485 ± 0.005	0.318 ± 0.005	*pduABJkNut*	0.458 ± 0.004	0.234 ± 0.005
	0 µM IPTG	**50 µM IPTG**		**0 µM IPTG**	**50 µM IPTG**

A hint, that the growth effect is mainly based on the *pdu* genes and not on the pMKEx1 plasmid is given by the integration strain MB001(DE3)::P_{T7}*pduABJknt* also showing a growth decline with the overproduction of PduABJknt (Table S7). In the chromosomal integration strain, the growth defect is less pronounced than in MB001(DE3) *pduABJknt*, however, the overproduction is also not as strong as only a single copy of the operon is present per cell.

Table S7: Growth rates of *C. glutamicum* MB001(DE3)::P_{T7}*pduABJknt* in the presence of different IPTG inducer concentrations. Given are the calculated growth rates of strains, whose growth curves are presented in Figure 19.

Strain	Growth rate (h^{-1})			
MB001(DE3)	0.548 ± 0.007	0.546 ± 0.006	0.559 ± 0.007	0.540 ± 0.003
MB001(DE3)::P_{T7}*pduABJknt*	0.558 ± 0.011	0.522 ± 0.0052	0.452 ± 0.008	0.428 ± 0.009
	0 µM	**20 µM**	**50 µM**	**100 µM**

6.3 Supplemental material – TEM of Pdu production strains

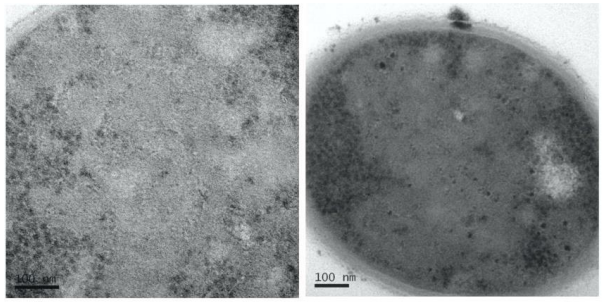

MB001(DE3) *pduABJKnut*

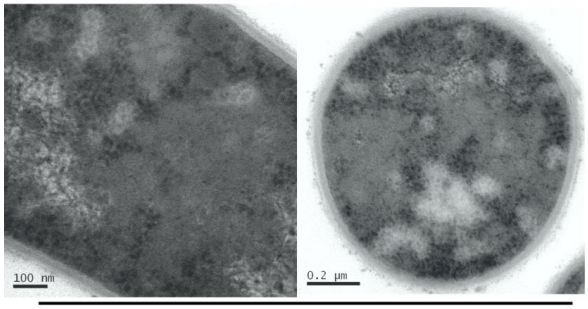

MB001(DE3) *pduABJKnt*

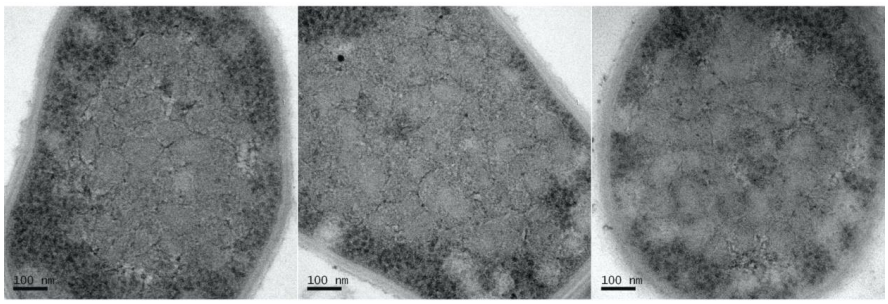

MB001(DE3) *pduABJkNut*

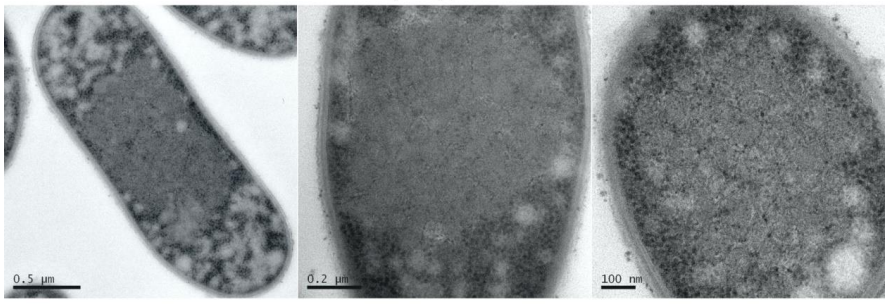

MB001(DE3) *pduABJkNu*

Figure S1: Transmission electron microscopy analysis of *C. glutamicum* MB001(DE3) Pdu production strains. Presented are additional images of strains compared in Figure 15.

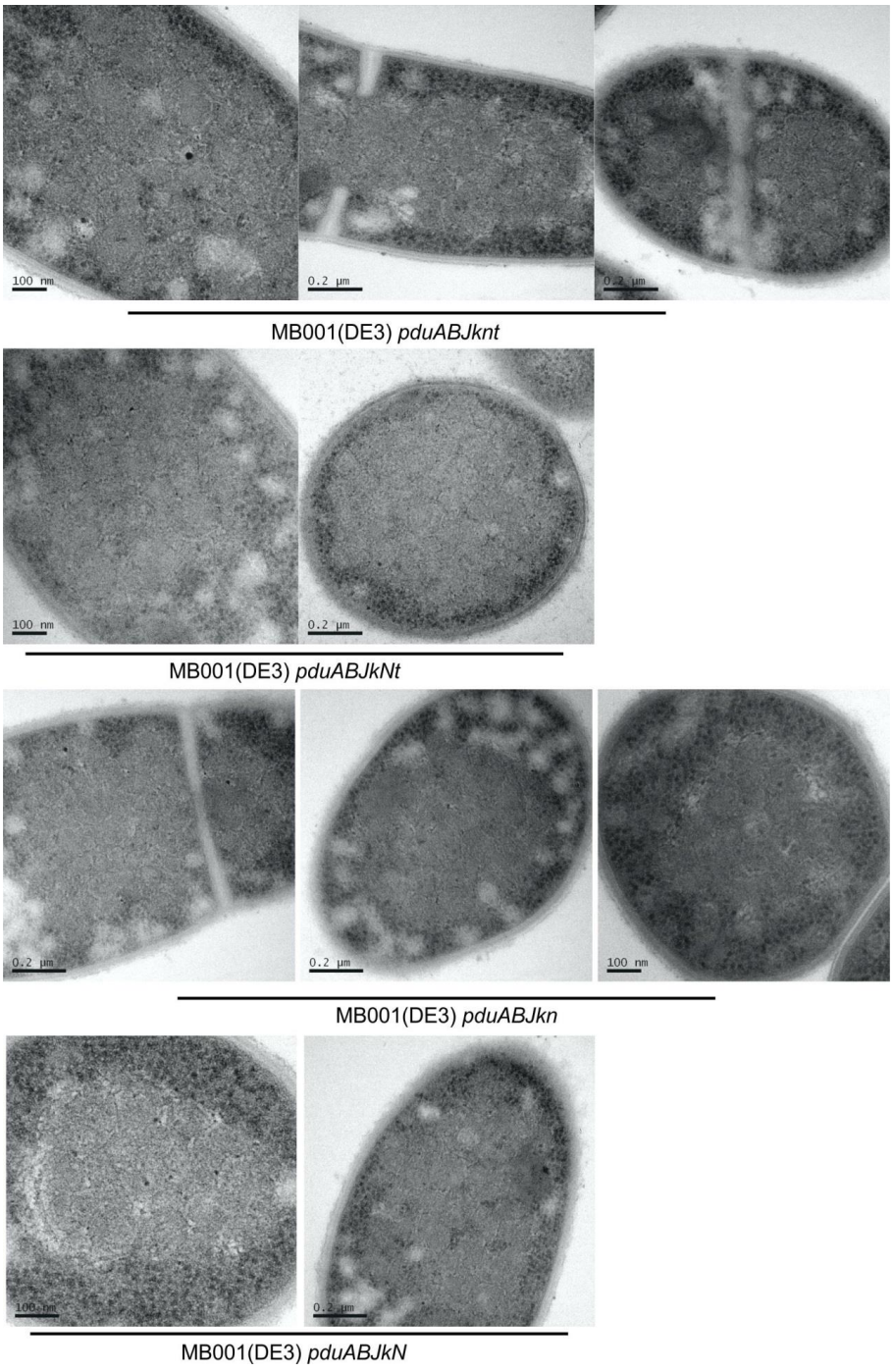

Figure S1 (continued): Transmission electron microscopy analysis of *C. glutamicum* MB001(DE3) Pdu production strains. Presented are additional images of strains compared in Figure 15.

Table S8: Number of cells with ‚BMC-like' structures. 200 cells of each strain were analyzed on 'BMC-like' structures within the cells. Cells were counted to contain 'BMC'-like if they contained at least one closed BMC-like structure.

Strain	Cells with 'BMC'-like	No BMCs	Total	% of cells with 'BMC'-like
MB001(DE3) *pduABJKNUT*	8	192	200	4%
MB001(DE3) *pduA*$_{PDZlig}$*BJknt*	115	85	200	58%
MB001(DE3) *pduA*$_{GBDlig}$*BJknt*	68	132	200	34%
MB001(DE3) *pduA*$_{SH3lig}$*BJknt*	45	155	200	23%
MB001(DE3) *pduABJknt*	91	109	200	46%
MB001(DE3) *pduABJkNt*	76	124	200	38%
MB001(DE3) *pduABJKnut*	12	188	200	6%
MB001(DE3) *pduABJkNut*	105	95	200	53%
MB001(DE3) *pduABJkn*	51	149	200	26%
MB001(DE3) *pduABJkN*	57	143	200	29%
MB001(DE3)::P$_{T7}$*pduABJknt*	38	162	200	19%
MB001(DE3)	7	193	200	4%

6.4 Supplemental material – Ethanol production

Table S9: Effects of plasmid-based AdhB/Pdc variant and genomic PduA or PduABJknt coproduction on growth of MB001(DE3). Growth analysis was performed in a microbioreactor system (BioLector®) in CGXII supplemented with 2% glucose at 30 °C. Given are the calculated growth rates of the listed strains, whose growth curves were presented in Figure 30.

Strain	Ethanol production module	Growth rate (h^{-1})	
MB001(DE3)	-	0.510 ± 0.00	
	adhB_pdc	0.460 ± 0.00	
	D18-GSGS-adhB_P18pdc	0.457 ± 0.00	
	D18-10aa-adhB_P18pdc	0.457 ± 0.00	
MB001(DE3)::P_{T7}*pduA*	*adhB_pdc*	0.415 ± 0.01	0.280 ± 0.01
	D18-GSGS-adhB_P18pdc	0.413 ± 0.00	0.280 ± 0.00
	D18-10aa-adhB_P18pdc	0.416 ± 0.00	0.276 ± 0.01
MB001(DE3)::P_{T7}*pduABJknt*	*adhB_pdc*	0.460 ± 0.00	0.351 ± 0.00
	D18-GSGS-adhB_P18pdc	0.458 ± 0.00	0.359 ± 0.00
	D18-10aa-adhB_P18pdc	0.458 ± 0.01	0.362 ± 0.01
		0 µM IPTG	**50 µM IPTG**

Table S10: Ethanol titers during 'semi-anaerobic' cultivation after 24 h and 30 h. The whole experiment is described in the Results Section 3.4.1. The ethanol titers were determined within sample supernatants of biological duplicates. As the quantification limit of the HPLC is below 30 mM ethanol, for some strains ethanol titers could not be calculated.

Strain	Ethanol production module	Ethanol (mM) 24 h cultivation		Ethanol (mM) 30 h cultivation	
MB001(DE3)	*adhB_pdc*	<30		61.35	
	D18-GSGS-adhB_P18pdc	<30		59.07	
	D18-10aa-adhB_P18pdc	46.59		65.86	
MB001(DE3)::P_{T7}*pduA*	*adhB_pdc*	50.28	<30	68.81	35. 07
	D18-GSGS-adhB_P18pdc	34.13	37.75	47.65	47.88
	D18-10aa-adhB_P18pdc	36.60	38.02	44.10	49.74
MB001(DE3)::P_{T7}*pduABJknt*	*adhB_pdc*	52.06	45.52	66.59	49.48
	D18-GSGS-adhB_P18pdc	40.23	<30	48.76	39.43
	D18-10aa-adhB_P18pdc	44.87	45.24	71.95	56.19
		0 µM IPTG	**50 µM IPTG**	**0 µM IPTG**	**50 µM IPTG**

Table S11: Ethanol production titers during 'semi-anaerobic' cultivation after 48 h and 60 h. The whole experiment is described in the Results Section 3.4.1. The measurements were performed in biological duplicates after 48 h and 60 h of cultivation. The ethanol titers were determined within sample supernatants of biological duplicates by HPLC analysis. The values after 48 h of cultivation are also given in Figure 31 as bar chart. After 60 h, the ethanol values dropped in comparison to 48 h.

Strain	**Ethanol production module**	**Ethanol (mM) 48 h cultivation**		**Ethanol (mM) 60 h cultivation**	
MB001(DE3)	*adhB_pdc*	104.59		69.85	
	D18-GSGS-adhB_P18pdc	92.65		36.67	
	D18-10aa-adhB_P18pdc	113.80		52.50	
MB001(DE3)::P_{T7}*pduA*	*adhB_pdc*	135.46	68.67	51.26	76.99
	D18-GSGS-adhB_P18pdc	129.07	84.99	49.68	91.57
	D18-10aa-adhB_P18pdc	100.85	85.33	39.72	87.47
MB001(DE3)::P_{T7}*pduABJknt*	*adhB_pdc*	115.63	95.32	49.99	56.39
	D18-GSGS-adhB_P18pdc	89.14	85.84	66.01	52.26
	D18-10aa-adhB_P18pdc	85.23	126.29	75.70	68.50
		0 µM IPTG	**50 µM IPTG**	**0 µM IPTG**	**50 µM IPTG**

6.5 Supplemental material – Itaconate production

Table S12: Influence of Icd activity on itaconate production in listed strains. The Icd activity was lowered by the modification of the start codon from ATG to GTG in MB001(DE3)::*icd*(A1G) or TTG in MB001(DE3)::*icd*(A1T). Itaconate titers were determined after 25 h of cultivation under N-limitation conditions. Given are the itaconate titers presented in the bar chart in Figure 33.

Strain	Plasmid	Itaconate (mM)	Plasmid	Itaconate (mM)
MB001(DE3)::*icd*(A1G)	P_{tuf}*malEcad*	4.85 ± 0.06	P_{tuf}*P18malEcad*	2.03 ± 0.07
MB001(DE3)::*icd*(A1T)	P_{tuf}*malEcad*	4.98 ± 0.10	P_{tuf}*P18malEcad*	2.84 ± 0.12
MB001(DE3)::*icd*(A1G)	*acn_malEcad*	2.58 ± 0.04	*D18acn_P18malEcad*	2.86 ± 0.04
MB001(DE3)::*icd*(A1T)	*acn_malEcad*	4.56 ± 0.12	*D18acn_P18malEcad*	4.48 ± 0.04

Table S13: Itaconate production and growth parameters of itaconate production strains containing plasmid-based or genomically integrated *pduABJKNUT* operon. Itaconate titers were determined after 25 h of cultivation under N-limitation conditions. The production of PduABJKNUT was induced with the addition of IPTG. Given are the itaconate titers presented in the bar chart in Figure 34 and the growth rates of the respective strains.

Strain	Plasmid	Itaconate (mM)		Growth rate (h^{-1})	
MB001(DE3) *pduABJKNUT*	*malEcad_acn*	0.13 ± 0.01	0.00 ± 0	0.35 ± 0.01	0.23 ± 0.01
	P18malEcad_D18acn	0.09 ± 0.01	0.00 ± 0	0.30 ± 0.01	0.19 ± 0.01
	pVWEx2	ND	ND	0.30 ± 0.01	0.25 ± 0.01
		0 µM IPTG	**20 µM IPTG**	**0 µM IPTG**	**20 µM IPTG**
MB001(DE3) ::P_{T7}*pduABJKNUT*	*malEcad_acn*	0.74 ± 0.07	0.32 ± 0.02	0.45 ± 0.01	0.37 ± 0.00
	P18malEcad_D18acn	0.81 ± 0.06	0.47 ± 0.05	0.44 ± 0.01	0.36 ± 0.01
	pVWEx2	ND	ND	0.42 ± 0.01	0.44 ± 0.01
		0 µM IPTG	**150 µM IPTG**	**0 µM IPTG**	**150 µM IPTG**

Table S14: Itaconate production and growth parameters of listed strains in MB001(DE3)::*icd*(A1G) ::P_{T7}*pduABJknt* background. Itaconate titers were determined after 25 h of cultivation under N-limitation conditions. Given are the itaconate titers presented in the bar chart in Figure 35A and the growth rates calculated from the growth curves presented in Figure 35B and C.

Strains	Plasmid	Itaconate (mM)		Growth rate (h^{-1})	
MB001(DE3)::*icd*(A1G) ::P_{T7}*pduABJknt*	*acn_malEcad*	1.39 ± 0.01	0.97 ± 0.02	0.45 ± 0.01	0.39 ± 0.01
	D18acn_P18malEcad	1.45 ± 0.02	0.83 ± 0.01	0.42 ± 0.02	0.38 ± 0.01
		0 µM IPTG	**150 µM IPTG**	**0 µM IPTG**	**150 µM IPTG**
MB001(DE3) ::*icd*(A1G)::P_{T7}*pduA*	*acn_malEcad*	1.29 ± 0.06	0.18 ± 0.01	0.47 ± 0.01	0.28 ± 0.01
	D18acn_P18malEcad	1.41 ± 0.02	0.23 ± 0.02	0.44 ± 0.01	0.29 ± 0.01
		0 µM IPTG	**150 µM IPTG**	**0 µM IPTG**	**150 µM IPTG**

Erklärung

Ich versichere an Eides Statt, dass die Dissertation von mir selbständig und ohne unzulässige fremde Hilfe unter Beachtung der „Grundsätze zur Sicherung guter wissenschaftlicher Praxis an der Heinrich-Heine Universität Düsseldorf“ erstellt worden ist. Die Dissertation wurde in der vorgelegten oder in ähnlicher Form noch bei keiner anderen Institution eingereicht. Ich habe bisher keine erfolglosen Promotionsversuche unternommen.

Düsseldorf, den 09.07.2017

Band / Volume 154
Gate-All-Around Silicon Nanowire Tunnel FETs for Low Power Applications
G. V. Luong (2017), ii, 136 pp
ISBN: 978-3-95806-259-7

Band / Volume 155
Graphene Devices for Extracellular Measurements
D. Kireev (2017), ix, 169 pp
ISBN: 978-3-95806-265-8

Band / Volume 156
Nanoscale 3D structures towards improved cell-chip coupling on microelectrode arrays
S. D. Weidlich (2017), II, 154 pp
ISBN: 978-3-95806-278-8

Band / Volume 157
Interface phenomena in $La_{1/3}Sr_{2/3}FeO_3$ / $La_{2/3}Sr_{1/3}MnO_3$ heterostructures and a quest for p-electron magnetism
M. Waschk (2017), ix, 205 pp
ISBN: 978-3-95806-281-8

Band / Volume 158
Physics of Life
Lecture Notes of the 49th IFF Spring School 2018
26 February – 09 March 2018, Jülich, Germany
ed. by G. Gompper, J. Dhont, J. Elgeti, C. Fahlke, D. Fedosov, S. Förster, P. Lettinga, A. Offenhäusser (2018), ca 1000 pp
ISBN: 978-3-95806-286-3

Band / Volume 159
Identifizierung von Bindungsdeterminanten von Tat-Vorläuferproteinen an den TatBCRezeptorkomplex während der Tat-abhängigen Proteintranslokation in *Escherichia coli*
A. Ulfig (2018), 186 pp
ISBN: 978-3-95806-290-0

Band / Volume 160
***Corynebacterium glutamicum* – a novel platform for the production of plant polyphenols**
N. Kallscheuer (2018), X, 98 pp
ISBN: 978-3-95806-291-7

Band / Volume 161
Neurons on 3D polymer nanostructures
A. Belu (2018), vii, 135 pp
ISBN: 978-3-95806-296-2

Band / Volume 162
Tailoring and Characterisation of Bioelectronic Interfaces
A. Markov (2018), 75 pp
ISBN: 978-3-95806-298-6

Band / Volume 163
Epitaxy of group IV Si-Ge-Sn alloys for advanced heterostructure light emitters
N. von den Driesch (2018), viii, 149 pp
ISBN: 978-3-95806-300-6

Band / Volume 164
Impact and Regulatory Control of the CGP3 Prophage in *Corynebacterium glutamicum*
E. Pfeifer (2018), IV, 206 pp
ISBN: 978-3-95806-301-3

Band / Volume 165
Establishment of Bacterial Microcompartments in the Industrial Production Strain *Corynebacterium glutamicum*
I. Huber (2018), X, 114, XI-XXXIV pp
ISBN: 978-3-95806-302-0

Schlüsseltechnologien / Key Technologies
Band / Volume 165
ISBN 978-3-95806-302-0

Mitglied der Helmholtz-Gemeinschaft

JÜLICH
Forschungszentrum